Proposal E-138
Received 10/5/82

SLAC PROPOSAL - SON OF E130

NEW MEASUREMENTS OF ASYMMETRIES IN POLARIZED DEEP INELASTIC SCATTERING

Part I. First Determination of the Spin Dependent Structure Function of the Neutron A_1^N

Part II. First Determination of the Nucleon Structure Functions A_2^P (Proton) and A_2^N (Neutron)

Polarized e-p Collaboration

V.W. Hughes, Spokesman

K.P. Schüler, Co-spokesman

September, 1982

Title: New Measurements of Asymmetries in Polarized Deep Inelastic Scattering.

Part I. First Determination of the Spin Dependent Structure Function of the Neutron A_1^N. (Scattering of longitudinally polarized electrons from longitudinally polarized protons and deuterons.)

Part II. First Determination of the Nucleon Structure Functions A_2^P (Proton) and A_2^N (Neutron). (Scattering of longitudinally polarized electrons from transversely polarized protons and deuterons.)

Experimenters: V.W. Hughes (spokesman), Yale University.

K.P. Schüler (co-spokesman), Yale University.

Polarized e-p collaboration

Beam: Polarized electrons produced by photoemission from GaAs with polarized laser light. Magnitude of polarization $P_e = 0.4$; polarization switching by modulation of cw laser with Pockels cell; pulse repetition rate 120 pps; current: $10^{10} e^-$/1.6 μs pulse on target; energy (A-line): 22.66 GeV; beam dump east.

Target: Polarized proton (deuteron) target to be set up in end station A. Material irradiated NH_3 (ND_3). New cryostat of $^3He/^4He$ type (0.6 Kelvin @ 1 watt) will be built; magnet: longitudinal type for part I exists, transverse type for part II will be built; polarizable nucleon fraction: ~0.2 (NH_3), ~0.3 (ND_3); maximum polarization: $P_p \sim 0.85$, $P_d \sim 0.45$; depolarizing (1/e) dose ~ $10^{16} e^-/cm^2$ ~ 15 hours of beam.

Detectors: E-130 spectrometer needs to be set up in end station A for a scattering angle of 7°; Møller polarimeter also needs to be set up again in ESA.

Date when equipment ready: Fall of 1984

Running time required:

Checkout: Six weeks at 10 to 60 pps

	Part I	Part II
Data-taking (factored hours):	300	300
Irradiation; background and Møller measurements	100	100
Total No. of factored hours	400	400

TABLE OF CONTENTS

Abstract

New measurements of asymmetries in deep inelastic scattering of longitudinally polarized electrons by longitudinally and transversely polarized protons and deuterons are proposed as a continuation of our studies of the internal spin structure of nucleons. This experiment is designed to obtain the first information on the spin dependent structure function A_1^N of the neutron (Part I) and on the "second" spin dependent structure functions A_2^P and A_2^N for the proton and neutron (Part II). The kinematic range covered will be from about $x = 0.1$ to $x = 0.6$ with $Q^2 \simeq$ 2 to 6 $(\text{GeV}/c)^2$.

The results should be valuable to test further the Bjorken sum rule, scaling for spin dependent structure functions, and modern models of nucleon structure. Furthermore, in general, the understanding of high energy spin dependent hadron scattering requires this information on the spin dependent nucleon structure functions.

I. INTRODUCTION AND MOTIVATION

A brief review of the subject of the internal spin structure of the nucleon, including experimental information obtained from our SLAC experiments E80 and E130, is given in the published paper in Appendix I. The final results of E130 are given in Appendix II and will soon be submitted to Physical Review Letters and also be published as a SLAC-PUB.

We propose now new measurements on the internal spin structure of the nucleon as follows:

Part I. The "longitudinal" spin dependent structure function of the neutron, A_1^N.

Part II. The "transverse" spin dependent structure functions of the proton and the neutron, A_2^P and A_2^N.

As compared with our E130 experiment and with our earlier Son of E130 proposal (August, 1980), major new technical approaches are proposed here. The first concerns the polarized target, where we will use a new target material - irradiated NH_3 and ND_3 - which has a higher free proton and deuteron content than the conventional hydrocarbon targets and also much higher resistance to radiation damage. In addition, our target will operate at the lower temperature of a $^3He/^4He$ refrigerator. The second concerns the polarized electron source where we will use the GaAs type source rather than the atomic ^6Li type source. With these new technological approaches we project an increase in data-taking rate by a factor of 20. We also believe we will achieve improved reliability of operation.

Part I Neutron Spin Dependent Structure Function A_1^N.

In part I we propose to measure for the first time the spin dependent structure function of the neutron A_1^N. In general for a nucleon the quantity A_1 is defined as

$$A_1 = \frac{\sigma_{1/2} - \sigma_{3/2}}{\sigma_{1/2} + \sigma_{3/2}}$$

in which $\sigma_{1/2}$ ($\sigma_{3/2}$) is the total absorption cross section of the virtual photon by the nucleon when the z component (z is the direction of the virtual photon momentum) of angular momentum of the virtual photon plus nucleon is 1/2 (3/2). In the quark-parton model A_1 is given by (Close, 1978)

$$A_1 = \frac{\Sigma_i e_i^2 [q_i^{\uparrow} - q_i^{\downarrow}]}{\Sigma_i e_i^2 [q_i^{\uparrow} + q_i^{\downarrow}]}$$

in which i denotes quark i and $q_i^{\uparrow}(q_i^{\downarrow})$ is the probability the quark i has its spin parallel (antiparallel) to the nucleon spin.

Our experiment involves the measurement of spin dependent asymmetries in the scattering of longitudinally polarized electrons by longitudinally polarized protons and by longitudinally polarized deuterons. By appropriate subtraction we can determine the longitudinal asymmetry or structure function for the neutron A_1^N. The kinematic range to be covered is $0.1<x<0.6$ and $2<Q^2<6(\text{GeV/c})^2$.

It is important to know A_1^N for the following reasons:

(1) It is one of the four electromagnetic structure functions which characterize the neutron in deep inelastic scattering and hence is a fundamental property of the neutron. In particular, A_1^N provides information about the internal spin structure of the neutron.

(2) Knowledge of A_1^N is required to test the important Bjorken polarization sum rule which is based on the quark-parton model and on the proposition that the weak interactions of quarks and leptons are the same. (Bjorken, 1966, 1970)

The status of the experimental verification of the Bjorken sum rule is given in Appendix II. From our data on A_1^P, about 50% of the value of the integral predicted in the sum rule is obtained. Our proposed measurements on

A_1^N should determine a substantial fraction of the neutron's contribution to the sum rule. In addition, the improved precision of values of A_1^P, especially in the low x range, to be obtained in our proposed experiment will improve significantly our knowledge of the contribution of A_1^P to the sum rule.

(3) Present quark-parton models of the nucleon are, of course, not based on rigorous QCD calculations although some day they may be. However, these somewhat phenomenological and intuitive wavefunctions represent our current state of knowledge of nucleon structure. Measurement of A_1^N will provide a new structure function to test existing models of the nucleon and to help to develop improved models.

Figure 1 shows some theoretical predictions for A_1^N. All of these models predict rather small values of A_1^N in the experimentally accessible kinematic region of $x \lesssim 0.6$. Our data will be of reasonable precision and can test this general conclusion of the models. (See Fig. 13, p. 40) Other predictions for A_1^N are expected from the MIT bag model (R. Jaffe, 1982), source theory (J. Schwinger, 1982), a modern version of the quark-parton model including QCD effects (G. Altarelli, 1982). It is worth remarking that the contribution of gluons to the spin dependent structure functions is a largely unexplored matter.

According to an argument of Bjorken (Bjorken, 1982) A_1^P is approximately equal to the intrinsic spin asymmetry a_u associated with the up quark in the nucleon wavefunction for moderate x values, and A_1^N will provide new useful information about the intrinsic spin asymmetry a_d associated with the down quark.

(4) Knowledge of A_1^N is essential to the interpretation of spin dependent high energy phenomena involving the neutron.

More generally, knowledge of the internal spin structure of the nucleon is required to interpret such processes as spin dependent hadron-hadron scattering (Sivers, 1978; Babcock, et al., 1979; Hidaka, et al., 1979; Craigie, et al., 1981), the polarized

Drell-Yan process (Soffer and Taxil, 1979; Hidaka, et al., 1980), and production of polarized W or Z vector bosons in collisions of polarized protons in a high energy storage ring (Baldracchini, 1980; Hidaka, 1981; Hughes et al., 1981: Kinnunen and Lindfors, 1981; Paige et al., 1979).

A major experiment is planned to be run at CERN by the European Muon Collaboration in 1984 (EMC, 1974) to measure the asymmetry in deep inelastic scattering of longitudinally polarized muons by longitudinally polarized protons. A significant test of the predicted scaling of the spin dependent structure function A_1^P will be obtained from this CERN data at high Q^2 ($Q^2 \leq 60(\text{GeV/c})^2$) and our SLAC data with $2 < Q^2 < 10(\text{GeV/c})^2$. Indeed the proton data to be obtained in our proposed experiment will be more precise than that obtained in E-130 (by a factor of 2 to 3), and hence useful for the test of scaling. Figure 2 gives a theoretical prediction of scaling violation using $\Lambda = 0.1$ and 0.4 GeV.

Part II The Spin Dependent Structure Functions, A_2^P and A_2^N

Part II is designed to measure the second independent spin structure functions A_2^P and A_2^N which arise from the interference between transverse and longitudinal photon-nucleon amplitudes. The quantity A_2 can be expressed

$$A_2 = \frac{2\sigma_{TL}}{\sigma_{1/2} + \sigma_{3/2}}$$

where σ_{TL} is an interference term between the amplitude for the absorption of longitudinal and transverse virtual photons. σ_{TL} may be negative. A positivity limit requires

$$|A_2| \leq \sqrt{R}$$

where $R = \sigma_L/\sigma_T$ is the ratio of the cross sections for absorption of longitudinal and transverse virtual photons.

The spin structure function A_2 is a qualitatively new quantity. There is a sum rule related to $A_2(x)$. (Burkhardt and Cottingham, 1970) In the scaling limit simple parton models predict that $A_2 = 0$ (Altarelli, 1982).

More specific QCD theories give rather large values for A_2 (Jaffe, 1975; Hughes, 1977). Nonzero values of A_2 arise from quark masses and finite transverse momenta of the quarks (Joshipura and Roy, 1980; Altarelli, 1982). Some thoeretical predictions for A_2 are given in Fig. 3.

It is important to measure A_2 for the following reasons:

1) It has intrinsic interest for nucleon structure and QCD. Fig. 3 indicates our projected points plotted with respect to the bag model prediction.

2) The asymmetry with the transverse polarization direction of the target (the measurement required to determine A_2) is needed because a separate determination of A_1 and A_2 requires two measurements - one with a longitudinal polarization direction of the target and the other with a transverse direction. Hence our values of A_1^P from E-130 will be more accurately determined once the transverse measurement is done. This point may be particularly true for A_1^N if A_1^N actually turns out to be small. Furthermore, the separation of A_1 and A_2 becomes an essential requirement if one looks for the rather small scaling violations predicted by QCD.

3) Our measurement of A_2 will provide a lower limit to R because of the positivity relation $|A_2| < \sqrt{R}$. It is well known that the usual determination of R from unpolarized lepton scattering at two different spectrometer angles is plagued with large systematic errors. Our measurement of A_2 will be done by flipping spin directions only and therefore is largely free of normalization errors.

References for I.

Abramowicz, H., et al., 1981, CERN Report CERN-EP/81-168, (sumbitted to Zeitschrift für Physik).

Altarelli, G., et al., Nucl. Phys. B69, 531 (1974).

Altarelli, G., 1982, Private communication.

Altarelli, G., Phys. Rep. 81, No. 1 (1982).

Babcock J., et al., Phys. Rev. D19, 1483 (1979).

Baldracchini, F., et al., "A Survey of Polarization Asymmetries Predicted by QCD," International Cetner for Theoretical Physics, Trieste, 1980.

Bjorken, J.D., Phys. Rev. 148, 1467 (1966).

Bjorken, J.D., Phys. Rev. D1, 1376 (1970).

Bjorken, J.D., 1982, Int. Symp. on High Energy Spin Physics, Brookhaven National Laboratory.

Burkhardt, H. and Cottingham, W.N., Ann. Phys. 56, 453 (1970).

Carlitz, R. and Kaur, J., Phys. Rev. Lett. 38, 673 (1977).

Close, F.E., Nucl. Phys. B80, 269 (1974).

Close, F.E., "An Introduction to Quarks and Partons" (Academic Press, London, 1979).

Craige, N.S., et al., "Polarization of Prompt Photons Produced at Lart P_T in Polarized Proton-Proton Collisions (preprint, 1981).

Darrigol, O. and Hayot, F., Nucl. Phys. B141, 391 (1978).

EMC (European Muon Collaboration), 1974, CERN Proposal SPSC-74-78, p. 63.

Hidaka, K., Monsay, E., and Sivers, D., Phys. Rev. D19, 1503 (1979).

Hidaka, K., Phys. Rev. D21, 1316 (1980).

Hidaka, K., Nucl. Phys. B192, 369 (1981).

Hughes, R.J., Phys. Rev. D16, 622 (1977).

Hughes, V.W., et al., 1981 Isabelle Workshop, BNL 51443, p. 600.

Jaffe, R.L., Phys. Rev. D11, 1953 (1975).

Jaffe, R., 1982, Private communication; Jaffe, R., and Ross, G.G., Phys. Lett. B93, 313 (1980).

Joshipura, A.D. and Roy, P., Phys. Lett. B92, 348 (1980).

Kaur, J., Nucl. Phys. B128, 219 (1977).

Kinnunen, R. and Lindfors, J., Nucl. Phys. B189, 63 (1981).

Kuti, J. and Weisskopf, V.F., Phys. Rev. D4, 3418 (1971).

Paige, F.E., et al., Phys. Rev. D19, 935 (1979).

Peierls, R.F., et al., Phys. Rev. D16, 1397 (1977).

Preparata, G., 1980, High Energy Physics with Polarized Beams and Polarized Targets, Proc. of the 1980 Int. Symposium, Lausanne, p. 121.

Schwinger, J., 1982, Private communication.

Schwinger, J., Nucl. Phys. B123, 223 (1977).

Sivers, D., High Energy Physics with Polarized Beams and Polarized Targets, ed. G.H. Thomas (AIP Conference Proceedings No. 51, Argonne, 1978), p. 505.

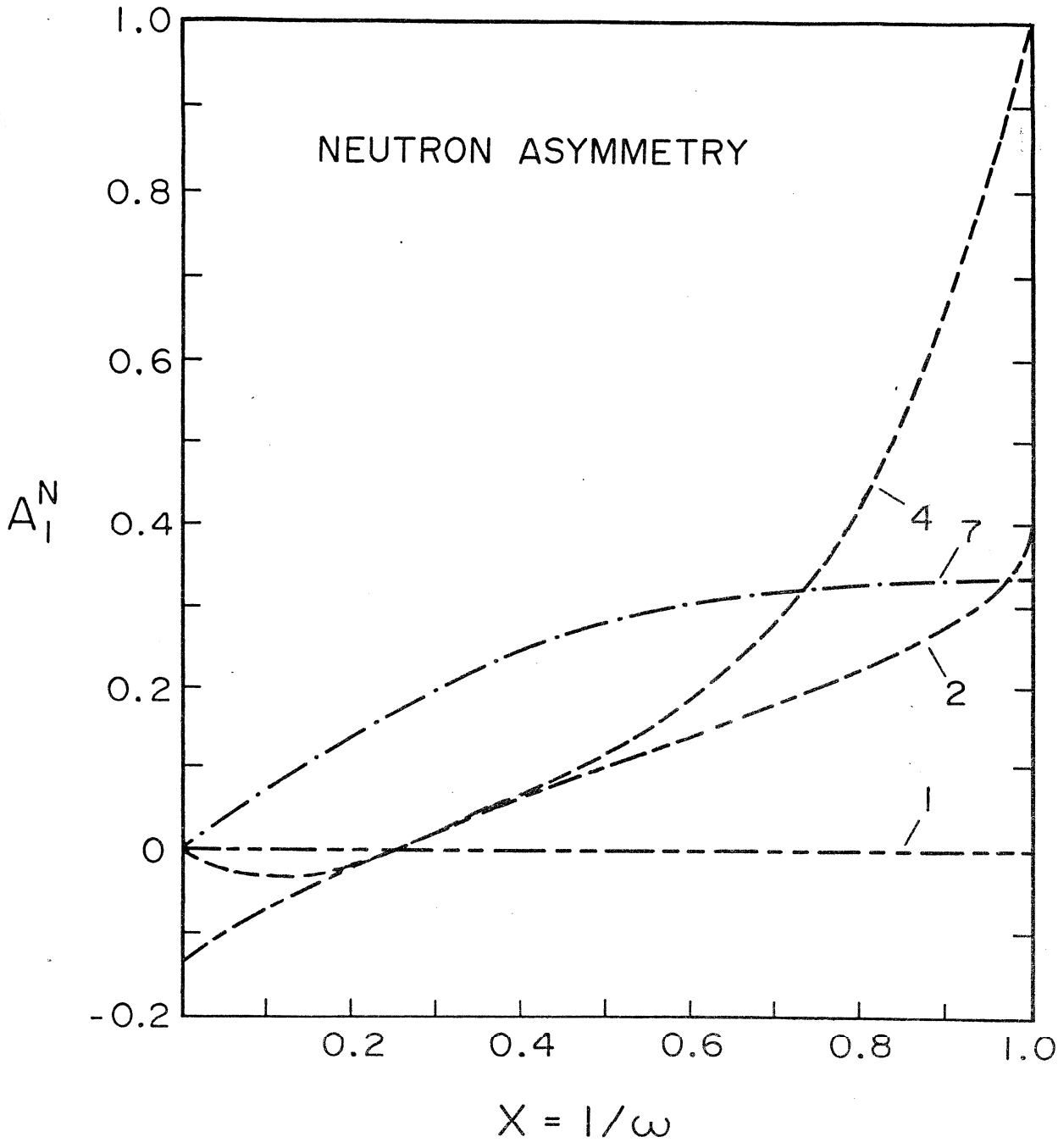

1. Symmetrical valence quark (Kuti, Weisskopf, 1971)
2. Current quarks (Close, 1974)
4. Unsymmetrical model (Carlitz, Kaur, 1977)
7. Quark-Geometrodynamics (Preparata, 1981)

Figure 1

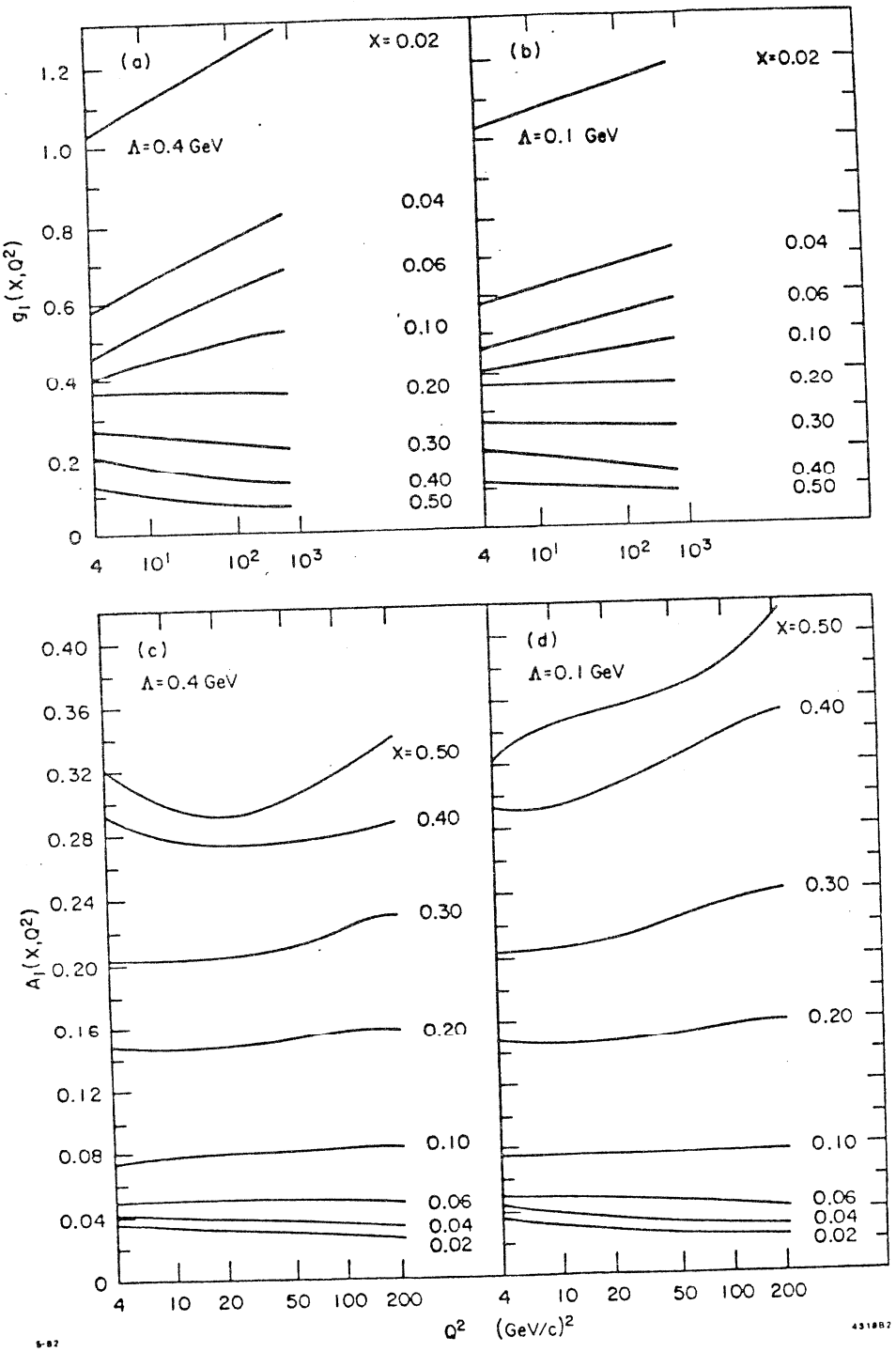

Figure 2. (a,b) Scaling violations of $g_1(x,Q^2)$ (Darrigol and Hayot, 1978) for two values of Λ, obtained by QCD and a broken SU(6) model (Close, 1974) at Q_o=2 GeV. (c,d) Scaling violations of $A_1(x,Q^2)$ obtained from (a,b) and known values of $F_1(x,Q2)$ (Abramowicz et al. 1981).

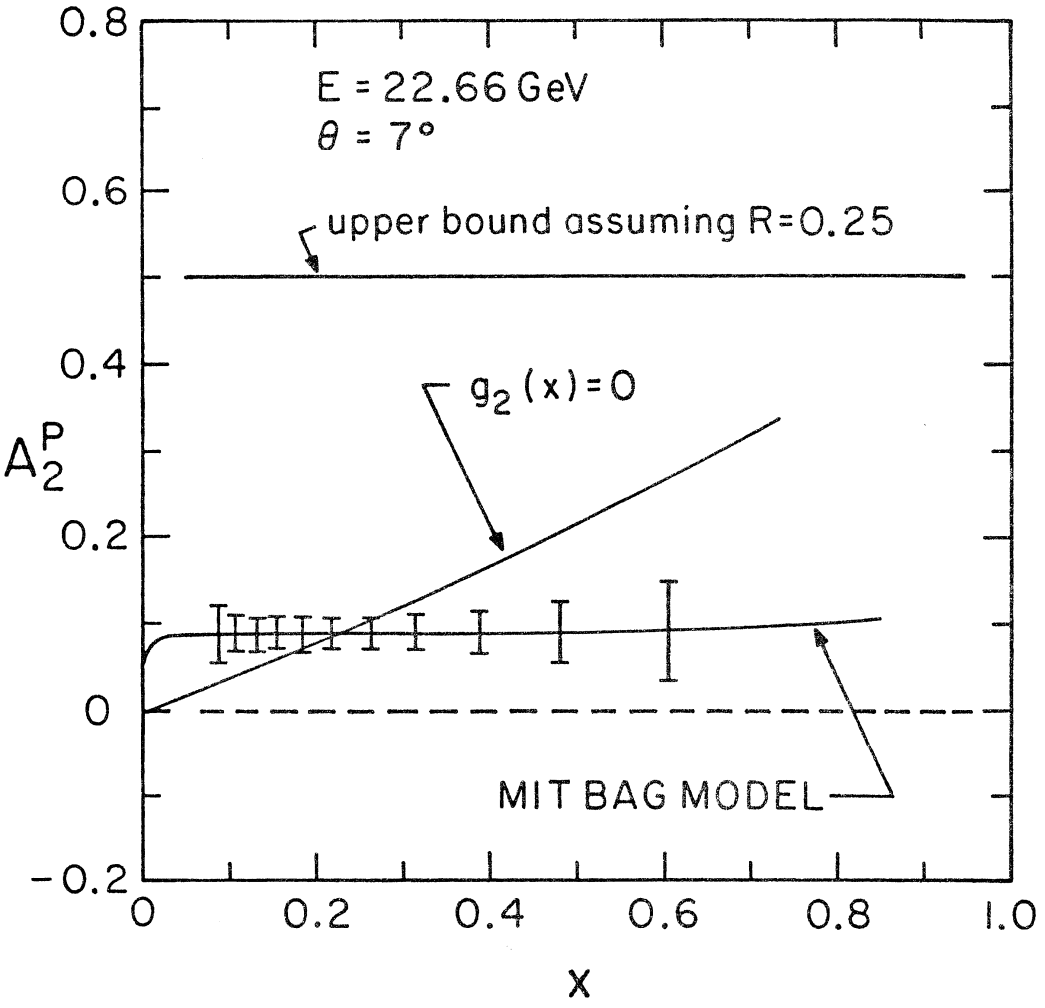
E = 22.66 GeV
θ = 7°
upper bound assuming R=0.25
g2 (x)=0
MIT BAG MODEL
A2P
0.8
0.6
0.4
0.2
0
-0.2
0
0.2
0.4
0.6
0.8
1.0
X

Figure 3

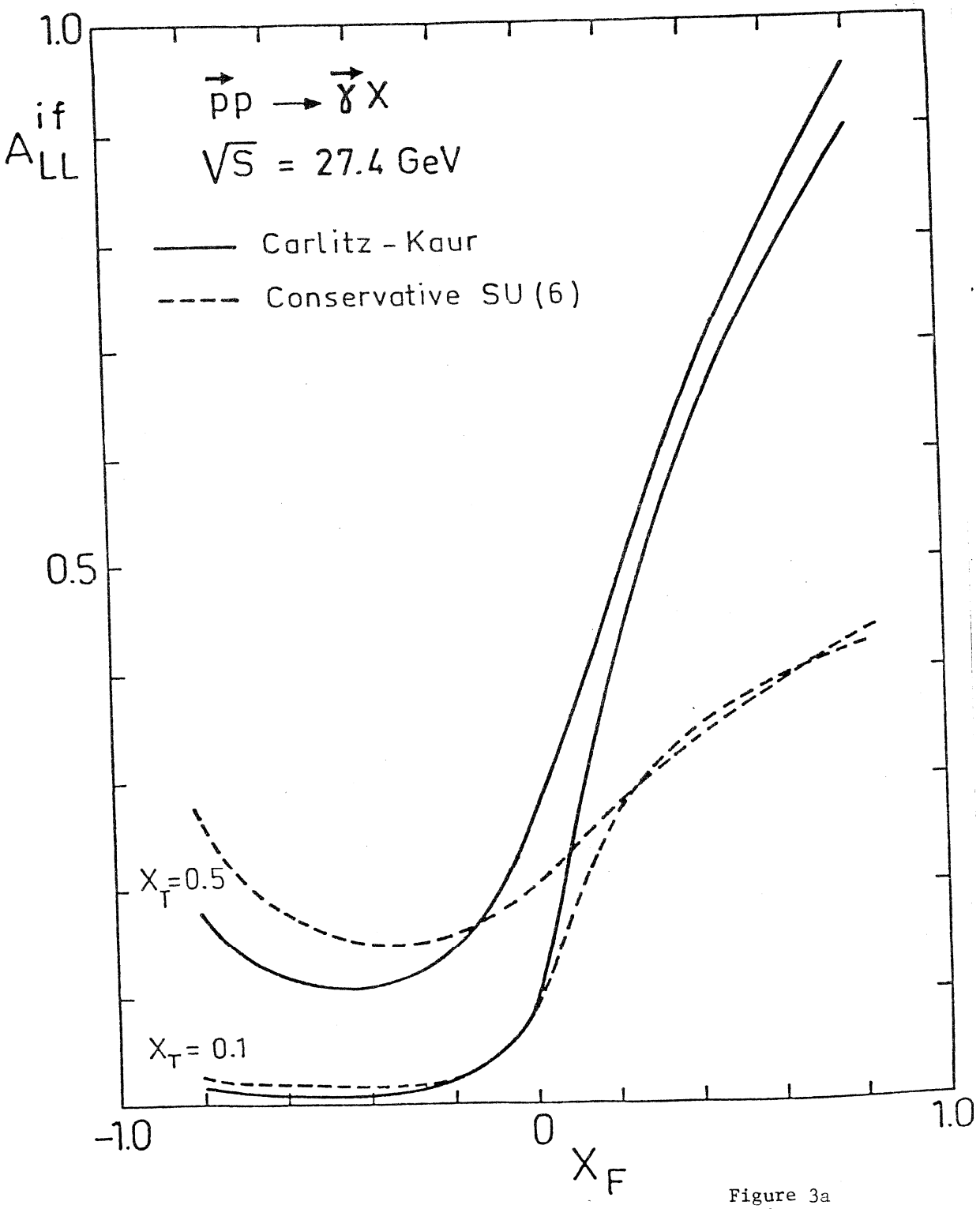

Figure 3a

(From K. Hidaka, 1981)

II. DESCRIPTION OF EXPERIMENT

II.1 Introduction

The experiment being proposed here - Son of E130 - is the same in principle as E130. The experiment E130 is described briefly in Appendix I and in more detail in several Physical Review Letters (Alguard et al., 1976, 1978). It involves the scattering of longitudinally polarized electrons by polarized protons and determination of the momentum and scattering angle of the electron in an inclusive experiment. We measure the asymmetry of spin dependence of the scattering rate. In Son of E130 we propose to use a polarized deuteron as well as a polarized proton target and also to use the transverse as well as the longitudinal target polarization direction.

The principal technical differences of Son of E130 from E130 are the use of a new polarized electron source and for the polarized target the use of a new target material - irradiated NH_3 and ND_3 - and a lower temperature operation. The polarized electron source and the polarized target are discussed in II.2 and II.3. The spectrometer-detector system, which is the same as used in E130 is discussed briefly in II.4. Kinematic conditions, counting rates, and expected results are given in II.5. II.6 details experimental facilities and personnel.

The projected factor of increase in data-taking rate in our present proposal as compared to the actual data-taking rate in our E130 experiment is about 20. The gain is accounted for as follows:

Increase for polarized electron beam ($P_e^2 I$) =	3.5	
Increase from polarized target ($F^2 P_p^2$)	(Proton)	(Deuteron)
Higher polarizable nucleon content (F^2) =	1.7	1.6
Higher polarization (P_p^2) (mainly from 0.5K operation) =	1.6	4.8
Total	9.5	27

About 3/4 of the data-taking time will involve the deuteron. Hence we take a weighted factor of increase of about 20.

References for II.1

1. M.J. Alguard et al., Phys. Rev. Lett. 37, 1258 (1976).
2. M.J. Alguard et al., Phys. Rev. Lett. 37, 1261 (1976).
3. M.J. Alguard et al., Phys. Rev. Lett. 41, 70 (1978).

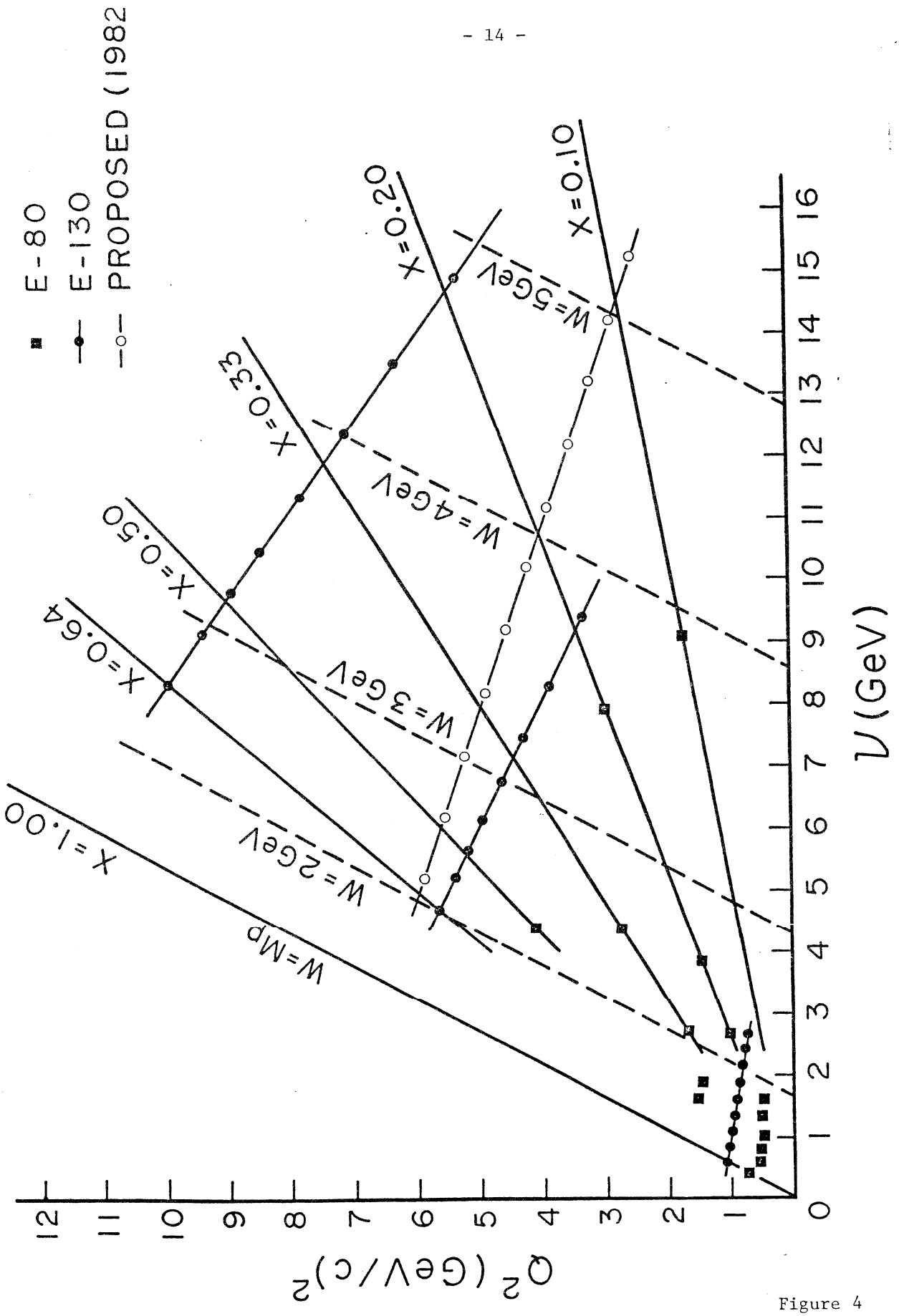

Kinematic points measured and proposed.

Figure 4

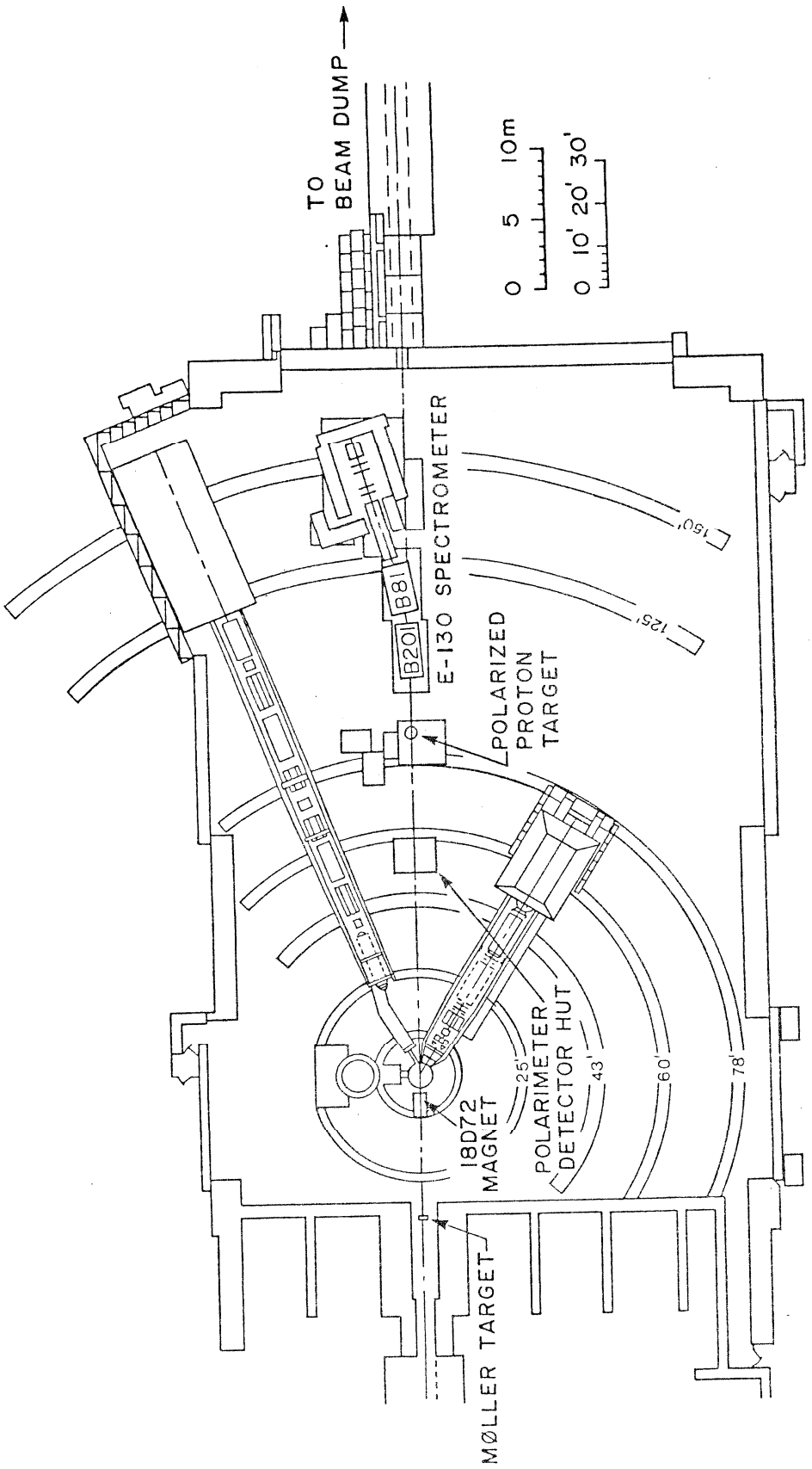

E-130 SET-UP IN END STATION A

Figure 5

II.2 Polarized Electron Source

Until recently the maximum beam current that could be tolerated on a polarized target was limited because of radiation damage. The evolution of a new technique (see polarized target section) that utilizes irradiated ammonia has changed the situation and higher beam currents become permissible, provided that the cryogenic problems related to beam heating of the target material can be managed.

For the proposed extension of E-130 we hope to use a beam current of $\sim 7 \times 10^9$ e^-/pulse, which is much larger than the current available in E-130;* (Alguard et al., 1979) and requires a solid state polarized electron source similar to the PEGGY II gun that was used in the parity experiment E-122 at SLAC (Prescott et al., 1978; Sinclair 1980). This type of source is based on photoemission of electrons from negative electron affinity gallium arsenide (GaAs) cathodes by circularly polarized laser light. Numerous versions of this kind of source exist now at various laboratories around the world and some important simplifications and improvements have been made.

The most important difference of the proposed new gun will be the use of an intense cw-krypton ion laser, commercially available, (Spectra Physics, 1982) instead of a flash lamp pumped dye-laser. This will result in very good pulse to pulse current stability (<1% according to specifications on laser noise). The electron beam current requirement ($\sim 7 \times 10^9$ e^-/pulse at the target) can be comfortably fulfilled with the cw-intensity of such a laser. The cw-output of the laser will be chopped with an electro-optical shutter to match the time structure of the accelerator. A quantum yield of 1% at the photocathode- a modest goal by the state of the art-will lead to 7×10^{10} e^-/pulse using the

---

*In E130 we used the polarized electron gun PEGGY I which is based on photo-ionization of a state selected lithium beam. It delivered an average current of 5×10^8 e^-/pulse @ 120 pulses per second at the target, the beam polarization was 81%

well matched krypton line at 752 nm (1.5 watts). Thus there is some room for nonoptimal performance and losses in transmission. The longitudinal polarization of the source can be switched by reversing the sense of the circular polarization of the laser light with a Pockels-cell. A GaAs source of this type using a cw laser is being developed by our group at Yale to be used with the MIT Bates electron linac for an experiment to measure parity violation in e^- - C elastic scattering at about 200 MeV (Souder et al.. 1977).

The physical principles of a GaAs-photoemission source and details of crystal preparation are described in a recent publication by Pierce et al. (Pierce et al., 1980). Using a GaAs (100)-type crystal a polarization of $P_e = 0.40$ should be obtainable (Pierce et al., 1980). This material is readily available. During the construction of the gun we will also study in as much as we can different cathode materials with a potential for higher polarization and/or more convenient laser lines. The following choices can presently be considered: (a) GaAs (111) grown by molecular beam epitaxy (MBE): At 1.65 eV (750 nm) a polarization of $P_e = 0.49$ together with a quantum yield of y = 0.9% has been obtained (Alvarado et al. 1981) (b) $A\ell_{0.37}\,Ga_{0.63}As$ alloy (also grown by MBE): At 1.92 eV (650 nm) a polarization value of $P_e = 0.45$ with y = 0.8% has recently been reported (Ciccacci et al., 1982). In this case the intense krypton-ion laser line at 647 nm with 3.5 watts of power can be used with advantage. (c) $GaAs_{0.6}P_{0.4}$ crystals: These crystals have shown polarizations of $P_e \simeq 0.4$ with quantum yields of y = 1% at 1.92 ev. (Conrath et al., 1979) At present a major uncertainty in these crystal studies is the question of whether samples of the above mentioned alloys or epitactically grown layers will be available to us. There has been some additional relevant research on the solid state crystals (Garwin, 1981; Zoroabedian, 1981).

The tentative plan is to locate this polarized electron source in the injection tunnel near the place where the SLAC GaAs polarized electron was located for E122.

References for II.2

1. M.J. Alguard et al., Nucl. Instrum. Methods 163, 29 (1979).

2. S.F. Alvarado et al., Z.f. Phys. B44, 259 (1981).

3. F. Ciccacci et al., J. Appl. Phys. 53, 4395 (1982).

4. D. Conrath et al., Appl. Phys. 20, 1955 (1979).

5. E. Garwin et al., SLAC-PUB-2715, April 1981.

6. D.T. Pierce et al., Rev. Sci. Instrum. 51, 478 (1980).

7. C.Y. Prescott et al., Phys. Lett. 77B, 347 (1978).

8. C.K. Sinclair, High Energy Physics with Polarized Beams and Polarized Targets, (Proceedings of the 1980 International Symposium, Lausanne, 1980), ed. C. Joseph and J. Soffer, (Birkhäuser Verlag, 1981) p. 27.

9. P.A. Souder et al., Bates proposal 14, 1977.

10. Spectra Physics Model 171-01, or similar.

11. P. Zoroabedian, SLAC Report 248 (Ph.D. dissertation, 1981).

Table 1

Characteristics of Polarized Electron Source

Characteristic	Value
Pulse length	1.5 μs
Repetition rate	120 pps
Intensity (at high energy)	7×10^9 e^-/pulse
Polarization	0.4

II.3 Polarized Target

The polarized target system that would be used in this experiment differs substantially from the present Yale-SLAC polarized target, which was used in experiments E-80 and E-130. The most significant improvements will be the use of new target materials and a new refrigeration system. The use of new polarized targets materials, irradiated NH_3 and ND_3, will provide a higher polarizable nucleon fraction and will enable the target to operate in an intense beam without requiring a substantial fraction of down time for target annealing and replacement. The target system will utilize a new refrigeration system operating at 0.55 K with a 50 kG superconducting magnet in order to achieve high deuteron polarizations. Because the target is to be used in a relatively intense beam, the refrigerator will have a large cooling power (~1 W at 0.55 K) and will include a subcooled ^4He bath around the actual target for improved heat transfer from the target material to the refrigerator. The anticipated operating characteristics of the new target system are given in Table 2. The characteristics of our present system are given for comparison.

The recent development of irradiated NH_3 and ND_3 as polarized target materials represents a major advance in polarized target technology (Niinikoski et al., 1979; Hartel, 1981; Seely et al., 1982). (A publication describing the results of our studies on irradiated NH_3 and ND_3 is given in Appendix 3). The polarizable nucleon fractions for NH_3 and ND_3 are higher than the polarizable nucleon fractions for conventional hydrocarbon targets by approximately 29%. Furthermore, the radiation resistance of the polarization in NH_3 and ND_3 is approximately thirty times greater than that for conventional hydrocarbon targets, such as butanol (the target material used in E-80 and E-130). The increased radiation resistance of NH_3 and ND_3 targets is an important factor in making the use of intense beams possible.

In all polarized target materials, the nuclear polarization decreases

during the course of the experiment due to radiation damage. The polarization may be recovered by annealing (warming up) the target material. After approximately 6 anneals, it becomes necessary to replace the target material. Annealing and target replacement can introduce a substantial amount of down time for the experiment. For the beam intensities we propose here, it would not be practical to use conventional hydrocarbon target materials because the radiation resistance of the polarization in these materials is relatively low. With irradiated NH_3 and ND_3 targets, however, we are able to use higher beam intensities than were previously practical, while maintaining a higher average target polarization and a better duty factor for the target. NH_3 and ND_3 targets must be irradiated before they may be polarized. This may be accomplished by irradiating the targets insitu (i.e., in the target system) using an unpolarized beam. We have computed duty factors for the target assuming a beam current of 7×10^{11} e^-/s. For NH_3 we anticipate that 8% of the total time available will be spent on annealing/target changing and unpolarized irradiation to establish target polarization. For ND_3, we expect a 20% down time for target changes/anneals and unpolarized irradiation to establish target polarization. (For butanol, we would expect 50% down time under the same conditions). The down time for ND_3 is greater than that for NH_3 because the ND_3 targets must be reirradiated after each anneal to establish polarization. Irradiated NH_3 targets were recently used in a polarized target experiment at Brookhaven (D. Crabb, 1982) and the EMC is planning to use irradiated NH_3 as the target material in the two liter polarized proton target at CERN (J. Court; T. Niinikoski, 1982).

The 40 MeV Linac, now under construction in the Cryogenics building at SLAC, will be used for further studies on irradiated NH_3 and ND_3 targets. This facility will also be used to test the new target system. During the experiment, we may wish to use the 40 MeV Linac to irradiate NH_3 and ND_3

target material in liquid argon in order to reduce the time required to initially polarize the targets.

Initial design work for the new refrigeration system has been completed. A schematic drawing of the refrigerator is given in Figure 6. This refrigerator will utilize a conventional ^{3}He evaporation cryostat to achieve a target bath temperature of 0.55 K with an applied heat load of 1 W. The actual target will be immersed in a bath of subcooled ^{4}He at a pressure of 1 atmosphere. Traditionally, the target would be placed directly in the evaporating ^{3}He bath; however, subcooled ^{4}He offers improved heat transfer characteristics and will enable us to use much higher beam currents than would otherwise be permitted. It should also be noted that at 0.5 K, the microwave power required for dynamic polarization is much lower than the microwave power required at 1 K. We are therefore able to devote a much larger fraction of the available cooling power to offset beam heating. (With the present target system, operating at 1 K, we require ~0.4 W of microwave power).

Heat will be transferred from the subcooled ^{4}He target bath to the ^{3}He evaporation cryostat via the ^{3}He/^{4}He heat exchanger. This heat exchanger is the most important component of the new refrigerator. As shown in Figure 7, the heat exchanger will consist of a single copper tube, approximately 18" long and 4" in diameter, with a 0.04" layer of sintered 350 mesh copper on the inside (^{4}He side) and 450 radial fins, extending to a diameter of 6.28", on the outside (^{3}He side). ^{3}He evaporation takes place around the outside of the heat exchanger. The fins are cut off at the top to form a vapor space, from which the ^{3}He is pumped. The inner wall of the heat exchanger tube forms the outer wall of the subcooled ^{4}He vessel. The sintered copper surface inside the heat exchanger will have a total surface area of

approximately 8×10^5 cm^2, which is 2000 times larger than the surface area of the target beads.

When operating with a target bath temperature of 0.55 K and a heat load of 1 W, we expect the ^{4}He consumption of the new refrigerator to be 25 ℓℓ/hr or less. The magnet dewar will require an additional 8 ℓℓ/hr of ^{4}He, bringing the total helium usage rate to 33 ℓℓ/hr. It should be stressed that this is an upper limit on the helium usage. There has been relevant research on high power low temperature cryostats at Bonn (Rennings, 1981), CERN (Niinikoski, 1982), and KEK (Fukushima et al., 1976).

In addition to the macroscopic heat transfer and cooling power requirements, we have also considered the potential transient heating and depolarization effects that may occur with an intense, pulsed beam. It is our opinion, and the opinion of others in the field, that depolarization of the target during the 1.6 μs beam pulse will not occur due to the long time constants involved in dynamic polarization. No transient depolarization effects were observed during experiment E-130. Furthermore, transient beam heating can be avoided quite easily by defocusing the beam.

Additional improvements in the polarized target will include a new NMR system, which is being acquired from Liverpool University. This NMR system has substantially better signal/noise and linearity characteristics than our present system and will enable us to reduce the uncertainty in the target polarization measurement. We are also in the process of upgrading our microwave system by replacing the carcinatron BWO tube with an EIO tube from Varian.

For the A_1 measurement (Part I), we plan to use the existing 50 kG superconducting solenoid. For the A_2 measurement, the 50 kG solenoid would be replaced by a 50 kG Helmholtz pair to obtain target polarization transverse to the beam direction.

References for II.3

1. J. Court, Liverpool University, private communication.

2. D. Crabb, University of Michigan, private communication.

3. M. Fukushima et al., "A Cryostat with a Large Cooling Power for Polarized Target," in High Energy Physics with Polarized Beams and Targets, ed. M.L. Marshak, (AIP Conf. Proceedings No. 35, Argonne, 1976) 519.

4. U. Härtel et al., "Experience with NH_3 as Target Material for Polarized Proton Targets at the Bonn 2.5 GeV Electron Synchrotron," and "First Dynamic Deuteron Polarization Measurements in Irradiated ND_3," in High Energy Physics with Polarized Beams and Polarized Targets, ed. Joseph and Soffer (Lausanne, 1980) 447, 451.

5. T.O. Niinikoski and J.-M. Rieubland, Phys. Lett. 72A, 141 (1979).

6. T.O. Niinikoski and J.-M. Rieubland, CERN-EP/82-51 (May 1982).

7. K. Rennings, "Ein Kryostat für Polarisationsexperimente am Bonner 2.5 GeV Synchrotron," Universität Bonn, Ph.D. Thesis, February 1981.

8. M.L. Seely et al., "Dynamic Nuclear Polarization of Irradiated Targets," SLAC-PUB 2874 (January, 1982).

Table 2

Polarized Target

Target System Characteristics

	Present Polarized Target System	Projected for New System
Temperature (at target)	1 K	0.6 K
Refriderant	^{4}He	^{3}He/subcooled ^{4}He
Target volume	25 cm^3	25 cm^3
Cooling power	0.750 W at 1.0 K	1 W at 0.6 K
^{4}He comsumption	12 ℓℓ/hr	.33 ℓℓ/hr
Magnetic field	50 kG	50 kG

Target Material Characteristics

	Present Polarized Target System	Projected for New System
Target Material	Butanol	Ammonia
Polarizable Nucleon Fraction	0.135 (C_4 H_9 OH) 0.238 (C_4 D_9 OD)	0.176 (NH_3) 0.300 (ND_3)

Operational Characteristics - Proton

	Present Polarized Target System	Projected for New System
Designed for Beam Current	2×10^{11} e^-/s	7×10^{11} e^-/s
Maximum Polarization	75%	95%
Average Squared Polarization	0.39 } For 2×10^{11} e^-/s	0.76 } For 7×10^{11} e^-/s
Duty Factor	68% } Beam Current	85% } Beam Current

Operational Characteristics - Deuteron

	Present Polarized Target System	Projected for New System
Designed for Beam Current	2×10^{11} e^-/s	7×10^{11} e^-/s
Maximum Polarization	25%	55%
Average Squared Polarization	0.043 } For 2×10^{11} e^-/s	0.23 } For 7×10^{11} e^-/s
Duty Factor	68% } Beam Current	78% } Beam Current

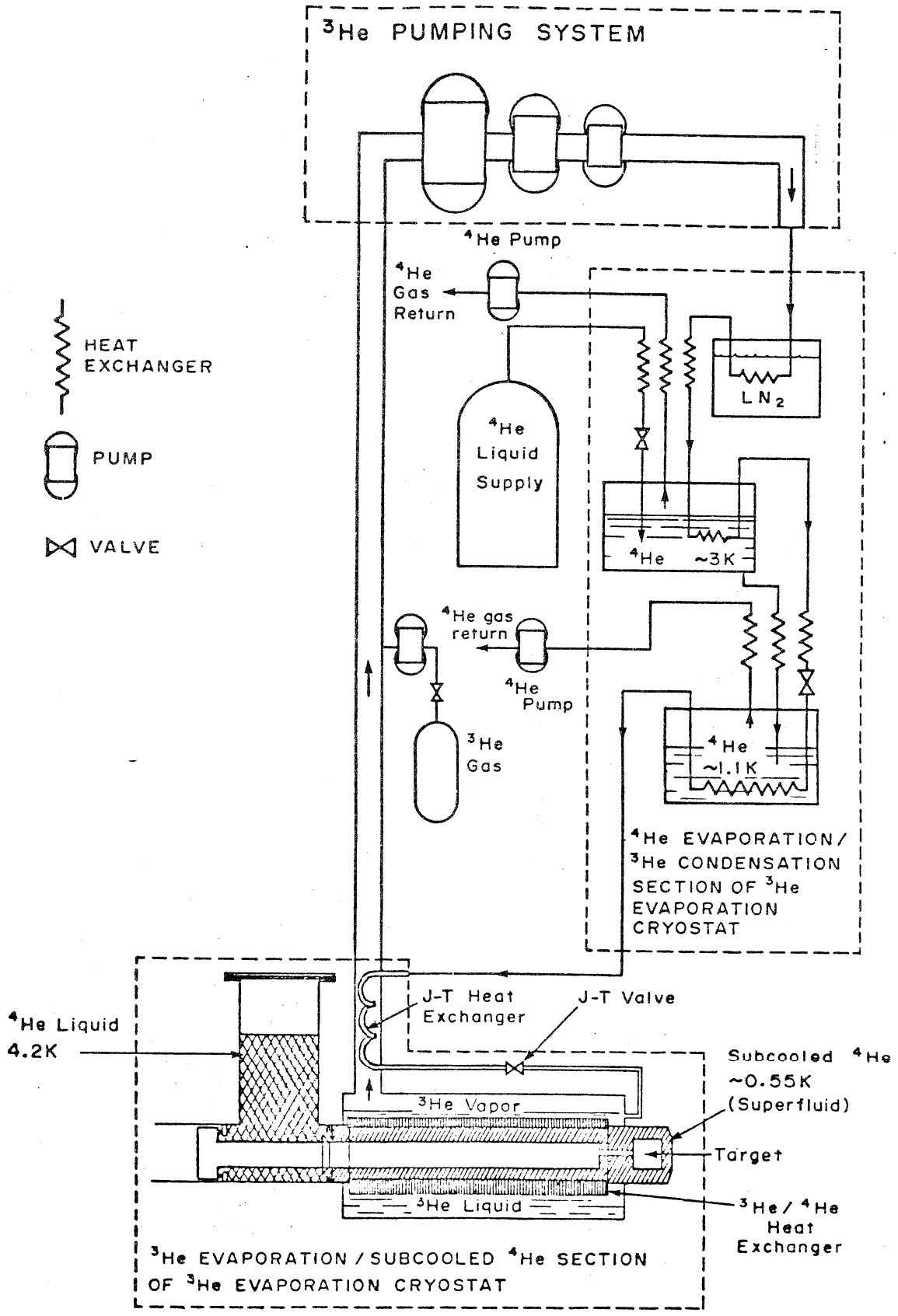
^{3}He PUMPING SYSTEM
^{4}He Pump
^{4}He Gas Return
HEAT EXCHANGER
PUMP
VALVE
^{4}He Liquid Supply
LN$_2$
^{4}He ~3K
^{4}He gas return
^{4}He Pump
^{3}He Gas
^{4}He ~1.1K
^{4}He EVAPORATION/ ^{3}He CONDENSATION SECTION OF ^{3}He EVAPORATION CRYOSTAT
J-T Heat Exchanger
J-T Valve
^{4}He Liquid 4.2K
Subcooled ^{4}He ~0.55K (Superfluid)
^{3}He Vapor
Target
^{3}He Liquid
^{3}He / ^{4}He Heat Exchanger
^{3}He EVAPORATION / SUBCOOLED ^{4}He SECTION OF ^{3}He EVAPORATION CRYOSTAT

Figure 6

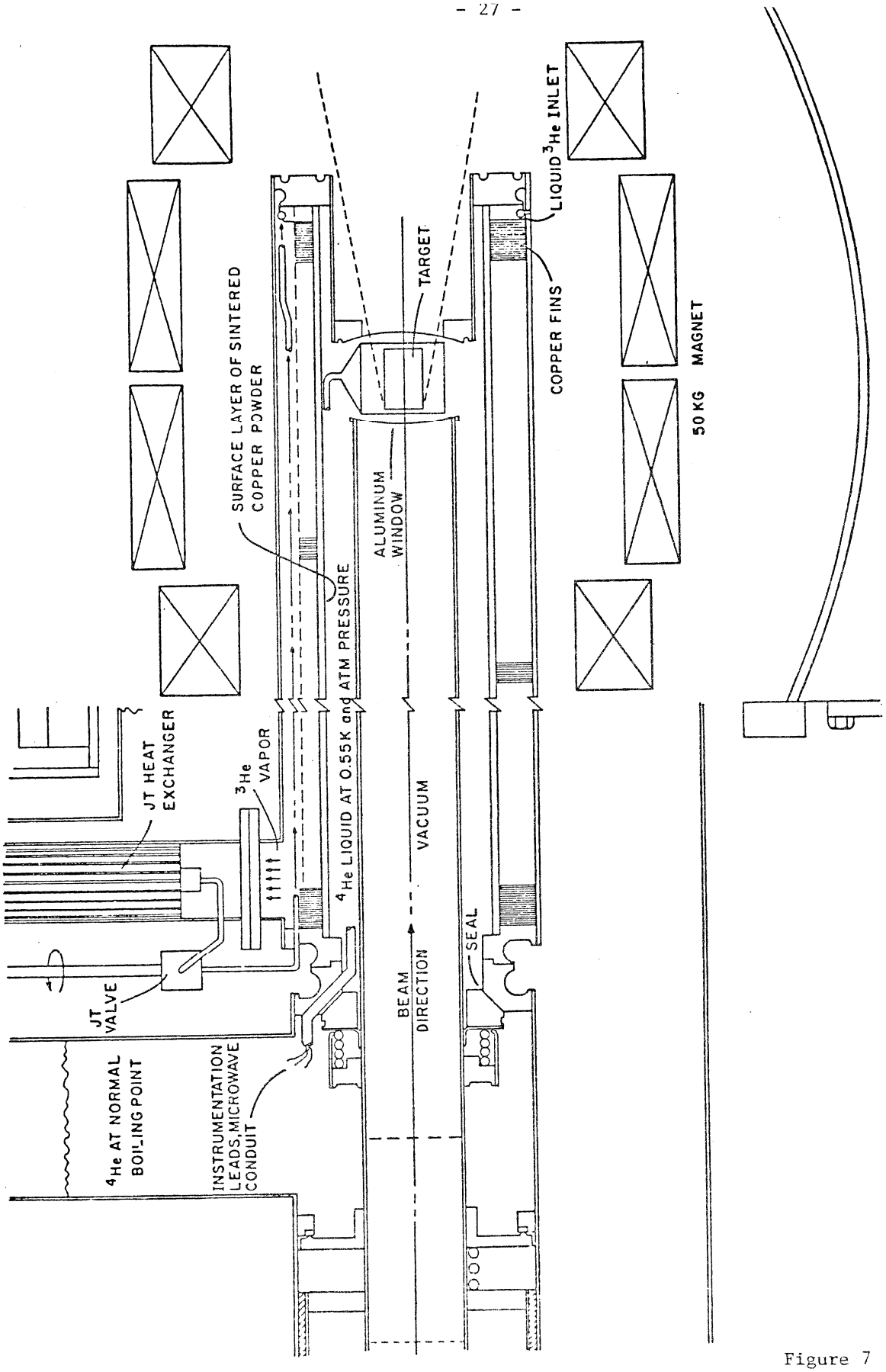
LIQUID ^{3}He INLET
TARGET
COPPER FINS
50 KG MAGNET
SURFACE LAYER OF SINTERED COPPER POWDER
ALUMINUM WINDOW
JT HEAT EXCHANGER
^{3}He VAPOR
^{4}He LIQUID AT 0.55K and ATM PRESSURE
VACUUM
SEAL
BEAM DIRECTION
JT VALVE
^{4}He AT NORMAL BOILING POINT
INSTRUMENTATION LEADS, MICROWAVE CONDUIT

Figure 7

II.4 Spectrometer-Detector

The E-130 spectrometer will be used at a fixed scattering angle of 7° for both parts of the proposal and needs to be set up again in end station A.

A schematic layout of the spectrometer is shown in fig. 8. It is of the non-focussing type and uses bending magnets from the standard 8 GeV/c and 20 GeV/c spectrometers at SLAC. The particle momenta are determined by ray tracing in a PWC-system. The spectrometer takes a very large momentum bite ($\Delta p/p \approx \pm 25\%$) and its acceptance (fig. 9) is approximately one (two) order(s) of magnitude larger than that of the 8 GeV/c (20 GeV/c) spectrometer. The momentum resolution $\Delta p/p$ of $\pm 1\%$ is actually better than we need in the deep inelastic region.

Electron identification is accomplished with a segmented total absorption lead glass shower counter and a 4 m long nitrogen gas Cerenkov counter which may be operated at subatmospheric pressure. In addition to the PWC system (≈4000 wires) there is a scintillator hodoscope with 12 x 16 segments and scintillator trigger counters. The useful detector area is 32 cm x 90 cm.

The detectors have been tested extensively under test beam conditions and performed quite well in the E-130 experiment at the spectrometer setting of 10°. Under these conditions we had very clean PWC tracks (1.01 track/trigger). Only the redundant, aperture defining scintillation counters proved rather useless due to sensitivity to soft background. The combined pion rejection capability of the lead glass and gas Cerenkov counters will also be sufficient at the 7° setting where the π/e ratio is expected to <14.

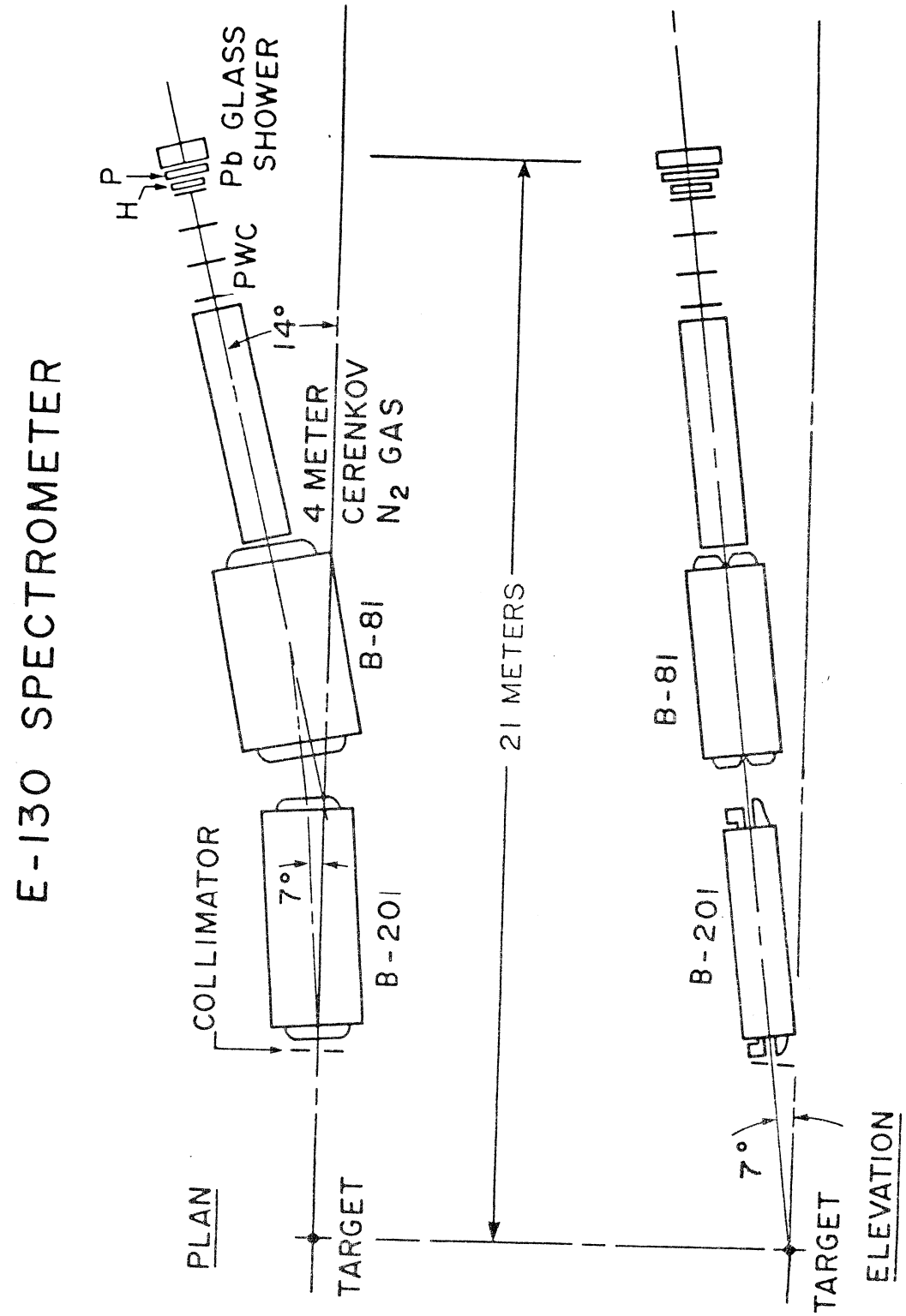
E-130 SPECTROMETER
P
H
Pb GLASS SHOWER
PWC
14°
4 METER CERENKOV N_2 GAS
B-81
21 METERS
COLLIMATOR
7°
B-201
PLAN
TARGET
B-81
B-201
7°
TARGET
ELEVATION

Figure 8

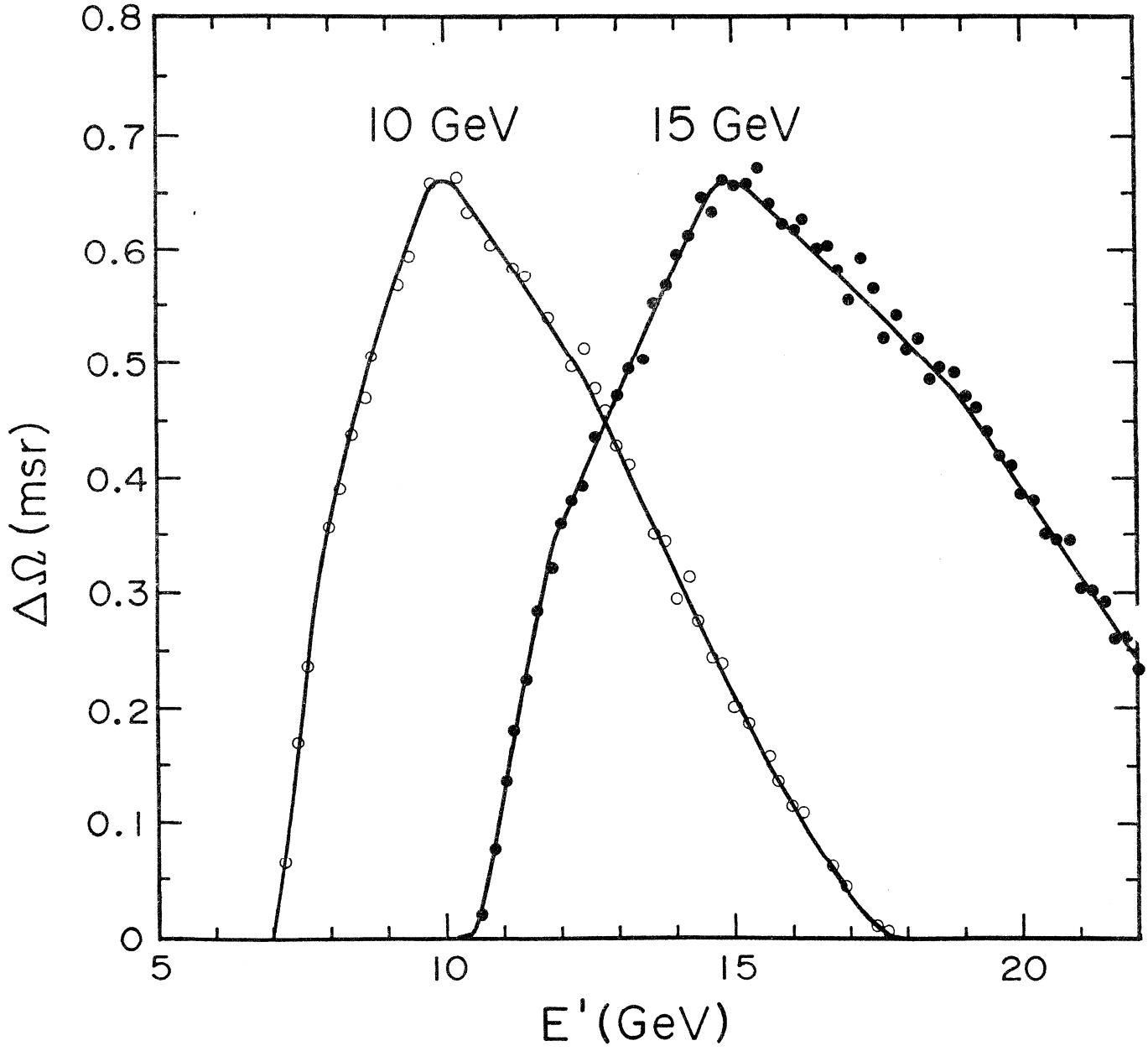

Acceptance of E-130 Spectrometer for Central Momentum Settings of 10 and 15 GeV/c.

Figure 9

II.5 Data Table, Statistical and Systematic Errors

Table 3 gives kinematic information and cross sections for a beam energy of E = 22.66 GeV and a scattering angle $\theta = 7^{o}$. Most of the variables used are defined in SLAC-PUB-2674 (See appendix I). There are also some new kinematic quantities relating to the transverse electron-nucleon asymmetry $A_T = d(\zeta A_1 - A_2)$. The factor d may be interpreted as a depolarization factor which degrades the electron polarization to a smaller virtual photon polarization and it is analogous to the factor D in the usual formula for the longitudinal asymmetry. A similar correspondence exists between the factors ζ and η.

From the measured longitudinal and transverse asymmetries A and A_T one obtains the spin structure functions

$$A_1 = \frac{A/D+\eta A_T/d}{1+\zeta\eta} \quad \text{and} \quad A_2 = \frac{\zeta A/D-A_T/d}{1+\zeta\eta}$$

In our earlier measurements of the longitudinal asymmetry A of the proton the kinematic conditions were usually such that the kinematic factor η was small and therefore $A_1 \simeq A/D$. At large values of the scaling variable x, however, the longitudinal and transverse terms compete and must both be measured in order to separate A_1 and A_2.

Part I (longitudinal target polarization). The counting rates for NH_3 and ND_3 targets (Tables 4,5) are based on the nucleon cross sections listed in Table 3. No radiative corrections have been made to the cross sections and counting rates. The solid angle $\Delta\Omega$ of the spectrometer varies with E' and is largest near the central momentum. In order to cover a broad range of x-values we plan to operate the spectrometer at central momentum settings of 10 GeV/c and 15 GeV/c. The individual columns of the tables are further explained in the footnotes. The polarizable nucleon fraction of

the target material (weighted by cross section) is plotted in Fig. 10.

In 300 factored hours (NH_3 + ND_3) we will obtain a statistical accuracy comparable to systematic errors. We have assumed overall systematic errors of 5% (relative) for the proton and 7% for the deuteron measurements. In Fig. 11 and 12 we have plotted the projected data points with respect to predictions of the unsymmetrical model of Carlitz and Kaur. The inner error bars indicate statistical errors, the outer error bars include systematic errors added in quadrature. Table 6 gives the resulting errors for the asymmetry of the neutron.* The projected neutron data has also been plotted in Fig. 13. The curve is again the prediction of the unsymmetrical model.

Part II (transverse target polarization). This type of measurement requires the replacement of the existing target magnet with a transverse field magnet. We plan to do such a measurement under otherwise identical conditions to Part I. i.e. the kinematic conditions will be the same. In 300 factored hours for Part II (NH_3 + ND_3) we obtain the same statistical precision for transverse asymmetries as for the longitudinal asymmetries listed in the Tables 4-6. The same holds for the two spin structure functions A_1 and A_2 because $d \simeq D$ and $\zeta \simeq \eta$ (Table 3). We have plotted the projected data of A_2^P for the proton in Fig. 3 on page 11.

---

*We have made the simplifying assumption that the polarization of the neutron is identical to that of the deuteron. Due to a small D-state admixture (6%) the neutron polarization will be slightly reduced to $P_n = 0.91\ P_d$. Also smearing effects have been neglected.

Table 3: Kinematics and Cross Sections (E = 22.66 GeV, θ = 7°)

E' (GeV)	ν (GeV)	Q^2 $(Gev)^2$	W (GeV)	ω	x	ε	$D^{(a)}$	η	$d^{(a)}$	ζ	F_2^P	$d^2\sigma/(d\Omega dE'/E')$ P $\frac{1}{2}$ (P+N) $(x10^{-30}cm^2/sr)$	
18.0	4.66	6.08	1.88	1.44	.695	.967	.187	.454	.185	.462	.050	.143	.098
17.5	5.16	5.91	2.16	1.64	.611	.960	.208	.399	.206	.407	.087	.220	.158
17.0	5.66	5.74	2.40	1.85	.541	.953	.230	.354	.227	.362	.127	.288	.216
16.5	6.16	5.57	2.62	2.07	.482	.945	.252	.316	.249	.325	.167	.340	.264
16.0	6.66	5.40	2.82	2.31	.432	.936	.275	.283	.270	.293	.205	.375	.299
15.5	7.16	5.24	3.01	2.57	.390	.925	.298	.255	.292	.265	.237	.396	.324
15.0	7.66	5.07	3.19	2.84	.352	.914	.321	.230	.314	.241	.265	.405	.337
14.5	8.16	4.90	3.36	3.13	.320	.902	.345	.208	.336	.220	.289	.404	.343
14.0	8.66	4.73	3.52	3.44	.291	.888	.369	.189	.358	.201	.308	.396	.342
13.5	9.16	4.56	3.68	3.77	.265	.873	.394	.172	.380	.184	.323	.384	.336
13.0	9.66	4.39	3.82	4.13	.242	.857	.418	.156	.402	.169	.334	.369	.327
12.5	10.16	4.22	3.97	4.52	.221	.840	.443	.142	.424	.155	.343	.352	.315
12.0	10.66	4.05	4.10	4.94	.203	.822	.469	.129	.445	.143	.350	.334	.302
11.5	11.16	3.88	4.24	5.39	.185	.802	.494	.118	.466	.132	.354	.316	.288
11.0	11.66	3.72	4.36	5.89	.170	.781	.520	.107	.487	.122	.356	.298	.274
10.5	12.16	3.55	4.49	6.43	.155	.758	.545	.097	.506	.113	.358	.281	.260
10.0	12.66	3.38	4.61	7.03	.142	.734	.571	.088	.526	.104	.358	.264	.246
9.5	13.16	3.21	4.73	7.70	.130	.709	.597	.080	.544	.096	.357	.248	.233
9.0	13.66	3.04	4.85	8.43	.119	.682	.623	.072	.561	.089	.356	.233	.220
8.5	14.16	2.87	4.96	9.26	.108	.654	.649	.065	.577	.082	.354	.219	.208
8.0	14.66	2.70	5.07	10.18	.098	.624	.674	.058	.591	.076	.352	.206	.196
7.5	15.16	2.53	5.18	11.23	.089	.593	.700	.052	.604	.070	.350	.194	.186
7.0	15.66	2.36	5.28	12.43	.080	.561	.725	.046	.615	.064	.347	.183	.175
6.5	16.16	2.20	5.39	13.81	.072	.527	.750	.041	.623	.059	.344	.172	.166
6.0	16.66	2.03	5.49	15.43	.065	.492	.774	.036	.629	.054	.341	.162	.157

$$A = D(A_1 + \eta A_2), \qquad D = \frac{E - E'\varepsilon}{E(1+\varepsilon R)}, \qquad \eta = \frac{\varepsilon(Q^2)^{1/2}}{E - E'\varepsilon}$$

$$\varepsilon = \frac{1}{1+2(1+\nu^2/Q^2)\tan^2 1/2\theta}$$

$$A_T = d(\zeta A_1 - A_2), \qquad d = \left(\frac{2\varepsilon}{1+\varepsilon}\right)^{1/2} D, \qquad \zeta = \frac{1+\varepsilon}{2\varepsilon}\,\eta$$

(a) We assume $R = \sigma_L/\sigma_T = 0.25$

Table 4: Kinematics and Counting Rates for Proton A_1 - Data

$E = 22.66$ GeV, $\theta = 7°$

E' (GeV)	ν (GeV)	Q^2 $(GeV)^2$	W (GeV)	x		$\Delta\Omega$[a] (msr) 15 GeV / 10 GeV	events[b] per pulse 15 GeV / 10 GeV	events[c] ($\times 10^6$) 15 GeV / 10 GeV	total	stat. error Δ (10^{-4}) (d)	f_p	stat. error A_p	D	error of $A_1^p + \eta A_2^p$ stat.	syst.	(e) total
18.0	4.66	6.08	1.88	.695	.611	.55 / .01	.040 / .001	1.72 / .02	1.74	7.6	.191	.0125	.208	.060	.039	.072
17.0	5.66	5.74	2.40	.541	.482	.60 / .07	.078 / .009	3.36 / .20	3.56	5.3	.182	.0091	.252	.036	.035	.050
16.0	6.66	5.40	2.82	.432	.390	.65 / .16	.108 / .027	4.66 / .58	5.24	4.4	.176	.0077	.298	.026	.031	.041
15.0	7.66	5.07	3.19	.352	.320	.65 / .26	.122 / .049	5.28 / 1.06	6.34	4.0	.172	.0072	.345	.021	.028	.035
14.0	8.66	4.73	3.52	.291	.265	.53 / .37	.104 / .073	4.50 / 1.58	6.08	4.0	.168	.0075	.394	.019	.026	.032
13.0	9.66	4.39	3.82	.242	.221	.41 / .47	.081 / .093	3.51 / 2.00	5.51	4.3	.166	.0080	.443	.018	.023	.029
12.0	10.66	4.05	4.10	.203	.185	.25 / .56	.049 / .110	2.12 / 2.38	4.50	4.7	.164	.0089	.494	.018	.021	.028
11.0	11.66	3.72	4.36	.170	.155	.03 / .63	.006 / .121	.27 / 2.62	2.89	5.9	.162	.0114	.545	.021	.020	.029
10.0	12.66	3.38	4.61	.142	.130	.61	.116	2.52	2.52	6.3	.161	.0122	.597	.020	.018	.027
9.0	13.66	3.04	4.85	.119	.108	.46	.087	2.06	2.06	7.0	.160	.0136	.649	.021	.016	.027
8.0	14.66	2.70	5.07	.098	.089	.18	.034	.74	.74	12.0	.159	.0231	.700	.033	.015	.036
7.0	15.66	2.36	5.28	.080		Total:	.59 / .72	25.4 / 15.8	41.2							

(a) Central momentum of Spectrometer set to 10 GeV and 15 GeV, respectively.

(b) Assumes 7×10^9 e^-/pulse, a 3.8 cm long NH_3 target of density 0.6 g/cm^3.

(c) Assumes 50 hours @ 120 pps (spectrometer set to 10 GeV),
100 hours @ 120 pps (spectrometer set to 15 GeV),
and a 20% loss due to beam rastering.

(d) $\Delta = P_e P_p f_p A_p$ is the raw counting asymmetry

(e) $A_1^p + \eta A_2^p = A_p/D = \Delta/(P_e P_p f_p D)$,

We assume $P_e = 0.40$, $\langle P_p \rangle = 0.80$, $f_p = 0.85\ f_2^p(NH_3)$,

We assume a systematic error of $\pm 0.05\ \sqrt{x}$ for $A_1^p + \eta A_2^p$.

Table 5: Kinematics and Counting Rates for Deuteron A_1 - Data

$E = 22.66$ GeV, $\theta = 7°$

E' (GeV)	ν (GeV)	Q^2 $(GeV)^2$	W (GeV)	x		ΔΩ (msr)	events[a] per pulse	events[b] ($\times 10^6$)		stat. error Δ (10^{-4})	stat. error A_d [c]	D	error of $A_1^d + \eta A_2^d$ [d]		
						15 GeV / 10 GeV	15 GeV / 10 GeV	15 GeV / 10 GeV	total				stat.	syst.	total
18.0	4.66	6.08	1.88	.695											
					.611	.55 / .01	.044 / .001	3.80 / .04	3.84	5.1	.0125	.208	.060	.038	.071
17.0	5.66	5.74	2.40	.541											
					.482	.60 / .07	.087 / .010	7.52 / .43	7.95	3.5	.0086	.252	.034	.032	.047
16.0	6.66	5.40	2.82	.432											
					.390	.65 / .16	.122 / .030	10.54 / 1.30	11.84	2.9	.0071	.298	.024	.024	.036
15.0	7.66	5.07	3.19	.352											
					.320	.65 / .26	.139 / .056	12.01 / 2.42	14.43	2.6	.0064	.345	.019	.023	.030
14.0	8.66	4.73	3.52	.291											
					.265	.53 / .37	.120 / .084	10.37 / 3.63	14.00	2.7	.0066	.394	.017	.020	.026
13.0	9.66	4.39	3.82	.242											
					.221	.41 / .47	.093 / .107	8.04 / 4.62	12.66	2.8	.0067	.443	.015	.018	.023
12.0	10.66	4.05	4.10	.203											
					.185	.25 / .56	.057 / .128	4.92 / 5.53	10.45	3.1	.0076	.494	.015	.016	.022
11.0	11.66	3.72	4.36	.170											
					.155	.03 / .63	.007 / .140	.60 / 6.05	6.65	3.9	.0096	.545	.018	.015	.023
10.0	12.66	3.38	4.61	.142											
					.130	.61	.135	5.83	5.83	4.1	.0100	.597	.017	.013	.021
9.0	13.66	3.04	4.85	.119											
					.108	.46	.101	4.36	4.36	4.8	.0118	.649	.018	.012	.022
8.0	14.66	2.70	5.07	.098											
					.089	.18	.040	1.73	1.73	7.6	.0186	.700	.027	.011	.029
7.0	15.66	2.36	5.28	.080											
						Total:	.67 / .83	57.8 / 35.9	93.7						

(a) Assumes an ND_3 target, all other conditions as for previous table.

(b) Assumes 100 hours @ 120 pps (spectrometer set to 10 GeV),
200 hours @ 120 pps (spectrometer set to 15 GeV).

(c) $A_d = \Delta/(P_e P_d f_d)$, we assume $P_e P_d f_d = 0.041$

($P_e = 0.40$; $\langle P_d \rangle = \langle P_p \rangle = \langle P_n \rangle = 0.40$; $f_d = 0.85\ f_2^d(ND_3) = 0.255$.

(d) $A_1^d + \eta A_2^d = A_d/D$

Table 6: Neutron A_1 - Data
E = 22.66 GeV, θ = 7°

E' (GeV)	ν (GeV)	Q^2 $(GeV)^2$	W (GeV)	x		stat. error A_d (a)	stat. error A_p (a)	σ_p/σ_n	stat. error A_n (b)	D	error of (c) $A_1^n + \eta A_2^n$ stat.	syst.	total
18.0	4.66	6.08	1.88	.695	.541	.0071	.0074	1.90	.0250	.230	.109	.082	.136
16.0	6.66	5.40	2.82	.432	.352	.0049	.0053	1.51	.0147	.321	.046	.053	.070
14.0	8.66	4.73	3.52	.291	.242	.0047	.0053	1.35	.0132	.418	.032	.039	.050
12.0	10.66	4.05	4.10	.203	.170	.0059	.0070	1.26	.0160	.520	.031	.030	.043
10.0	12.66	3.38	4.61	.142	.119	.0076	.0090	1.20	.0195	.623	.031	.024	.040
8.0	14.66	2.70	5.07	.098									

(a) See deuteron and proton data from previous tables

(b) $A_n \simeq (1 + \sigma_p/\sigma_n)A_d - (\sigma_p/\sigma_n)A_d$

(c) $A_1^n + \eta A_2^n = A_n/D$

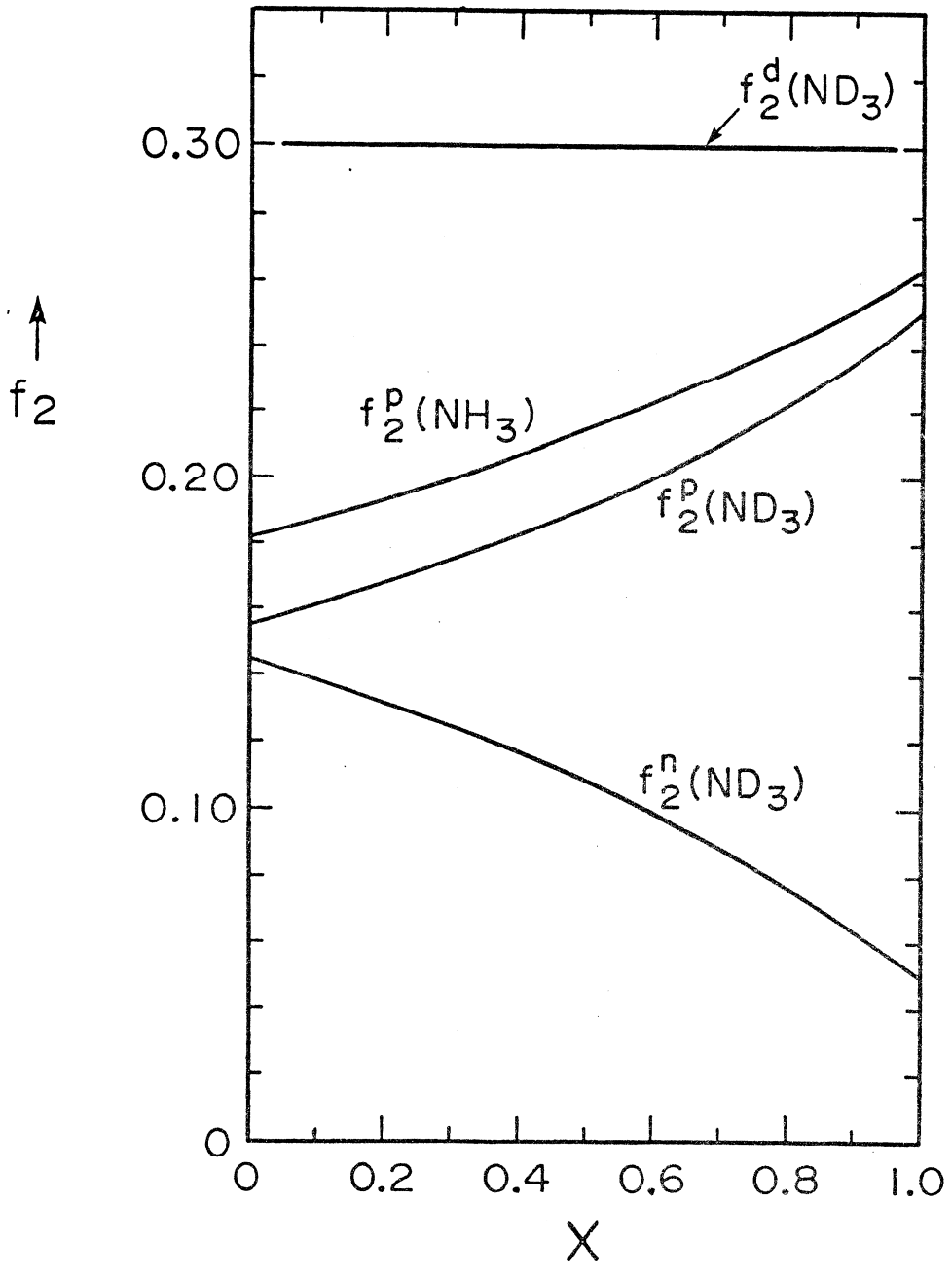

Fraction of polarizable protons and neutrons in NH_3 and ND_3 (weighted by cross section) vs. scaling variable x.

Using $\sigma_n/\sigma_p = 0.918 - 0.724\ x$ (A. Bodek et al. Phys. Rev. D20, 1471 (1979)) and neglecting polarizability of nitrogen and nuclear effects. Note that $f_2^d(ND_3) = f_2^p(ND_3) + f_2^n(ND_3)$.

Figure 10

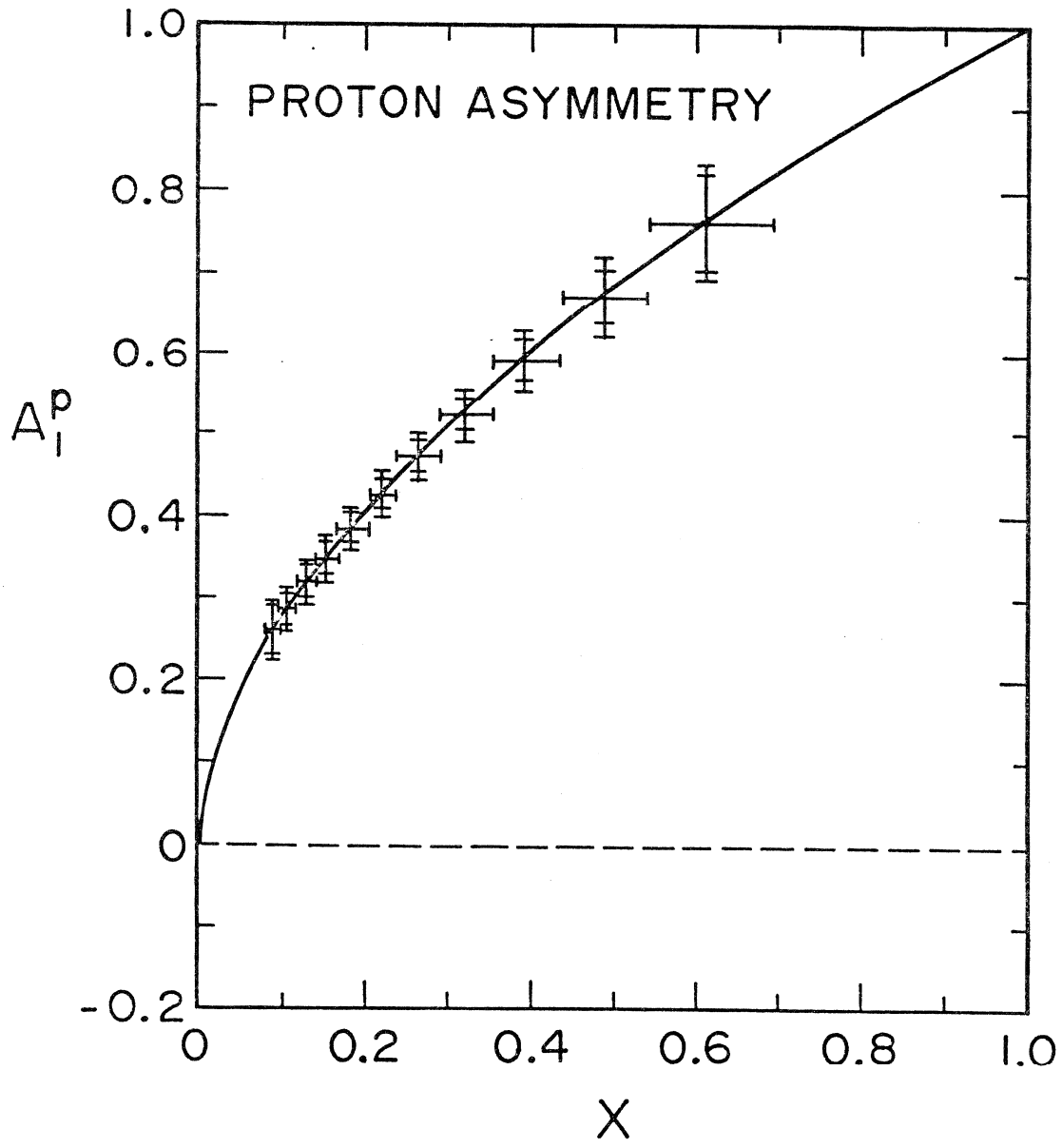

Figure 11

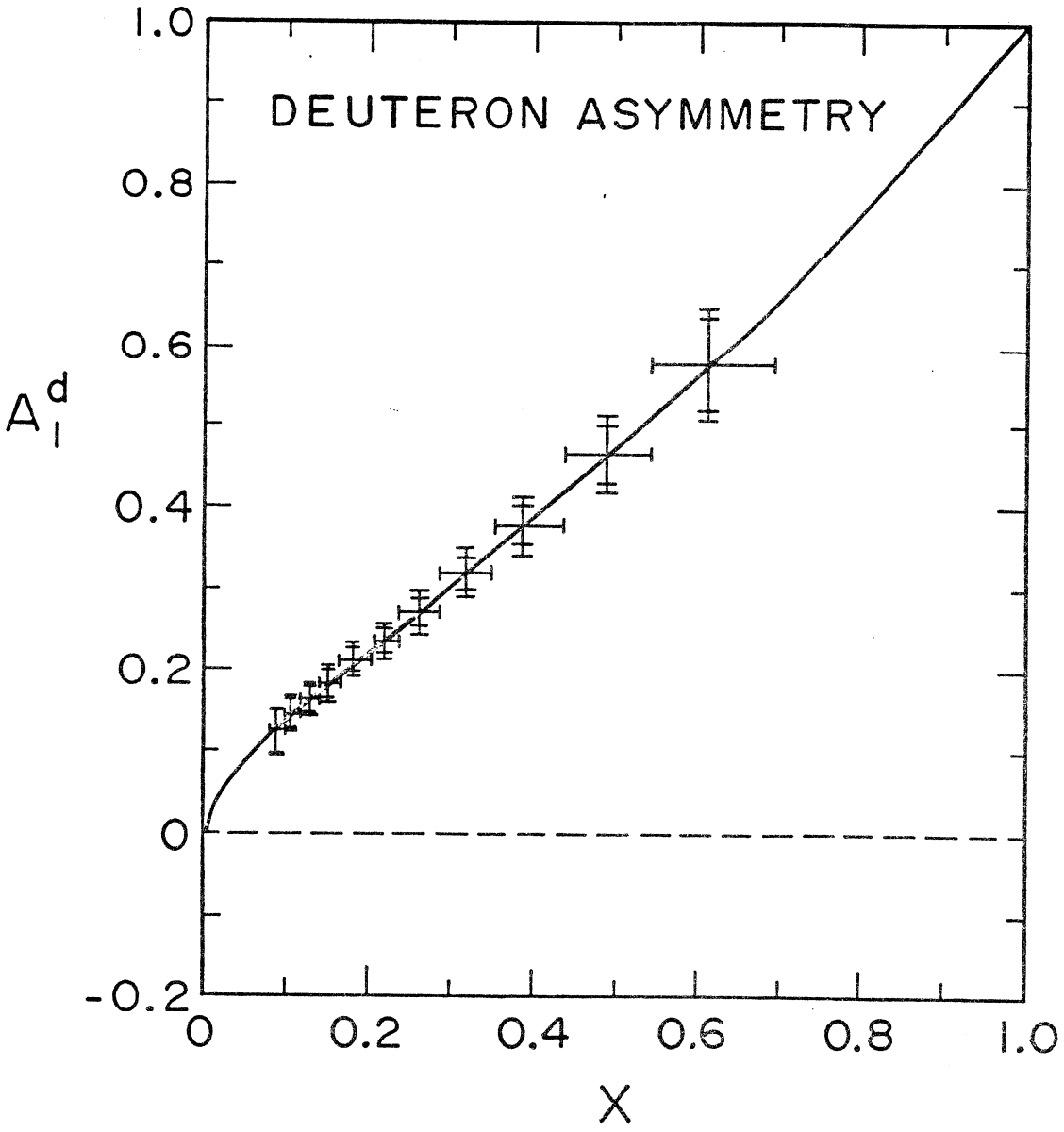

Figure 12

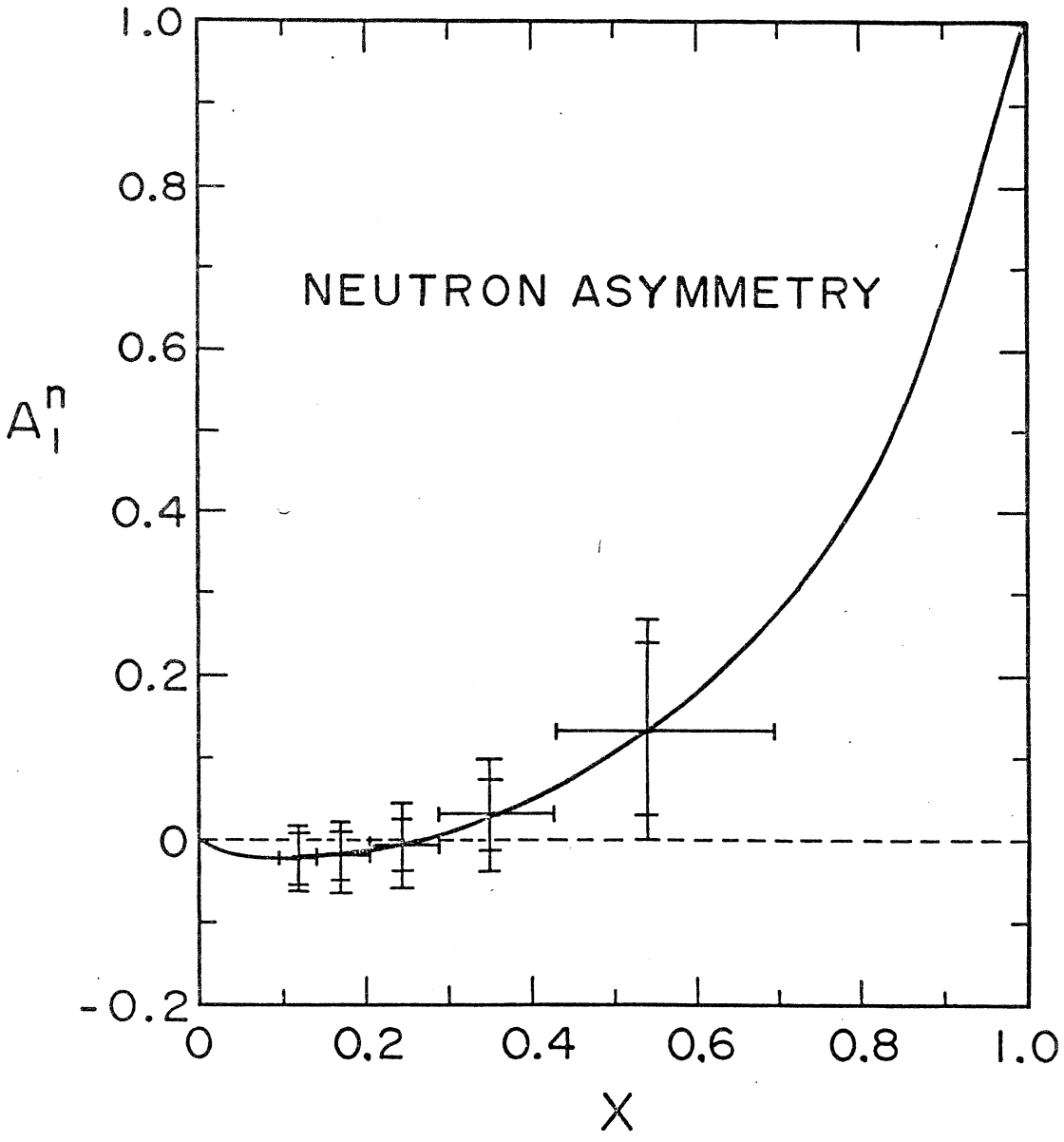

Solid curve Carlitz-Kaur prediction. Plotted points are projected experimental data.

Figure 13

II.6 Experimental Facilities and Personnel

The following tables are included in this subsection.

Table 7: Required Equipment and Facilities

Item (Status)	Responsibility
Polarized Electron Source (GaAs-type):	
Source (to be built, see following list)	Yale-Bielefeld
70 keV beam transport	SLAC
Camac link to Counting House (existing)	SLAC
Polarized Target	
New ^{3}He pumping system (on order)	Yale-Tsukuba
New ^{3}He/^{4}He cryostat (to be built)	Yale-SLAC-KEK-Tsukuba-Argonne
^{3}He recovery system	SLAC
Low energy linac (being set up)	SLAC
New microwave source (EIO) (have)	Yale
New NMR/DNMR (to be built)	Yale
Transverse field magnet & dewar (to be built)	KEK-Tsukuba
Operational costs: ^{3}He, ND_3	Yale
liquid ^{4}He (~800 l/day)	SLAC
LN_2 (~1000 l/week)	SLAC
Move target from cryo-building to ESA	SLAC-Yale
ESA and Countinghouse	
E-130 spectrometer (to be set up)	SLAC-Yale
Moller polarimeter (to be set up)	SLAC-Yale
Standard beam monitors, as in E-130	SLAC
VAX/780 computer	SLAC
Beam steering hardware incl. LSI-11 computer	SLAC
Electronics (HEEP and LEEP equipment as in E-130, see following list)	SLAC

Table 8: Manpower, Services, Equipment and Materials Requested from SLAC:

Polarized electron beam:

At injector: 70 keV beam transport and associated instrumentation (source itself will be built by the experimenters); 70 kV power supply (existing).

At high energy: standard beamline hardware used in E-130: computer controlled beam steering and energy adjustment using resonant and traveling wave type position monitors and vernier klystrons; setup of associated microwave electronics and small computer; Helmholtz steppers, toroids, roller screens, Faraday cup, Møller polarimeter, beam dump east.

Polarized target

40 MeV irradiation facility (in progress); manpower support requested for construction of new cryostat over a period of about 1 yr: 15 mm of of engineering, design, and drafting; 12 mm fabrication (additional 12 mm of fabrication at Yale), helium liquefaction (^{4}He) ~ 800 ll/day (maximum heat load condition during data-taking; this is 3 x the existing liquefaction capacity at the cryogenics building, for testing of the target the existing capacity will suffice); ~ 1000 ll/week of LN_2; ^{3}He recovery system; moving target from cryogenics building to end station A (riggers, plumbers, electricians).

Detector

The E-130 spectrometer needs to be set up again in end station A, at a scattering angle of 7^o. Cable requirements identical to experiment E-130.

Computers

Requirements identical to E-130: VAX/780 (with LSI-11 intake data buffer) in ESA counting house for online data-taking; LSI-11 for beam steering (linked to VAX via CAMAC), CAMAC links to injector and Yale-owned PDP-11 (target computer); ~250 computer tapes (6250 BPI); 6-12 months access to VAX for offline analysis.

Electronic equipment

Requirments idential to E-130: see HEEP and LEEP equipment list.

Table 9: SLAC Electronic Equipment used in E130 and needed for Son of E130

HEEP EQUIPMENT

Item	Model No.	Quanity
ADC, 12 channel	LRS 2249A	3
Analog MPX	LRS 2232A	3
Bipolar fan in	127B	1
Bipolar fan in	LRS 127D	3
CAMAC crate		8
Coinc.	EGG C 144/N	2
Coinc.	J 103	11
Coinc. latch	C 124	5
Crate controller	CCA-2	5
Dataway display	Joerger DD	2
Droege boxes	VK 5900	6
Dual amp (adjustable gain)	LRS 333	1
Dual disc.	161	1
Dual scalers	Jorway 80	26
Fan in/out	J 102	11
Gate & delay gen.	Ortec	2
Gate generator	GG 200/N	3
Gate generator	Joerger GG	4
Gate generator	108-177-29-RO	1
Level Translator	RS 688 AL	1
Linear fan in/out	428	1
Linear fan out	128	1
Logic	LRS 364A	1
Multilevel output	446-601	1
Nim bins with 6v		5
Nim bins w/o 6v		13
Octal disc.	LRS 620	1
Octal disc.	620 AL	1
Octal disc.	LRS 623	7
Quad coinc.	622	3
Quad disc.	321 B	1
Quad scalers	Joerger S1	13
QVT-old model modified	QVT	2
QVT	30001/3157/DPPQ7	1
16 channel DCR	LRS 2340B	4
Strobed coinc.	C 126/N	5
Switch input register	BiRa 2501	2
TSI-dual scalers		6
12 channel ADC	2249A	1
12 channel Amplifier	612	3
12 channel scaler	LRS 2551	1
Updating disc.	TR204AN	13
Verification Module	135-102	2
Bipolar fan in	128	1

LEEP EQUIPMENT

Data Pulsers	2
485 scopes	2
475 scopes	1
H.P. scope	1
Ligna Sweep	1
Misc. D.C. Power Supplies	4

Table 10: Polarized Electron Source: Cost Estimate

Vacuum (chamber, pumps, insulator, valves, etc.)	$ 50,000
Optics (laser, Pockel-cells, etc.)	70,000
Instrumentation	25,000
Machine shop	40,000
Salaries & Wages (design, drafting)	20,000
Travel	15,000
Shipping	10,000
Total Cost	$230,000

Table 11: Group Proposing Experiment

Yale

I. Beltrami
S. Dhawan
V. Hughes
D. Lu
R. Oppenheim
P. Schüler
M. Seely
P. Souder
Students

Bielefeld

G. Baum
W. Raith

KEK-Tsukuba

S. Hiramatsu
K. Kondo
Y. Mori
K. Morimoto
I. Nakano
Students

SLAC

R. Miller
S. St. Lorant

ANL

D. Hill
H. Spinka
A. Yokosawa
Postdoc

CCNY

M. Lubell
Student

Berne

U. Moser

Saclay

N. de Botton

Appendix I: High-Energy Physics with Polarized Beams and and Polarized Targets, ed. C. Joseph and J. Soffer (Birkhauser Verlag, 1981) p. 331-343.

SLAC-PUB-2674
February 1981
(T/E)

INTERNAL SPIN STRUCTURE OF THE PROTON FROM HIGH ENERGY POLARIZED e-p SCATTERING*

Vernon W. Hughes
Gibbs Laboratory, Physics Department
Yale University, New Haven, Connecticut 06520

G. Baum, M.R. Bergström, P.R. Bolton, J.E. Clendenin, N.R. DeBotton, S.K. Dhawan, R.A. Fong-Tom, Y.-N. Guo, V.-R. Harsh, K. Kondo, M.S. Lubell, C.-L. Mao, R.H. Miller, S. Miyashita, K. Morimoto, U.F. Moser, I. Nakano, R.F. Oppenheim, D.A. Palmer, L. Panda†, W. Raith, N.Sasao, K.P. Schüler, M.L. Seely, J. Sodja, P.A. Souder, S.J. St. Lorant, K. Takikawa, M. Werlen

University of Bern, Switzerland; University of Bielefeld, Germany; Institute of High Energy Physics, Beijing, China; National Laboratory for High Energy Physics, KEK, Tsukuba, Japan; Kyoto University, Japan; SACLAY, Saclay, France; Stanford Linear Accelerator Center, Stanford, California; University of Tsukuba, Ibaraki, Japan; and Yale University, New Haven, Connecticut.

ABSTRACT

A review is given of our experimental knowledge of the spin dependent structure functions of the proton, which is based on inclusive high energy scattering of longitudinally polarized electrons by longitudinally polarized protons in both the deep inelastic and resonance regions, and includes preliminary results from our most recent SLAC experiment. Implications for scaling, sum rules, models of proton structure, and the hyperfine structure interval in hydrogen are given. Possible future directions of research are indicated.

INTRODUCTION

The internal spin structure of the proton (and neutron), or the spin dependent structure functions, is a central aspect of nucleon structure. Knowledge of this spin structure is important to the development and testing of theories and models of nucleon structure, as well as to the understanding of spin dependent phenomena involving hadrons, such as polarized hadron-hadron scattering at high energies.

Spin dependent structure functions of the proton can be studied by high energy e-p scattering of polarized electrons by polarized protons,[1] which is especially interesting in the deep inelastic regime where the impulse approximation of e^- scattering from the constituent partons or quarks is valid. However, resonance region scattering at lower energy and momentum transfer is also informative about proton spin structure. Figure 1 indicates the kinematics of polarized e-p inclusive scattering in which the momentum and scattering angle of the scattered electron are measured. The e-p asymmetry, A, which is the normalized difference between the differential scattering cross sections with electron and proton spins anti-parallel and parallel, is the quantity measured. Tables 1 and 2 give definitions and relations for the quantities relevant to asymmetry. Thus far only inclusive scattering with longitudinal electron and proton spins has been measured.

* Work supported in part by the Department of Energy under contracts DE-AC03-76SF00515 and DE-AC02-76ER03075, and by John Simon Guggenheim Memorial Foundation Fellowship, 1978-1979, to VWH.

† Deceased.

(Invited paper presented at the 1980 International Symposium on High Energy Physics with Polarized Beams and Polarized Targets, Lausanne, Switzerland, September 25 - October 1, 1980.)

$q = (p - p')$

$Q^2 = -q^2 = 4EE' \sin^2 \frac{\theta}{2}$

$\tau = Q^2/4M^2$

$\nu = E - E'$

$\omega = 2M\nu/Q^2$

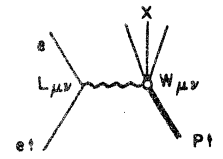

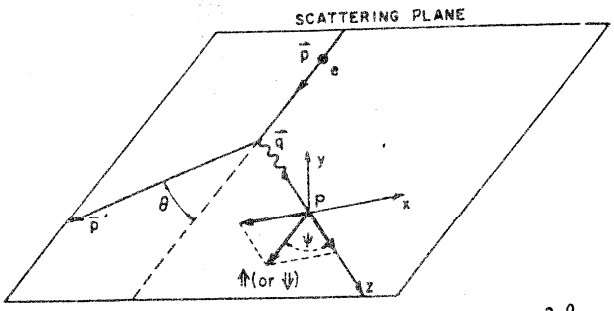

Fig. 1. Kinematics for the scattering of longitudinally polarized electrons by longitudinally polarized protons.

$$\frac{d^2\sigma}{d\Omega dE'} = \left(\frac{d\sigma}{d\Omega}\right)_{MOTT} L_{\mu\nu} W_{\mu\nu} \qquad \left(\frac{d\sigma}{d\Omega}\right)_{MOTT} = \frac{\alpha^2}{4E^2} \frac{\cos^2 \frac{\theta}{2}}{\sin^4 \frac{\theta}{2}}$$

$$A \equiv \frac{\frac{d^2\sigma}{d\Omega dE'}(\uparrow\downarrow) - \frac{d^2\sigma}{d\Omega dE'}(\uparrow\uparrow)}{\frac{d^2\sigma}{d\Omega dE'}(\uparrow\downarrow) + \frac{d^2\sigma}{d\Omega dE'}(\uparrow\uparrow)}$$

2 – 81
4028A1

CROSS SECTION AND ASYMMETRY

$$\frac{d^2\sigma}{d\Omega dE'} = \left(\frac{\alpha^2 \cos^2 \frac{\theta}{2}}{4E^2 \sin^4 \frac{\theta}{2}}\right) \left[W_2 + 2\tan^2 \frac{\theta}{2} W_1 \pm 2\tan^2 \frac{\theta}{2} (E + E' \cos\theta) M G_1 \pm 8 EE' \tan^2 \frac{\theta}{2} \sin^2 \frac{\theta}{2} G_2\right]$$

$$\begin{matrix} +(A) \\ -(P) \end{matrix}$$

$$\frac{d^2\sigma}{d\Omega dE'} = \left(\frac{d\sigma}{d\Omega}\right)_M \left(\frac{1}{\varepsilon(1+\nu^2/Q^2)}\right) W_1 \left|1 + \varepsilon R \pm (1-\varepsilon^2)^{1/2} \cos\psi A_1 \pm \left[2\varepsilon(1-\varepsilon)\right]^{1/2} \sin\psi A_2\right|$$

$$\varepsilon = \left[1 + 2(1+\nu^2/Q^2) \tan^2 \frac{\theta}{2}\right]^{-1}$$

$$R = \sigma_L/\sigma_T; \; \sigma_T = (\sigma_{1/2} + \sigma_{3/2})/2$$

$$A = \frac{d\sigma(+\,+) - d\sigma(+\,+)}{d\sigma(+\,+) + d\sigma(+\,+)}$$

$$A = D(A_1 + \eta A_2)$$

$$D = \frac{E - E'\varepsilon}{E(1+\varepsilon R)} = \frac{(1-\varepsilon^2)^{1/2} \cos\psi}{(1+\varepsilon R)}$$

$$\eta = \frac{\varepsilon (Q^2)^{1/2}}{E - E'\varepsilon} = \left(\frac{2\varepsilon}{1+\varepsilon}\right)^{1/2} \tan\psi \simeq \tan\psi$$

$$A_1 = \frac{\sigma_{1/2} - \sigma_{3/2}}{\sigma_{1/2} + \sigma_{3/2}}$$

$$A_2 = \frac{2\sigma_{TL}}{\sigma_{1/2} + \sigma_{3/2}}$$

$|A_1| \leq 1; \; |A_2| \leq \sqrt{R}$ (POSITIVITY LIMITS)

2 – 81
4028A16

Table 1. Cross section and asymmetry for scattering of longitudinally polarized electrons by longitudinally polarized protons.

$$W^{\mu\nu}_{[A]} = M\epsilon^{\mu\nu\rho\sigma} q_\rho s_\sigma G_1 + \frac{1}{M}\epsilon^{\mu\nu\rho\sigma} q_\rho \left[(p\cdot q)s_\sigma - (s\cdot q)p_\sigma\right] G_2$$

$$\sigma_{1/2} = \frac{4\pi^2\alpha}{K}(W_1 + M\nu G_1 - Q^2 G_2) \qquad \sigma_L = \frac{4\pi^2\alpha}{K}\left[W_2\left(1+\frac{\nu^2}{Q^2}\right) - W_1\right]$$

$$\sigma_{3/2} = \frac{4\pi^2\alpha}{K}(W_1 - M\nu G_1 + Q^2 G_2) \qquad \sigma_{TL} = \frac{4\pi^2\alpha}{K}\sqrt{Q^2}\,(MG_1 + \nu G_2)$$

$$\sigma_T = (\sigma_{1/2} + \sigma_{3/2})/2 = \frac{4\pi^2\alpha}{K} W_1 \qquad K = \nu - \frac{Q^2}{2M}$$

IN THE SCALING LIMIT $[\nu, Q^2 \to \infty;\ x \text{ FIXED}]$

$$MW_1(\nu, Q^2) \to F_1(x); \quad \nu W_2(\nu, Q^2) \to F_2(x)$$

$$M^2 \nu G_1(\nu, Q^2) \to g_1(x); \quad M\nu^2 G_2(\nu, Q^2) \to g_2(x)$$

$$A_1 = \frac{\sigma_{1/2} - \sigma_{3/2}}{\sigma_{1/2} + \sigma_{3/2}} \simeq \frac{2x}{F_2}\left(g_1 - \frac{2Mx}{\nu} g_2\right)(1+R) \to \frac{2x}{F_2} g_1$$

$$A_2 = \frac{\sigma_{TL}}{\sigma_T} \simeq \frac{\sqrt{Q^2}}{\nu} \frac{2x}{F_2}(g_1 + g_2)(1+R) \to 0$$

$$A_2' = \frac{\nu}{\sqrt{Q^2}} A_2 \simeq \frac{2x}{F_2}(g_1 + g_2)(1+R) \to \frac{2x}{F_2}(g_1 + g_2)$$

FOR THE $\simeq$ EXPRESSIONS FOR A_1, A_2 AND A_2' ALL QUANTITIES EXCEPT R ARE TAKEN IN THE SCALING LIMIT. $(\nu/2Mx \gg 1)$.

2-81
4028A17

Table 2. Some definitions and relations of structure functions and asymmetries.

YALE-SLAC EXPERIMENT

The Yale-SLAC experiments to measure A were initiated in 1971 with the approval of the SLAC E80 experiment. All the results from this experiment have been published.[2-5] Data-taking for a second experiment SLAC E130 was completed in April, 1980, and preliminary results have been reported.[6]

The experimental technique for SLAC E80 has been described in our above publications. The polarized electron source[7] is based on photoionization of spin polarized Li atoms, and the polarized proton target[8] is based on dynamic nuclear polarization using the hydrocarbon butanol. The SLAC 8 GeV/c spectrometer was used as the detector in SLAC E80. The principal new feature of SLAC E130 was the use of a new large acceptance spectrometer. The experimental set-up for SLAC E130 is shown in Fig. 2. The new spectrometer is shown in Fig. 3. It utilizes two large dipole magnets (B201 and B81) and a detector system which consists of a 1 m diameter × 4 m long N_2 gas Cerenkov counter, a 4000 wire PWC system, a

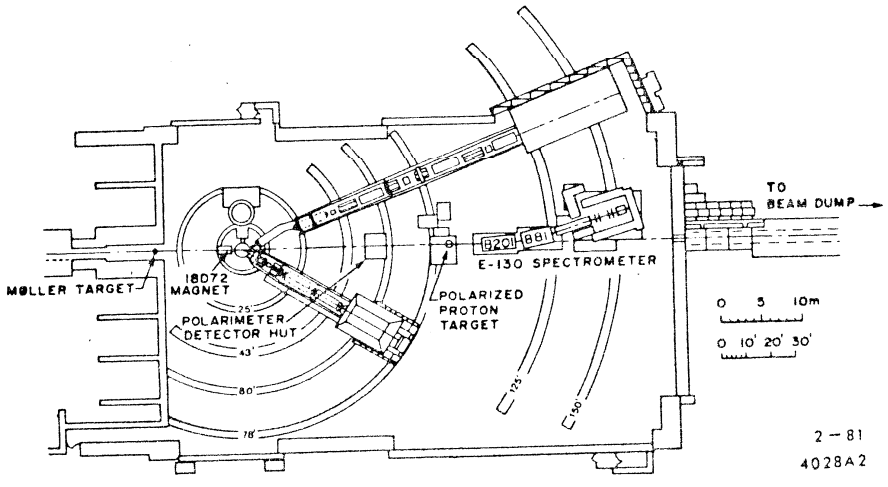

Fig. 2. SLAC E130 experimental set-up in end station A.

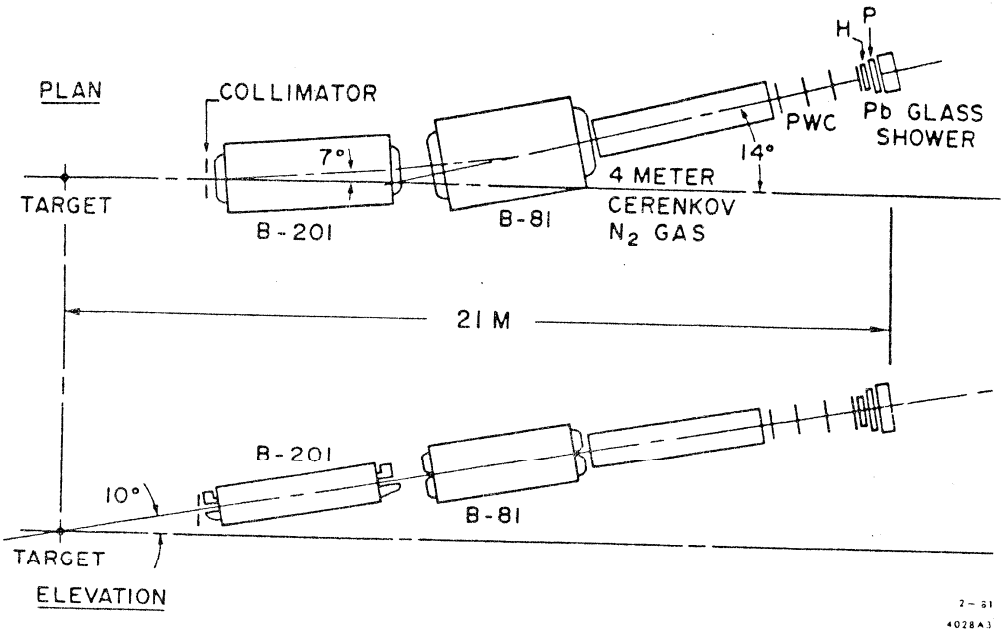

Fig. 3. SLAC E130 spectrometer.

hodoscope, and a segmented lead glass shower counter. The spectrometer may cover momenta up to 18 GeV/c, and its acceptance $\int d\Omega\, dp/p$ is 0.3 msr with the total momentum acceptance $\Delta p/p$ being about 50%. The momentum resolution of the spectrometer $\delta p/p$ is better than ±1%. For the measurement of the electron polarization P_e by Møller scattering,[9] a new feature was the detection of the two scattered electrons in coincidence. Counting rates and various sources of systematic errors in SLAC E130 are indicated in Table 3.

The kinematic points for which data have been obtained in SLAC E80 and in SLAC E130 are shown in Fig. 4, where proposed data points for a new experiment are also indicated.

$$\Delta = \frac{N(\uparrow\downarrow)-N(\uparrow\uparrow)}{N(\uparrow\downarrow)+N(\uparrow\uparrow)}, \quad \text{RAW ASYMMETRY}$$

$$\Delta = P_e P_p F A$$

$$A = \frac{d\sigma(\uparrow\downarrow)-d\sigma(\uparrow\uparrow)}{d\sigma(\uparrow\downarrow)+d\sigma(\uparrow\uparrow)}, \quad \text{INTRINSIC e-p ASYMMETRY}$$

$$P_e \simeq 0.8,\ P_p \simeq 0.6,\ F \simeq 0.1$$

$$\Delta \simeq 0.05\, A$$

COUNTING RATE VARIES FROM 0.01 TO 1/PULSE OR 1 TO 100/s.

SOURCE OF ERROR	COMMENT
COUNTING STATISTICS (Δ)	DOMINANT ERROR 1×10^{-3} TO 3×10^{-3} IN Δ 10% TO 30% OF Δ
P_e	$\delta P_e/P_e \sim 5\%$; MÖLLER SCATTERING
P_p	$\delta P_p/P_p \sim 5\%$; NMR
F	$\delta F/F \sim 5\%$; C, CH_2 CROSS SECTIONS
RADIATIVE CORRECTIONS	WHEN COMBINED WITH COUNTING ERROR, OVERALL ERROR IS 1.1 TO 1.5 TIMES COUNTING ERROR
BACKGROUND ASYMMETRY	≲ 1% OF Δ MISIDENTIFIED PIONS FROM PHOTOPION PRODUCTION OFF POLARIZED PROTONS
PEGGY BEAM ASYMMETRIES	
ENERGY	$\lesssim 10^{-4}$ IN Δ
ANGLE	$< 10^{-4}$ IN Δ
POSITION	$< 10^{-4}$ IN Δ

2-81
4028A18

Table 3. Counting rates and sources of error.

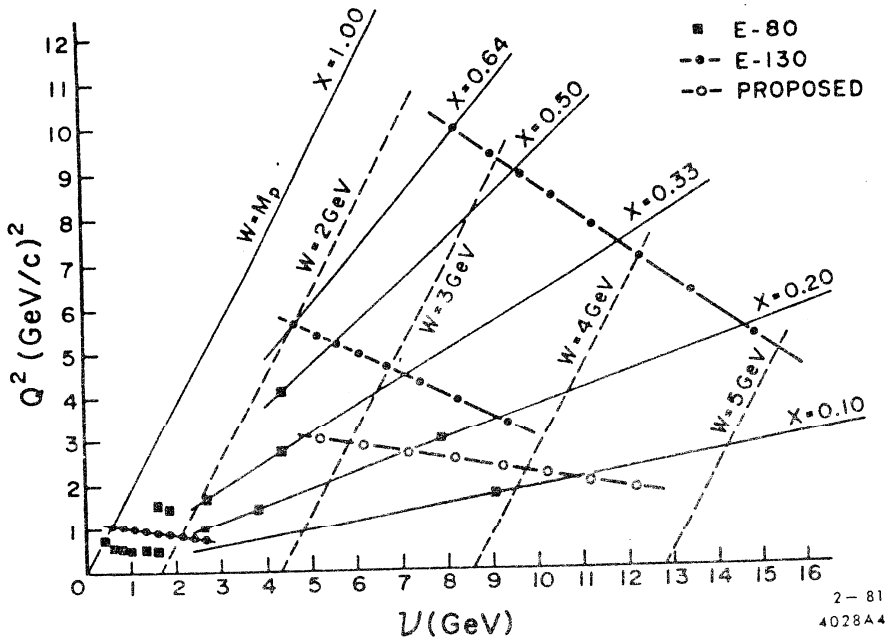

Fig. 4. Kinematic points where data have been taken.

DEEP INELASTIC DATA AND THEIR IMPLICATIONS

All the available deep inelastic asymmetry data are shown in Fig. 5, where the open diamonds are the published SLAC E80 results and the closed squares are the preliminary results for SLAC E130. The E130 results are "on-line" results, which must be checked and refined by off-line analysis. Furthermore radiative corrections are not yet included. All errors are one standard deviation total errors, which include the statistical counting error and systematic errors associated with P_e, P_p and F, added in quadrature. The new E130 data extend considerably our knowledge of the virtual photon-proton asymmetry A/D to higher Q^2 and higher x. A significant verification of the predicted scaling behavior[10] of A_1

$$A_1(\nu,Q^2) \to A_1(x) \text{ as } \nu,Q^2 \to \infty \text{ ; } \quad (1)$$
$$x \text{ fixed}$$

at about the 10% level over the Q^2 range from 1 to 10 $(GeV/c)^2$ is apparent from Fig. 5, where the dashed horizontal lines correspond to the average A_1 values for the three plots.

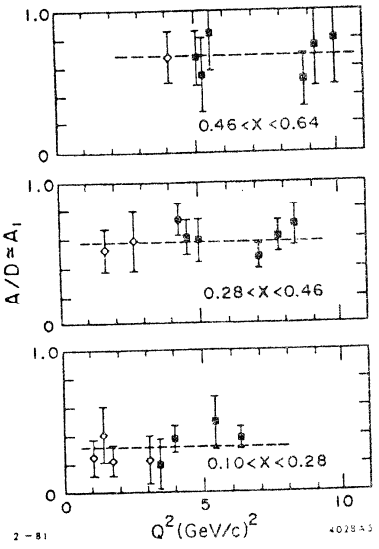

Fig. 5. Measured values of the asymmetry A/D in SLAC E80 (open diamonds) and SLAC E130 (closed squares).

For Fig. 6 for a given x value data for different Q^2 have been combined assuming that the A/D values are independent of Q^2. These data are fit by the curve $A_1(x) = (0.90 \pm 0.05)x^{\frac{1}{2}}$.

The Bjorken sum rule is given in Eq. (2)

$$\int_0^1 \left[A_1^p F_2^p/(1+R^p) - A_1^n F_2^n/(1+R^n)\right]\frac{dx}{x} = \frac{1}{3}\left|\frac{g_A}{g_V}\right| = (0.417 \pm 0.003) \quad (2)$$

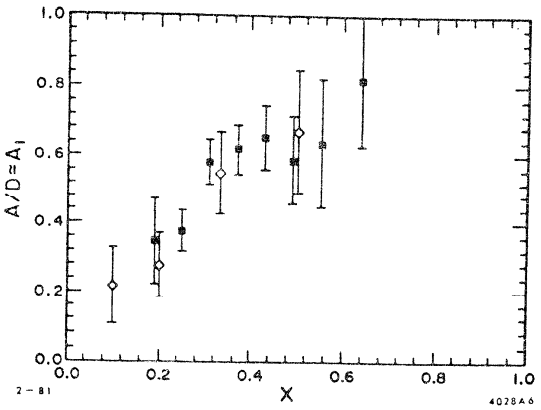

Fig. 6. Measured values of A/D vs x. Points were obtained from Fig. 5 data assuming A/D values are independent of Q^2.

in which quantities are defined in Fig. 1 and Tables 1 and 2; in addition, the superscripts p and n refer to proton and neutron, and g_V and g_A are the vector and axial vector coupling constants for neutron beta decay. The Bjorken sum rule was originally derived[11,12] from commutation relations based on the algebra of currents for the quark model. It can also be derived[13] from quantum chromodynamics (QCD) and is often written

$$\int_0^1 \left[g_1^p(x) - g_1^n(x)\right]dx = \frac{1}{6}\left|\frac{g_A}{g_V}\right| . \quad (3)$$

In the above forms the sum rule is only valid in the scaling limit.

A comparison of our data with the Bjorken sum rule is indicated in Fig. 7. Values of the quantity $A_1F_2/(1+R)$ are plotted vs x. The solid curve is a plot of the quantity $A_1F_2/(1+R)$ for the proton using the fit to our data of $A_1 = 0.90x^{\frac{1}{2}}$, $R = 0.25$ [14] and experimental values[15] of F_2 with $Q^2 = 4$ (GeV/c)^2, which is approximately the mean Q^2 for our data points. The integral under the solid curve in the range of our data from x = 0.10 to 0.64 is about 0.23

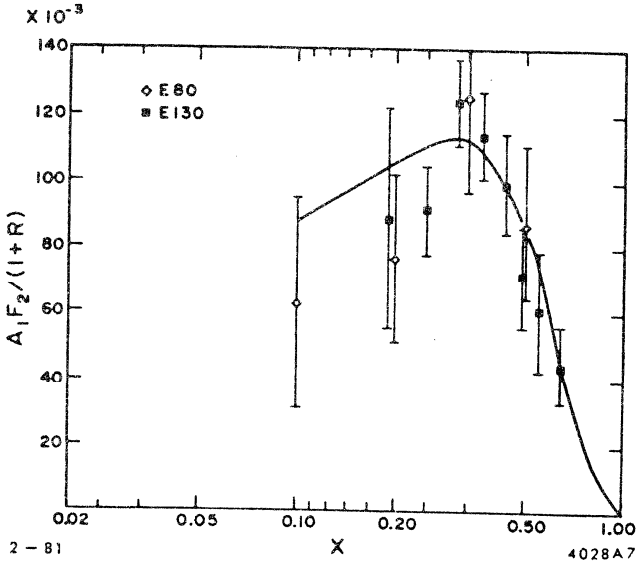

Fig. 7. Experimental values of $A_1^pF_2^p/(1+R^p)$ vs x, relevant to a test of the Bjorken sum rule.

or about 0.6 of the value predicted by the Bjorken sum rule. Clearly data at lower x are needed, and in addition an extrapolation to low x based on Regge theory can be made.[4] Since there is no experimental information about A_1 for the neutron, the neutron contribution to the integral must be ignored.. Our data on A_1^p are clearly consistent with the Bjorken sum rule.

Quantum chromodynamic corrections to the Bjorken sum rule have been calculated. The leading correction in the strong coupling constant $\alpha_s(Q^2)$ is given by:[13,16]

$$\int_0^1 dx \left(g_1^p - g_1^n\right) = \frac{1}{6}\left|\frac{g_A}{g_V}\right|\left(1 - \frac{\alpha_s}{\pi}\right) \qquad (4)$$

in which $\alpha_s = [12\pi/(33-2f)]\left[\ell n\left(Q^2/\Lambda^2\right)\right]^{-1}$ where f is the number of quark flavors and Λ is a free parameter. Higher order QCD corrections, including target mass effects, have also been evaluated.[17-20] Significant tests of these QCD corrections require additional experimental data as indicated below.

Another derivative form of the Bjorken sum rule due to Ellis and Jaffe[21] expresses separately a sum rule for the proton and for the neutron in the scaling limit:

$$\int_0^1 dx\ g_1^p = \left|\frac{g_A}{g_V}\right| \frac{(1.78)}{12} \qquad (5)$$

and

$$\int_0^1 dx\ g_1^n = \left|\frac{g_A}{g_V}\right| \frac{-(0.22)}{12} \qquad (6)$$

As compared to the Bjorken sum rule of Eq. (3), these sum rules involve the additional approximation that strange quarks do not contribute to the polarization asymmetry. According to Eqs. (5) and (6), the neutron contributes about 10% to the Bjorken sum rule.

Comparison of our data on A_1^p with theoretical values provides a major test for our understanding of nucleon structure. The generally accepted theory of quantum chromodynamics involving quarks and gluons has not yet been successfully applied from its own first principles to calculate either spin independent or spin dependent structure functions. However, perturbative QCD does make some important predictions about nucleon structure functions including A_1 for x near 1, which is the high momentum tail of the wave function. The models of nucleon structure[22] picture the proton as consisting of three valence quarks, two u quarks and a d quark, together with gluons and a sea of quark-antiquark pairs, and the neutron as two d quarks and a u quark together with gluons and the sea. The early models[23] assumed SU(6) symmetry for the wave function. However, experimental data on F_2^n/F_2^p and on A_1^p at large x required that SU(6) symmetry breaking be introduced. The important and unsymmetrical aspect of the wave function for the proton (neutron) near $x = 1$, which is predicted by perturbative QCD,[24] is the occurrence with high probability of a single u(d) quark with large x and a diquark with isotopic spin $I = 0$ and spin component $S_z = 0$. Of the various models for

the proton wave function which are intended to represent the nonperturbative QCD solution perhaps the most basic is the MIT bag model[22,25] which incorporates confinement.

A comparison of our data on $A_1^p(x)$ with various model predictions is shown in Fig. 8. We should remark that some earlier nonquark models of the proton predicted negative values for A_1, but all quark models predict that A_1 is positive.[3,23] Hence our earliest data indicating that A_1 is positive provided a crucial test of the quark model.[3] In the quark model A_1 can be written

$$A_1(x) = \frac{\sum_i e_i^2\left[q_i^{\uparrow} - q_i^{\downarrow}\right]}{\sum_i e_i^2\left[q_i^{\uparrow} + q_i^{\downarrow}\right]} \qquad (7)$$

in which the sum is over the quarks i, e_i is the quark i charge, and $q_i^{\uparrow}(q_i^{\downarrow})$ is the probability for quark i to have its spin parallel (antiparallel) to the target nucleon spin. A_1 clearly provides a measure of the probability that the quark spins are aligned with the nucleon spin. Only models 4 and 6 agree well with the experimental data. Curve 4 provides an unsymmetrical model of the quark distributions involving SU(6) breaking, Regge theory at small x, the Melosh transformation, and agreement with the Bjorken sum rule. Curve 6 is based on Schwinger's source theory, which is not a quark model.

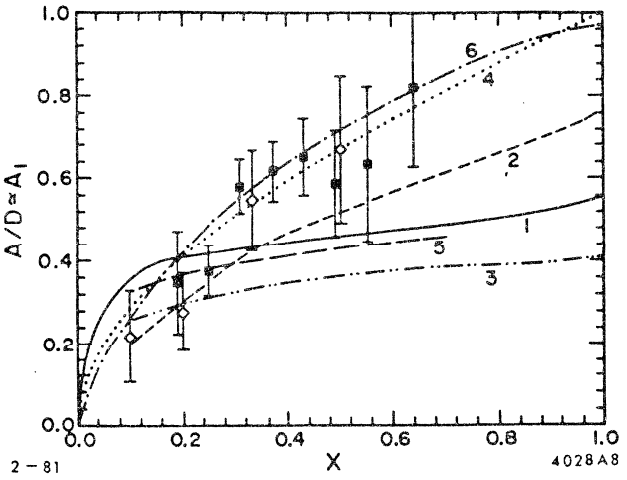

Fig. 8. Experimental values of $A/D \simeq A_1$ compared to theoretical predictions for A_1^p. The models are as follows: (1) a relativistic symmetric valence-quark model of the proton;[23] (2) a model incorporating the Melosh transformation which distinguishes between constituent and current quarks;[26] (3) a model introducing nonvanishing quark orbital angular momentum;[27,28] (4) an unsymmetrical model[29,30] in which the entire spin of the proton is carried by a single quark in the limit of $x = 1$; (5) the MIT bag model of quark confinement;[25,31] (6) source theory.[32]

RESONANCE REGION DATA AND THEIR IMPLICATIONS

The first exploratory experiment at SLAC on polarized e-p scattering in the resonance region, which was a part of E80, has recently been reported.[5] Figure 9a displays the measured asymmetry values, and Fig. 9b shows the contributions to the differential cross section from resonances and background. Our measured asymmetries A/D are predominantly large and positive throughout the entire range in missing mass W except in the region of the $\Delta(1232$ MeV) resonance, where A/D is expected to be negative because of magnetic dipole excitation. In principle our measured asymmetry values can be predicted from a multipole analysis of complete but unpolarized electroproduction data. Figure 10 displays the predictions

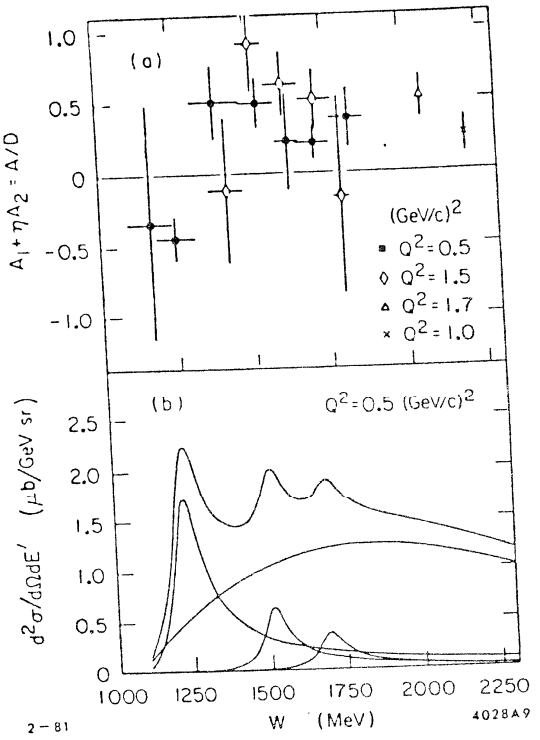

Fig. 9. (a) Asymmetry vs missing mass W. (b) Differential cross section vs W. Also shown is a decomposition into individual resonances and the background.

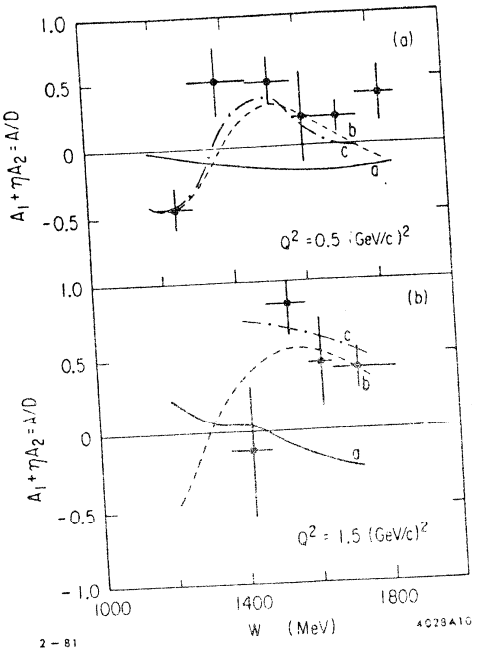

Fig. 10. (a) Asymmetry data at $Q^2 \simeq 0.5$ $(GeV/c)^2$ compared with a multipole analysis performed by Devenish and Gerhardt: curve a, Born terms alone; curve b, Born terms plus $\Delta(1232)$; and curve c, Born terms plus all resonances. (b) Same for $Q^2 \simeq 1.5$ $(GeV/c)^2$.

based on a multipole analysis of single pion electroproduction data only, which accounts for about 1/2 of the differential cross section. The agreement between these predictions and our data is rather good, and hence indicates that the net asymmetry contributed by other channels than single pion production cannot be very different from our measured asymmetries. Figure 11 indicates that scaling applies for our resonance region data except at the $\Delta(1232)$ point, and hence that the spin dependent behavior is also consistent with a global duality mechanism in analogy to the unpolarized case.

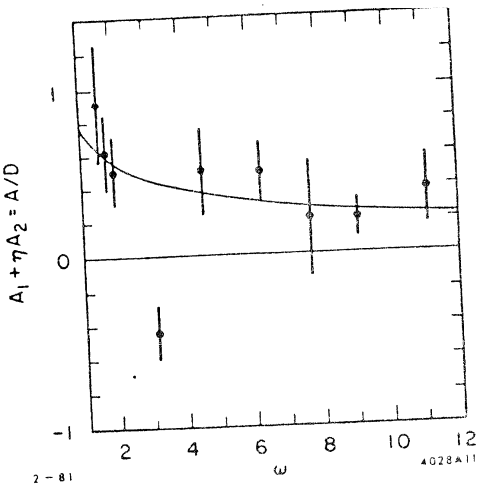

Fig. 11. Asymmetry vs scaling variable ω. The curve $0.78\omega^{-\frac{1}{2}}$ is a fit to deep-inelastic data ($W > 2$ GeV) of SLAC E80. The data points are the resonance-region results ($W < 2$ GeV) of SLAC E80.

THE FUTURE

We turn now to more futuristic aspects. An experiment[33] entitled Son of E130 has been proposed at SLAC to measure A_1 (neutron) and A_2 (proton), about which we have no experimental information. Determination of A_1^n can be done by measuring asymmetries for both the deuteron and the proton. Determination of A_2^p can be done by measuring asymmetries in scattering longitudinally polarized electrons by transversely polarized protons, and observing scattered electrons in the plane determined by the directions of the incident electron and the proton polarizations. In addition, this experiment would determine A_1^p to relatively high precision for values of x as low as 0.07. Both the data on A_1^n and the higher precision data on A_1^p at the lower x values would improve our test of the Bjorken sum rule.

Some theoretical predictions for A_1^n are shown in Fig. 12. On the basis of the spin-isospin part of the SU(6) wave function, $A_1^n = 0$ for all x (curve 1). Perhaps the most interesting prediction (curve 4) is that

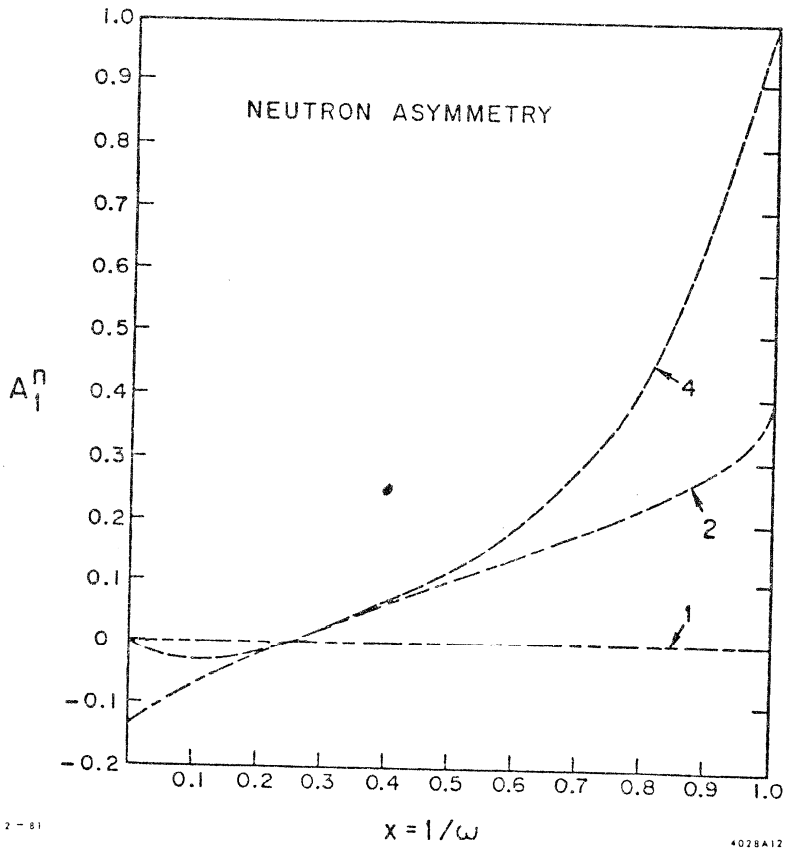

Fig. 12. Theoretical predictions for A_1 (neutron). The models are as follows: (1) a relativistic symmetric valence-quark model of the neutron;[23] (2) a model incorporating the Melosh transformation which distinguishes between constituent and current quarks;[26] (4) an unsymmetrical model[29,30] in which the entire spin of the neutron is carried by a single quark in the limit of $x = 1$.

of the unsymmetrical model of Carlitz and Kaur which agrees so well with the A_1^p data. It is seen that A_1^n is small over most of the range of x but becomes large at x near 1, where a single quark carries the entire spin of the neutron.

The structure function A_2 arises from an interference between amplitudes for absorption of virtual longitudinal and transverse photons by the proton.[3] In the scaling limit A_2 becomes zero, and there is a positivity bound[34] $|A_2| < R^{\frac{1}{2}}$. Physically A_2 arises from transverse momenta of the quarks. Figure 13 shows various theoretical predictions for A_2 for the kinematics of our proposed Son of E130 experiment. The positivity limit of $|A_2| < R^{\frac{1}{2}}$ is 0.5, since the best current value[14] of R in this kinematic range is $R = 0.25 \pm 0.10$. Parenthetically, this large experimental value for R, which is expected theoretically to be zero in the scaling limit, poses a problem for QCD theory, which may be related to higher-twist terms; the comparison of theory and experiment for A_2 can be expected to pose a similar problem. In addition, Fig. 13 shows the prediction of the MIT bag model,[25,31] a prediction based on our A_1^p data together with a relation between A_1 and A_2 given by the approximate Wandzura-Wilczek sum rule,[17,35] and a prediction given from $g_2(x) = 0$ which is consistent[23] with SU(6). Data on A_2 are important for comparison with these and other[36] theories for A_2. In addition, data on A_2 are important to our experimental determination of A_1, since we measure $A/D = A_1 + \eta A_2$, and we only obtain a value of A_1 provided ηA_2 is sufficiently small. With the positivity bound for A_2, the value of ηA_2 for E80-E130 data is between 0.2 and 0.8 times the experimental one standard deviation error in our determination of A/D.

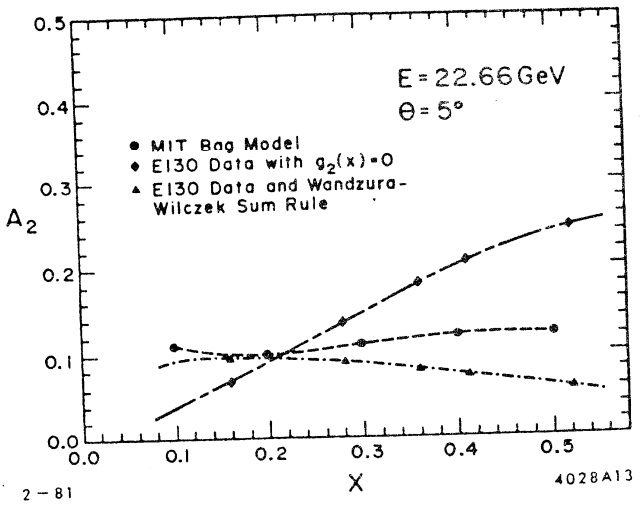

Fig. 13. Theoretical predictions for A_2 (proton) for the kinematics of the Son of E130 proposal.

Further significant tests of the scaling behavior of A_1 will only come with the availability of additional data on A_1 at higher Q^2, which is planned at CERN by the European Muon Collaboration[37] in the Q^2 range up to about 60 $(GeV/c)^2$. Figure 14 shows predictions of scaling violations of g_1 predicted[38] by QCD; they amount to about a 10% variation over the Q^2 range from 2 to 60 $(GeV/c)^2$ in the accessible range of x, and are of different sign for low and intermediate values of x. Since our measured quantity A_1 is equal to $2xg_1(1+R)/F_2$, the known scaling violations in F_2 must also be considered.

It is well known in the theory of atomic hyperfine structure[39,40] that a significant contribution to the hfs interval $\Delta\nu$ in hydrogen arises from the spin dependent polarizability of the proton. Figure 15 gives the experimental and theoretical values[41] for $\Delta\nu$. The contribution

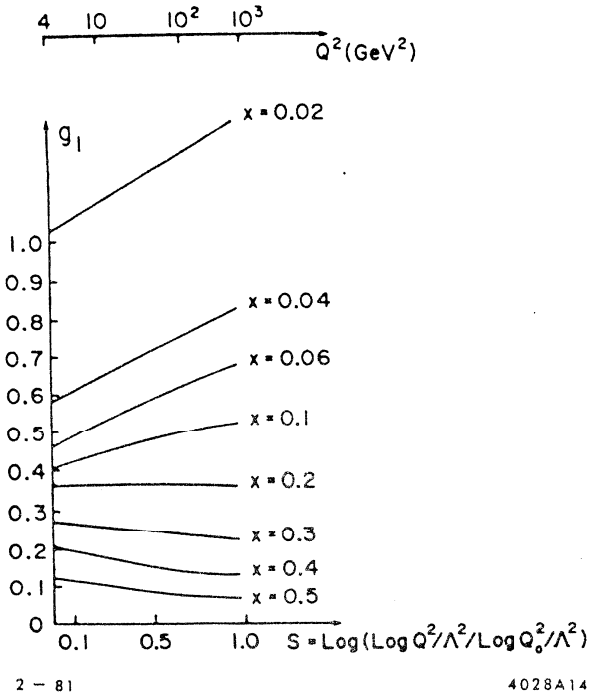

Fig. 14. Theoretical prediction[38] of scaling violation for g_1, with the parameter values $Q_0 = 2$ GeV/c and $\Lambda = 0.4$ GeV/c.

HYPERFINE INTERVAL IN HYDROGEN; EFFECT OF PROTON POLARIZABILITY

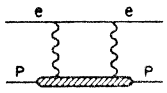

$\Delta\nu_{expt.} = 1\,420\,405\,751.766\,7(10)$ Hz

$\Delta\nu_{theory} = \Delta\nu_F(1+\delta_{QED}+\delta_P)$ $\quad \Delta\nu_F$ = Fermi value; δ_{QED} = QED corrections; δ_P = Proton recoil and structure term

$\delta_P = \delta_P(\text{rigid}) + \delta_P(\text{polarizability}) = -34.6(9) \times 10^{-6} + \delta_P(\text{pol})$

$$\delta_P(\text{pol}) = \frac{\alpha}{\pi}\frac{m_e}{M}\frac{1}{2(1+\mu_A)}\int_0^\infty \frac{d(-q^2)}{(-q^2)}\left[\Delta_1(q^2)+\Delta_2(q^2)\right]$$

$$\Delta_1(q^2) = \frac{9}{4}\left[F_2(q^2)\right]^2 + 5M^3\int_{\nu_1(q^2)}^\infty \frac{d\nu}{\nu}\beta_1\left(\frac{\nu^2}{-q^2}\right)G_1(\nu,q^2)$$

$$\Delta_2(q^2) = 3M^2\int_{\nu_1(q^2)}^\infty \frac{d\nu}{\nu^2}\beta_2\left(\frac{\nu^2}{-q^2}\right)q^2\,G_2(\nu,q^2)$$

$$\beta_1(x) \equiv \frac{4}{5}(-3x+2x^2+2(2-x)\sqrt{x(1+x)});\ \beta_2(x) \equiv 4x(1+2x-2\sqrt{x(1+x)})$$

$F_2(q^2)$ = Pauli form factor; $F_2(0) = \mu_A$; $\nu_1(q^2) = m_\pi + \dfrac{(m_\pi^2 - q^2)}{2M}$

2 – 81 4028A15

Fig. 15. Hyperfine structure interval $\Delta\nu$ in hydrogen. The Feynman diagram and the expression given for δ_p (pol) indicate the contribution of the spin dependent polarizability of the proton to $\Delta\nu$.

of the spin dependent polarizability is designated δ_p (pol). The principal theoretical uncertainty in $\Delta\nu$ is due to δ_p (pol), for which a positivity bound $|\delta_p(\text{pol})| \lesssim 3$ ppm has been calculated.[42] The quantity δ_p (pol) can be expressed[43] in terms of the spin dependent structure functions G_1 and G_2 which are measured in polarized e-p scattering. Using our experimental data for A_1^p and the Wandzura-Wilczek relation,[35] we estimate the total contribution to δ_p (pol) to be $\lesssim$0.5 ppm from both the deep inelastic and resonance regions above a Q^2 value of ~5 (GeV/c)^2. The greatest contribution to δ_p (pol) comes from the small Q^2 region, including the proton resonances. Further experimental data and theoretical work should determine δ_p (pol) to a useful precision.

Finally we emphasize that knowledge of the internal spin structure of the nucleon, apart from its importance to our understanding of nucleon structure, is essential to the interpretation of spin dependent high energy phenomena involving hadrons. These include hadron-hadron scattering,[44–47] the polarized Drell-Yan process,[48,49] and production of polarized W or Z vector bosons in collisions of polarized protons in a high energy storage ring.[50,51]

REFERENCES

1. V. W. Hughes, High Energy Physics with Polarized Beams and Polarized Targets, ed. G. H. Thomas (AIP Conference Proceedings No. 51, Argonne, 1978), p. 171.
2. M. J. Alguard et al., Phys. Rev. Lett. 37, 1258 (1976).
3. M. J. Alguard et al., Phys. Rev. Lett. 37, 1261 (1976).
4. M. J. Alguard et al., Phys. Rev. Lett. 41, 70 (1978).
5. G. Baum et al., Phys. Rev. Lett. 45, 2000 (1980).
6. G. Baum et al., XXth International Conference on High Energy Physics, University of Wisconsin, July 17-23, 1980.
7. M. J. Alguard et al., Nucl. Instrum. Methods 163, 29 (1979).
8. W. W. Ash, High Energy Physics with Polarized Beams and Targets, ed. M. L. Marshak (American Institute of Physics, New York, 1976), p. 485.
9. P. S. Cooper et al., Phys. Rev. Lett. 34, 1589 (1975).
10. L. Galfi et al., Phys. Lett. B31, 465 (1970).
11. J. D. Bjorken, Phys. Rev. 148, 1467 (1966).
12. J. D. Bjorken, Phys. Rev. D1, 1376 (1970).
13. J. Kodaira et al., Phys. Rev. D20, 627 (1979).
14. L. F. Abbott et al., Phys. Rev. D22, 582 (1980).
15. A. J. Buras and K. J. F. Gaemers, Nucl. Phys. B132, 249 (1978).
16. J. Kodaira et al., Nucl. Phys. B159, 99 (1979).
17. S. Wandzura, Nucl. Phys. B122, 412 (1977).
18. J. Kodaira, Nucl. Phys. B165, 129 (1980).
19. S. Matsuda and T. Uematsu, Nucl. Phys. B168, 181 (1980).
20. C. S. Lam and B. A. Li, SLAC-PUB-2505 and 2506 (1980).
21. J. Ellis and R. Jaffe, Phys. Rev. D9, 1444 (1974).
22. F. E. Close, An Introduction to Quarks and Partons, Academic Press, London (1979).
23. J. Kuti and V. W. Weisskopf, Phys. Rev. D4, 3418 (1971).
24. G. R. Farrar and D. R. Jackson, Phys. Rev. Lett. 35, 1416 (1975).
25. R. L. Jaffe, Phys. Rev. D11, 1953 (1975).
26. F. E. Close, Nucl. Phys. B80, 269 (1974).
27. G. W. Look and E. Fischbach, Phys. Rev. D16, 211 (1977).
28. L. M. Sehgal, Phys. Rev. D10, 1663 (1974).
29. R. Carlitz and J. Kaur, Phys. Rev. Lett. 38, 673; 1102 (E) (1977).
30. J. Kaur, Nucl. Phys. B128, 219 (1977).
31. R. J. Hughes, Phys. Rev. D16, 662 (1977).
32. J. Schwinger, Nucl. Phys. B123, 223 (1977).
33. V. W. Hughes et al., SLAC Proposal Son of E130, August 1980.
34. M. G. Doncel and E. de Rafael, Nuovo Cimento 4A, 363 (1971).
35. S. Wandzura and F. Wilczek, Phys. Lett. B72, 195 (1977).
36. A. S. Joshipura and P. Roy, Phys. Lett. B92, 348 (1980).
37. E. Gabathuler, CERN Proposal by European Muon Collaboration (1974).
38. O. Darrigol and F. Hayot, Nucl. Phys. B141, 391 (1978).
39. S. J. Brodsky and S. D. Drell, Ann Rev. Nucl. Sci. 20, 147 (1970).
40. A. De Rujula et al., Phys. Lett. 33B, 605 (1970).
41. E. R. Cohen and B. N. Taylor, Jr., Phys. and Chem. Data 2, 663 (1973).
42. E. De Rafael, Phys. Lett. B37, 201 (1971).
43. R. L. Heimann, Nucl. Phys. B64, 429 (1973).
44. D. Sivers, High Energy Physics with Polarized Beams and Polarized Targets, ed. G. H. Thomas (AIP Conference Proceedings No. 51, Argonne, 1978), p. 505.

45. J. Babcock et al., Phys. Rev. D19, 1483 (1979).
46. K. Hidaka et al., Phys. Rev. D19, 1503 (1979).
47. N. Craigie et al., Phys. Lett. B96, 381 (1980).
48. J. Soffer and P. Taxil, Phys. Lett. B85, 404 (1979).
49. K. Hidaka et al., Phys. Rev. D21, 1316 (1980).
50. F. E. Paige et al., BNL-24919 (1978).
51. F. Baldracchini et al., "A Survey of Polarization Asymmetries Predicted by QCD," International Center for Theoretical Physics, Trieste, 1980.

Appendix II

Final Results of SLAC - E130

(To be published soon)

The final radiatively corrected electron-proton asymmetries A and virtual photon-proton asymmetries $A/D \simeq A_1$ are shown in Table I. The results for the high and low-Q^2 kinematic points are given separately first. For a given value of x, the A/D values for different Q^2 agree within errors, consistent with the predicted scaling relation $A_1(\nu,Q^2) \to A_1(x)$ as $\nu,Q^2 \to \infty$ with x fixed. Therefore, assuming scaling, the weighted averages of the $A_1(\nu,Q^2)$ values have been obtained for each x bin and are shown at the bottom of the table. Note that $A(\nu,Q^2)$ has also been combined in this way although it is not expected to scale.

The A/D asymmetry results from experiments E-130 and E-80 are plotted against Q^2 for three intervals of x in Figure I. The error bars include systematic errors. The data are clearly consistent, within errors, with the scaling predictions. The Q^2-combined asymmetries for each x bin are shown in Figure II, where the errors plotted are a quadrature sum of statistical and systematic errors. A fit to the data of the form $A_1 = c\sqrt{x}$ gives $c = 0.942 \pm 0.080\ (0.053)$, where the quantity in parenthesis is the statistical error only. The fit has a chi-square of 9.5 with 11 degrees of freedom.

Comparison with Models

Our results for $A/D \simeq A_1$ are compared with several theoretical predictions in Figure III. A summary of our confidence level in each of these models is presented in Table II.

TABLE I. Results of Asymmetry Measurements

HIGH Q**2 Point : (E0 = 22.659 GeV, TH = 10 Degrees)

X	Omega	Q**2	Nu	W	Delta	$A^{1)}$	D	$A^{2)}$	$A/D^{2),3)}$	$nA2^{4)}$
.19	5.26	5.32	14.93	4.85	0.030+/-0.009	0.439+/-0.137 (0.134)	0.68	0.461+/-0.163 (0.160)	0.69+/-0.24 (0.24)	<0.04
.25	4.00	6.32	13.47	4.45	0.017+/-0.003	0.248+/-0.049 (0.046)	0.61	0.263+/-0.056 (0.053)	0.44+/-0.09 (0.09)	<0.05
.31	3.22	7.14	12.28	4.09	0.020+/-0.003	0.279+/-0.047 (0.043)	0.55	0.289+/-0.053 (0.050)	0.53+/-0.10 (0.09)	<0.07
.37	2.70	7.83	11.28	3.77	0.026+/-0.004	0.358+/-0.054 (0.049)	0.50	0.366+/-0.060 (0.055)	0.74+/-0.12 (0.11)	<0.08
.43	2.32	8.41	10.43	3.46	0.021+/-0.005	0.288+/-0.064 (0.061)	0.46	0.294+/-0.070 (0.068)	0.65+/-0.16 (0.15)	<0.10
.49	2.04	8.92	9.70	3.18	0.020+/-0.006	0.257+/-0.085 (0.083)	0.42	0.261+/-0.094 (0.092)	0.62+/-0.22 (0.22)	<0.11
.55	1.81	9.35	9.06	2.92	0.018+/-0.009	0.228+/-0.118 (0.117)	0.39	0.231+/-0.124 (0.123)	0.60+/-0.32 (0.32)	<0.12
.64	1.56	9.91	8.25	2.54	0.017+/-0.010	0.212+/-0.126 (0.126)	0.35	0.214+/-0.131 (0.131)	0.61+/-0.38 (0.37)	<0.14

LOW Q**2 Point : (E0 = 16.185 GeV, TH = 10 Degrees)

X	Omega	Q**2	Nu	W	Delta	$A^{1)}$	D	$A^{2)}$	$A/D^{2),3)}$	$nA2^{4)}$
.19	5.26	3.34	9.38	3.89	-.001+/-0.007	-.011+/-0.117 (0.117)	0.59	0.008+/-0.140 (0.140)	0.01+/-0.24 (0.24)	<0.06
.25	4.00	3.88	8.28	3.54	0.014+/-0.003	0.212+/-0.047 (0.044)	0.51	0.224+/-0.054 (0.052)	0.44+/-0.11 (0.10)	<0.08
.31	3.22	4.31	7.41	3.23	0.020+/-0.003	0.310+/-0.047 (0.042)	0.45	0.319+/-0.053 (0.048)	0.71+/-0.12 (0.11)	<0.10
.37	2.70	4.65	6.71	2.96	0.018+/-0.003	0.270+/-0.049 (0.046)	0.40	0.277+/-0.054 (0.051)	0.69+/-0.14 (0.13)	<0.12
.43	2.32	4.94	6.13	2.72	0.015+/-0.004	0.215+/-0.055 (0.054)	0.36	0.220+/-0.062 (0.060)	0.60+/-0.17 (0.16)	<0.14
.49	2.04	5.18	5.64	2.50	0.014+/-0.005	0.192+/-0.067 (0.066)	0.33	0.196+/-0.075 (0.074)	0.59+/-0.23 (0.22)	<0.15
.55	1.81	5.39	5.22	2.30	0.013+/-0.006	0.178+/-0.087 (0.086)	0.30	0.180+/-0.092 (0.092)	0.59+/-0.30 (0.30)	<0.17
.64	1.56	5.64	4.70	2.01	0.017+/-0.006	0.231+/-0.080 (0.079)	0.27	0.232+/-0.085 (0.084)	0.85+/-0.31 (0.31)	<0.20

Combined Q**2

X	Omega	$A^{2)}$	$A/D^{2),3)}$
.19	5.263	0.204+/-0.106 (0.105)	0.35+/-0.17 (0.17)
.25	4.000	0.243+/-0.040 (0.037)	0.44+/-0.07 (0.07)
.31	3.226	0.305+/-0.040 (0.035)	0.61+/-0.08 (0.07)
.37	2.703	0.318+/-0.043 (0.037)	0.72+/-0.10 (0.08)
.43	2.326	0.252+/-0.048 (0.045)	0.63+/-0.12 (0.11)
.49	2.041	0.212+/-0.066 (0.064)	0.61+/-0.16 (0.16)
.55	1.818	0.198+/-0.075 (0.074)	0.59+/-0.22 (0.22)
.64	1.563	0.227+/-0.072 (0.070)	0.75+/-0.24 (0.24)

1) Measured values without radiative corrections.The total errors are statistical errors added in quadrature to the systematic errors ; the numbers in parenthesis are the 1-standard-deviation counting errors.
2) Radiatively corrected values.
3) Calculated using weighted average of D.
   Calculated upper limits using R = 0.25.

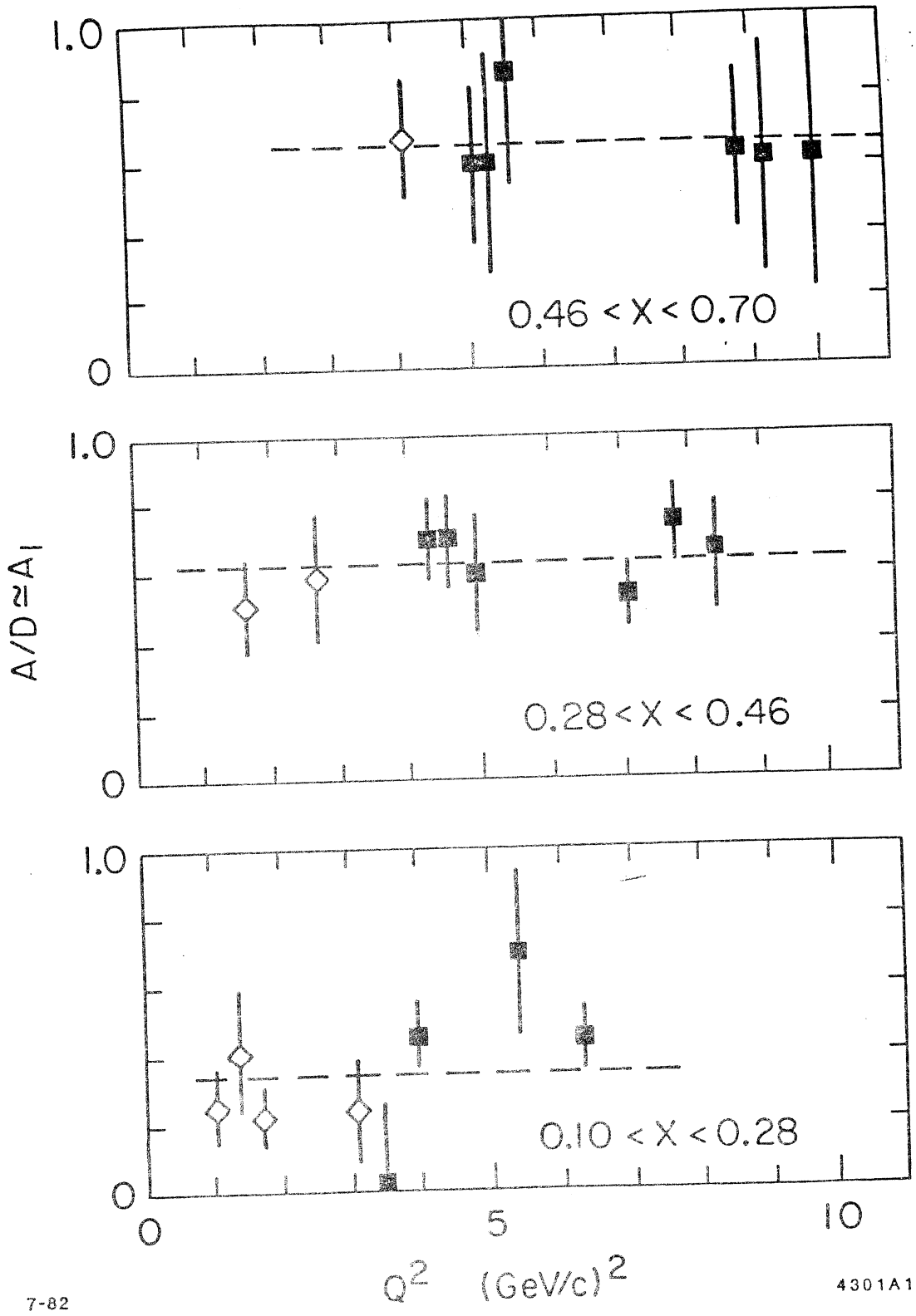

Figure I. Radiatively corrected values of the asymmetry A/D in three intervals of x for SLAC E-130 (closed squares) and revised SLAC E-80 data (open diamonds).

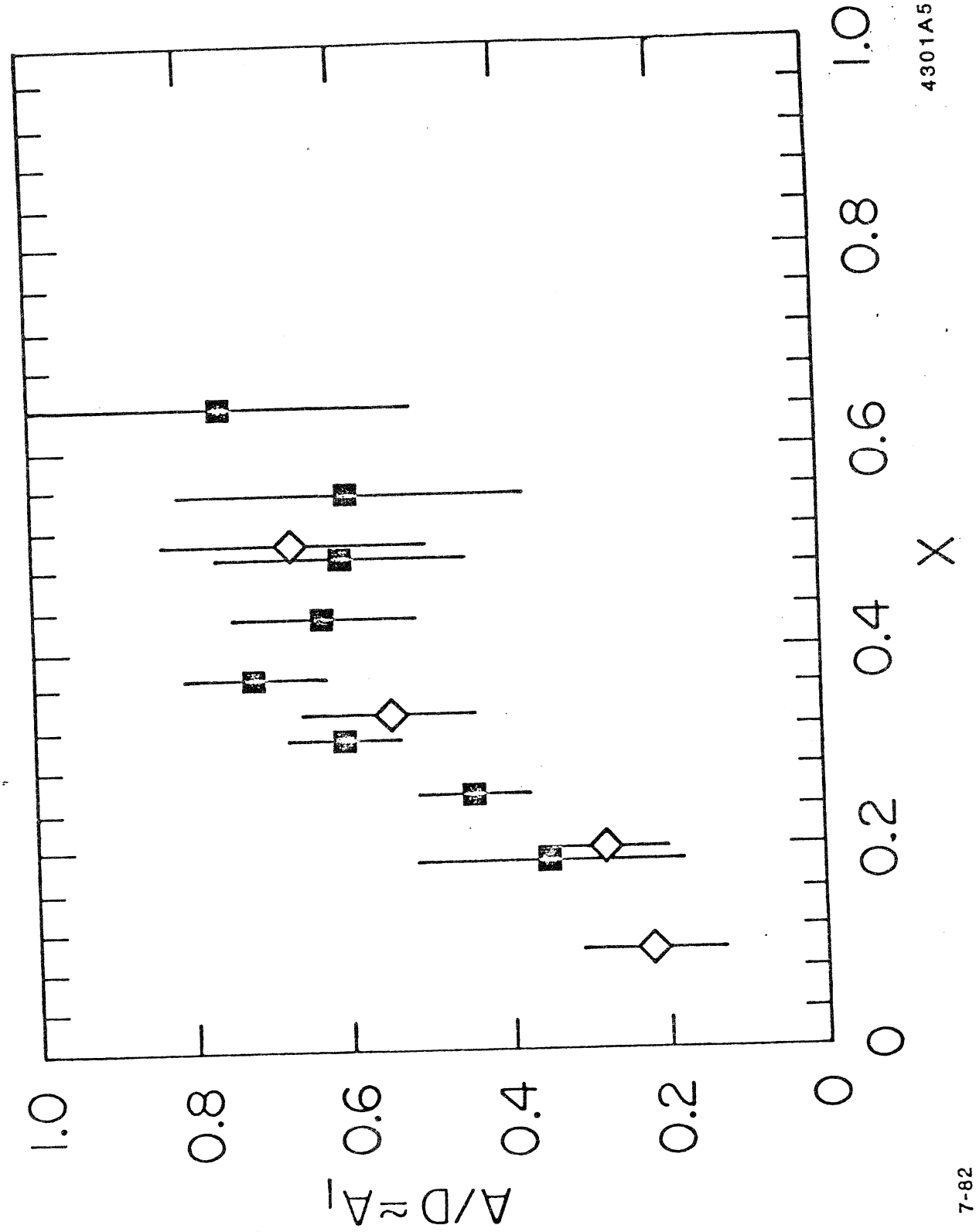

Figure II. Radiatively corrected values of A/D vs. x. Points are obtained from our data assuming that it scales. SLAC E-130 (closed squares) and revised SLAC E-80 data (open diamonds) are shown.

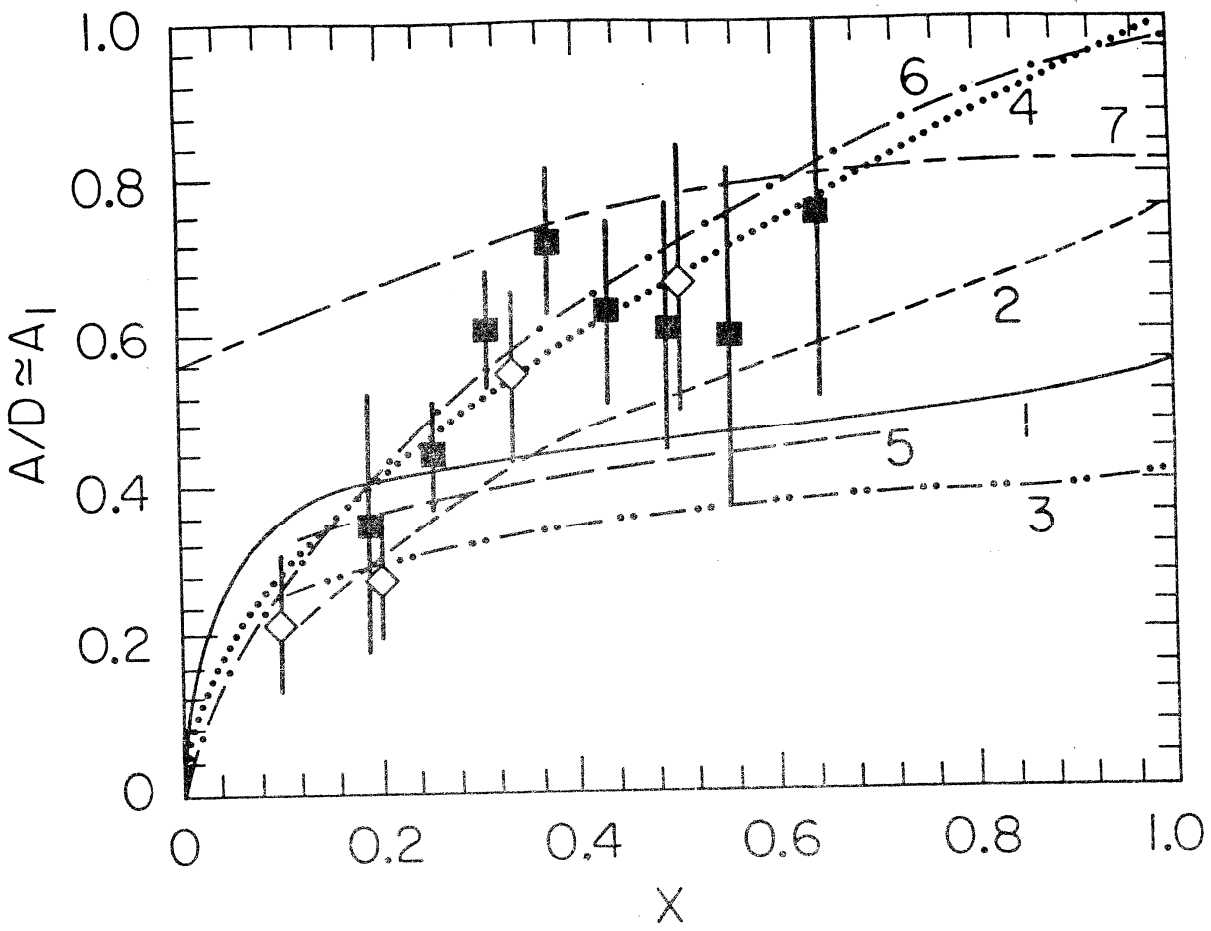

1. Symmetrical Valence Quark Model (Kuti, Weisskopf, 1971).
2. Current Quarks (Close, 1974).
3. Orbital Angular Momentum, (Look, Fischbach, Sehgal, 1977).
4. Unsymmetrical Model (Carlitz, Kaur, 1977).
5. MIT Bag Model (Jaffe, Hughes, 1977).
6. Source Theory (Schwinger, 1977).
7. Quark-Geometrodynamics (Preparata, 1981).

7-82

4301B2

Figure III. Comparison of A/D ≃ A_1 with various models.

Table II. Comparison of A/D with Models of A_1

#	Model Type	Originator(s)	χ^2/D.O.F.*	C.L.†
1	Symmetrical Valence Quarks	Kuti, Weisskopf	2.57	0.005
2	Current Quarks	Close	2.03	0.03
3	Orbital Angular Momentum	Look, Fischbach, Sehgal	4.92	<0.0001
4	Unsymmetrical Model	Carlitz, Kaur	.71	0.7
5	MIT Bag Model	Jaffe, Hughes	3.12	0.001
6	Source Theory	Schwinger	0.68	0.7
7	Quark-Geometrodynamics	Preparata	6.73	<0.0001

* Number of degrees of freedom = 10

† Confidence level

Taking into account the uncertainty in A_2, our data are consistent with (a) Schwinger's source theory (Schwinger 1977), (b) the unsymmetrical quark-parton model of Carlitz and Kaur (Carlitz and Kaur 1977, Kaur 1977), and possibly (c) the current quarks model due to Close (Close 1974).

Comparison with Bjorken and Ellis-Jaffe Sum Rules

The Bjorken sum rule is:

$$S_{Bj} = \int_0^1 \frac{dx}{x}\left[\frac{A_1^P F_2^P}{1+R^P} - \frac{A_1^N F_2^N}{1+R^N}\right] = \frac{1}{3}\left|\frac{g_A}{g_V}\right| = 0.418 \pm 0.002$$

In the absence of experimental information on A_1^N we approximate $A_1^N = 0$, since most quark-parton models of the neutron predict that A_1^N is small (except near $x \to 1$ where the contribution to the integral becomes negligible). Alternatively, we may exploit the Ellis-Jaffe sum rules which separately give the proton and neutron contributions according to

$$2\int_0^1 g_1^P(x)\,dx = \int_0^1 \frac{dx}{x}\,\frac{A_1^P(x)F_2^P(x)}{1+R^P} = \left|\frac{g_A}{g_V}\right|\frac{(0.89)}{3} = 0.372 \pm 0.002$$

$$2\int_0^1 g_1^n(x)\,dx = \int_0^1 \frac{dx}{x}\,\frac{A_1^N(x)F_2^N(x)}{1+R^n} = \left|\frac{g_A}{g_V}\right|\frac{(-0.11)}{3} = -0.046 \pm 0.0002$$

The integrand $A_1^P F_2^P/(1+R^P)$ is plotted for measured values of A_1^P in Figure IV. The F_2^P structure function has been evaluated using a parametrization produced by Buras and Gaemers (Buras and Gaemers 1978), and the quantity R^P has been set to the value obtained from the combined SLAC ep data (Hand 1977) of 0.25 ± 0.10. The solid curve is obtained from the fit to our data

$$A_1^P(x) = (0.94 \pm 0.08)\sqrt{x}$$

BJORKEN SUM RULE

$$S_{Bj} = \int_0^1 \frac{dx}{x}\left[\frac{A_1^p F_2^p}{(1+R^p)} - \frac{A_1^n F_2^n}{(1+R^n)}\right] = \frac{1}{3}\left|\frac{g_A}{g_V}\right| = 0.418 \pm 0.002$$

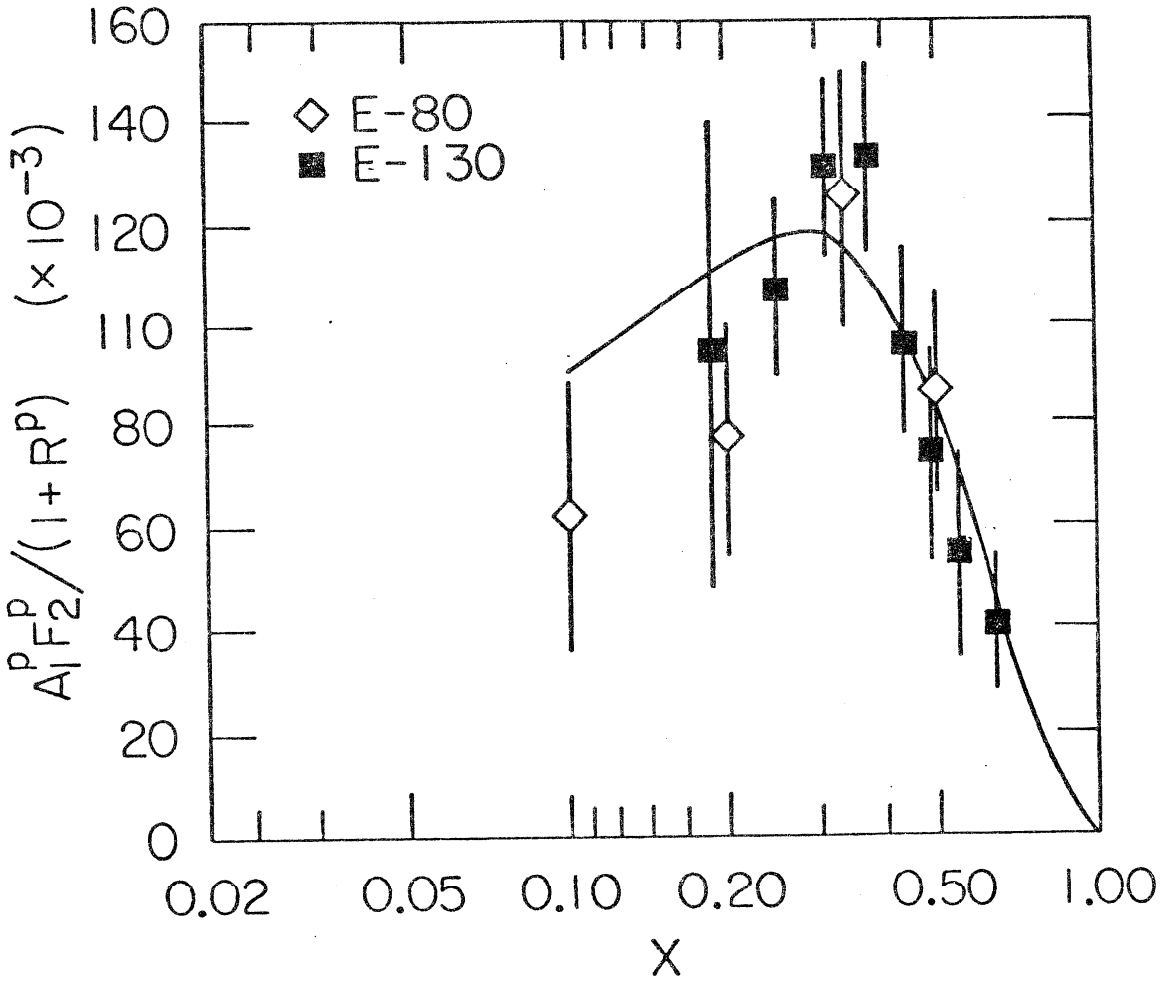

$A_1^p = (0.94 \pm 0.08)X^{1/2}$; Assume $A_1^n = 0$

F_2^p and R from unpolarized data

$S_{Bj}^{expt}(0.1 \le X \le 0.64) = 0.189$

7-82

4301B6

Figure IV

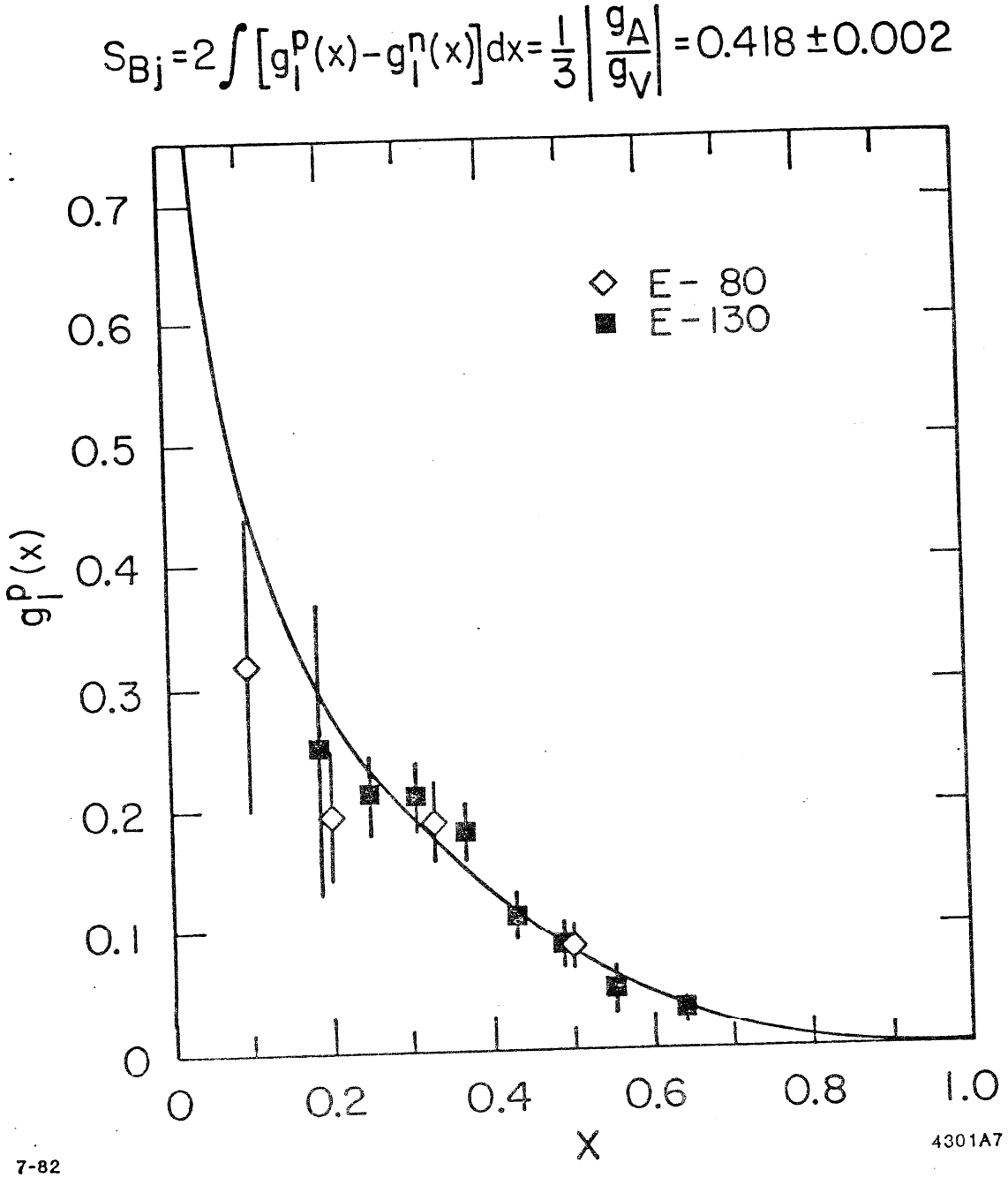

Figure V. Spin-dependent structure function of the proton, g_1^p (x) calculated from our combined A_1 data, the Buras-Gaemers parametrization of $F_2(x,Q^2)$, and assuming R=0.25. The solid curve is obtained from the fit to our data $A_1 = 0.94\sqrt{x}$ and $F_2(x)$ at a fixed value of Q^2=4 GeV^2.

and the F_2^P structure function evaluated at $Q^2 = 4$ GeV^2, which is nearly the mean Q^2 value of our data. The integral under this curve in our data interval of $0.1 < x < 0.64$ is 0.189 ± 0.016 which saturates 45% of the Bjorken sum rule.

Making the assumptions and following the same procedure as described above, the longitudinal spin-dependent structure function of the proton, $g_1^P(x) = A_1^P(x) F_2^P(x)/(2x(1+R^P))$ is shown in Figure V. The solid curve was obtained in a manner analogous to the solid curve that appears in Figure IV. The overall integral under this curve is

$$2\int_0^1 g_1^P(x)dx = 0.33 \pm 0.10$$

where the error includes (a) the experimental errors of A/D, (b) the errors due to the uncertainty of R and A_2, and (c) the error due to the extrapolation of A_1 as $x \to 0$.

In conclusion, this result is consistent with the Ellis-Jaffe sum rule for the proton. This implies that our results are also consistent with the Bjorken sum rule provided that the neutron contribution is as small (and has the same sign) as suggested by the Ellis-Jaffe sum rule for the neutron.

References

Buras, A.J. and Gaemers, K.J.F., 1978, Nucl. Phys. B132, 249.

Carlitz, R. and Kaur, J., 1977, Phys. Rev. Lett. 38, 673.

Close, F.E., 1974, Nucl. Phys. B80, 269.

Hand, L.N., 1977, Proc. of the Int. Symp. on Lepton & Photon Interactions at High Energies, Hamburg, 417.

Jaffe, R.L., 1975, Phys. Rev. D 11, 1953.

Kaur, J., 1977, Nucl. Phys. B128, 219.

Kuti, J. and Weisskopf, V.F., 1971, Phys. Rev. D 4, 3418.

Look, G.W. and Fischbach, E., 1971, Phys. Rev. D 16, 211.

Preparata, G., 1980, High Energy Physics with Polarized Beams and Polarized Targets, Proc. of the 1980 Int. Symp., Lausanne, p. 121.

Schwinger, J., 1977, Nucl. Phys. B123, 223.

Sehgal, L.M. 1974, Phys. Rev. D 10, 1663.

SLAC-PUB-2874
January 1982
(I)

DYNAMIC NUCLEAR POLARIZATION OF IRRADIATED TARGETS*

M. L. Seely, A. Amittay, M. R. Bergström, S. K. Dhawan,
V. W. Hughes, R. F. Oppenheim, K. P. Schüler and P. A. Souder
Yale University, New Haven, CT 06520

K. Kondo and S. Miyashita
University of Tsukuba, Ibaraki, Japan

K. Morimoto
K.E.K., Tsukuba, Japan

S. J. St. Lorant
Stanford Linear Accelerator Center
Stanford University, Stanford, California 94305

Y.-N. Guo
Institute of High Energy Physics, Beijing, China

A. Winnacker
University of Heidelberg, Heidelberg, W. Germany

ABSTRACT

We report studies of dynamics nuclear polarization of irradiated targets. The polarized target operated at a magnetic field of 5 T and a temperature of 1 K and was irradiated with the 20 GeV electron beam at the Stanford Linear Accelerator. Our results indicate that the temperature at which the target is irradiated is important. The maximum proton polarization attained with radiation was measured for some seven hydrogen-rich compounds. Irradiated NH_3 and ND_3 were polarized to high values of $P_p \simeq 0.75$ and $P_d \simeq 0.25$ with short values of polarization growth time T_p, and with radiation resistance of the polarization about a factor of 30 greater than for normal chemically-doped dydrocarbons. Hence irradiated NH_3 and ND_3 appear very promising as practical polarized target materials.

Submitted to Nuclear Instruments and Methods

* Work supported in part by the Department of Energy under contracts DE-AC03-76SF00515 (SLAC) and DE-AC02-76ER03075 (Yale), by the German Federal Ministry of Research and Technology, and by the Japan Society for the Promotion of Science.

I. INTRODUCTION

Polarized nucleon targets used in high energy physics experiments usually employ the method of dynamic nuclear polarization (DNP) to polari. the nucleons in an alcohol [1]. DNP requires the presence of paramagneti centers, which are customarily provided by a chemical dopant. These targets have a relatively low polarizable proton content, and suffer loss of polarization when subjected to high doses of ionizing radiation. If the paramagentic centers formed when the target is irradiated can be used in the DNP process, it becomes possible to use materials which have a relatively high hydrogen fraction, but are not easily doped by chemical means [2], such as NH_3 or HD. Furthermore, the polarization of such targets may be much more radiation resistant.

The earliest work on the use of radiation to produce a polarizable target was done on HD at Yale [3], using a bremsstrahlung beam with a maximum energy of 60 MeV. A proton polarization of 3.7% and a deuteron vector polarization of 0.4% were obtained by DNP, with a magnetic field (H) of 1.2 T and a temperature (T) of 1.2 K. Dynamic nuclear polarization of undoped butanol with a proton polarization of about 7% was obtained [4], using a 4 MeV bremsstrahlung beam with H = 2.5 T and T = 1 K. Recent encouraging results on the DNP of NH_3 irradiated in LN_2 with a proton beam (energy 580 MeV) were obtained at CERN [5], where a proton polarization of about 90% was obtained with H = 2.5 T and T < 0.5 K. However, a slow growth in polarization and a long spin-lattice relaxation time were observed. Furthermore, two explosions occurred when NH_3 was irradiated in LN_2.

In the Spring of 1979, we initiated our studies at the Stanford Linear Accelerator Center (SLAC), where our polarized target was set up in the high energy 20 GeV electron beam. In this paper we report our preliminary results for NH_3 and ND_3, as well as for a number of other substances with high hydrogen content. Earlier reports on our work have been made [6].

Important results on DNP of irradiated NH_3 and ND_3 have been reported [7] from Bonn. By using higher doses than used in the CERN experiment, the group achieved high proton polarizations with relatively short polarizing and spin lattice relaxation time constants in NH_3 targets irradiated with a 20 MeV electron beam. The Bonn group used liquid argon (80 K), rather than LN_2, to cool the targets during irradiation and did not observe any explosions. Relatively low deuteron polarizations were reported for ND_3.

II. EXPERIMENTAL METHOD AND RESULTS

The Yale-SLAC polarized target system [8] utilizes a ^4He cryostat to maintain 25 cm^3 (2.5 cm × 2.5 cm × 3.8 cm in the beam direction) of target material at 1 K, a superconducting magnet with a 50 kG field, a microwave system operating at 140 GHz, and an NMR system operating at 200 MHz (proton) or 30 MHz (deuteron). The targets were irradiated at SLAC with an electron beam delivered at 10 pulses per second with currents ranging from 2×10^9 to 5×10^{10} electrons per 1.5 μs pulse and with energies ranging from 6 to 20 GeV. The beam spot (~2 mm in diameter) was rastered over the target in a period of about 1 min. The irradiations and the measurements described here were conducted with the target at a temperature of 1 K. Irradiation of targets at higher temperatures in

the range of 20 K to 80 K (the temperatures were only poorly controlled) indicated that much larger radiation doses were required to achieve polarization than for irradiation at 1 K.

We have irradiated and studied dynamic polarization in the materials shown in Table I. For most of these materials, the low polarizations observed make them uninteresting as candidates for polarized target materials. Ammonia and deuterated ammonia, however, offer high polarization and show great promise as polarized target materials. We will therefore present the results of our studies on NH_3 and ND_3 in more detail.

The ammonia targets were prepared by slowly freezing (in a period of about 1 hour) approximately 30 cm^3 of liquid ammonia to produce a clear solid, which was then crushed and sifted to select fragments approximately 1.5 mm in diameter. In our earlier studies [6], we found that the microcrystaline beads, produced by rapidly freezing droplets of liquid ammonia (droplets were allowed to fall directly into LN_2), disintegrated rapidly when irradiated at 1 K. In slowly frozen ammonia, the rate of disintegration is significantly reduced. The problem of finely divided ammonia target material migrating from the target cup, which plagued our earlier studies, was eliminated through the use of slowly frozen ammonia and a redesigned target cup.

The polarization behavior of one of our ammonia targets is shown in fig. 1. The polarization rises smoothly with dose and levels off at the value of ~60% as the target is initially irradiated. Annealing the target at temperatures between 10 K and 40 K causes the polarization to increase to its maximum value of ~75%. A dose of 9×10^{14} e^-/cm^2 given subsequent to the second anneal caused the polarization to decrease from ~75% to ~68%

For an exponential decrease this corresponds to a depolarizating (1/e) dose of 0.9×10^{16} e^-/cm^2, which is about 30 times larger than for butanol. Actually the decay was not exponential and was relatively slower at high doses. The rate at which the radiation dose could be applied was limited by beam heating and by the cooling power of our cryostat, and hence much longer irradiation times than were available to us would have been required for more detailed studies of radiation damage.

The observed time constants for polarization growth (T_p) and free polarization decay or proton spin-lattice relaxation (T_1) were measured as a function of dose for unannealed targets and are plotted in fig. 2. From a least squares fit to these data, we find that T_p and T_1 decrease roughly as $(\text{dose})^{-1}$. Contrary to the situation in doped materials, the ratio T_p/T_1 changes very little in the 10^{14} to 10^{15} e^-/cm^2 dose range, implying an almost constant proton polarization and a very large depolarizing dose. Annealing at 40 K increases T_1 and T_p by roughly a factor of two, indicating a partial anneal of paramagnetic centers. Annealing at an even lower temperature (~10 K) resulted in an increase in T_1 alone. The observation of anneals of different character at these low temperatures indicates that the effectiveness of radiation depends strongly on the temperature.

Our ND_3 targets were prepared in the same manner as the NH_3 targets. The deuteron polarization rises smoothly as the target is initially irradiated (fig. 3). The maximum polarization achieved was ~25%. Annealing the target did not increase the polarization. The depolarizing (1/e) dose for ND_3 was approximately 1.3×10^{16} e^-/cm^2.

The time constants for polarization growth and free polarization decay are plotted as a function of dose for unannealed ND_3 targets in

figs. 4 and 5. The time constants plotted in figs. 4 and 5 are based on the sum and difference, respectively, of the right (R) and left (L) peak heights of the enhanced deuteron NMR signal. The sum corresponds to the vector polarization while the difference corresponds to the tensor polarization. All four time constants, $T_p(R+L)$, $T_p(R-L)$, $T_1(R+L)$ and $T_1(R-L)$ decrease with dose roughly as $(\text{dose})^{-1}$.

Annealing irradiated ND_3 targets at 10 K resulted in a slight increase in T_1 and T_p. Annealing the targets at 40 K increased T_1 and T_p for the vector polarization by an order of magnitude and greatly reduced the polarization. It was necessary to reirradiate targets annealed at 40 K to recover full polarization.

The absolute polarizations for ND_3 reported here were calculated by the ratio method [9]. While we were able to observe a TE signal, it was too small to allow accurate measurements. The many small structures in the ND_3 enhanced signal, fig. 6, may be due to different orientations of the ND_3 molecules in the crystal field. The fact that our fragments of target material are predominantly single crystals may make these structures more prominent than those observed by other groups using microcrystaline ND_3 target material.

III. CONCLUSIONS

Substantial improvements in polarized nucleon targets are possible by using irradiated ammonia or deuterated ammonia as the target materials. The polarizations attained in NH_3 and ND_3 are as high as those attained with doped hydrocarbons and the depolarizing doses for both materials are more than an order of magnitude above the depolarizing doses for conven-

tional materials. Annealing, if necessary, can be done at much lower temperatures than e.g. in butanol and hence much more quickly. Moreover, the polarizable nucleon content of NH_3 and ND_3 is about 30% greater than that of butanol.

In our recently completed E130 experiment [10] at SLAC we measured the asymmetries in the deep inelastic scattering of polarized electrons by polarized protons. The polarized electron source [11] was based on photoionization of a polarized ^6Li atomic beam and provided about 6×10^{10} polarized e^-/s (polarization $\simeq 0.8$), the polarized target was a butanol (porphyrexide-doped) target. The use of an irradiated NH_3 polarized target in this experiment would have been dramatically superior. Thus for NH_3 the fraction of polarizable protons to total number of nucleons is 0.175, whereas this fraction is 0.135 for butanol. Also since radiation damage would have been small for NH_3, the proton polarization would always have been close to its maximum value. Hence for the same statistical accuracy in the asymmetry the data-taking time would have been only about 0.5 of that used with the butanol target. Furthermore, whereas with our butanol target, radiation damage necessitated either annealing or replacing the target every 2 to 4 hrs. - a process taking about 45 min. - with an NH_3 target these frequent down-times and interruptions of data-taking would have been avoided. In order to reverse the target polarization we might have annealed our NH_3 target (rapidly at 10 K) infrequently.

With the much higher radiation resistant NH_3 polarized targets it is possible to consider doing a polarized e-p scattering experiment with a much higher intensity polarized electron beam. Indeed a higher intensity polarized e^- beam of at least 10^{12} e^-/s (but with lower polarization $\simeq 0.4$)

can be provided by photoelectron emission from GaAs using polarized laser light [12]. Optimum use of such a high intensity electron beam will require a cryostat of high cooling power and may involve problems of transient heating of the polarized bead material. However, the gain in data-taking rate would be substantial and important. Similarly the availability of irradiated ND_3 as a polarized target provides an excellent target of polarized neutrons.

We would like to acknowledge the important contribution of the SLAC Low Temperature Research Group, in constructing and maintaining our polarized target. R. Stanek of Argonne National Laboratory helped during a part of our data-taking period. We are grateful to K. Althoff, D. Hill, W. Meyer and T. O. Niinikoski for useful discussions and information. We would also like to thank Dr. R. E. Taylor of SLAC for encouragement and support, and Dr. S. Ecklund for facilitating our use of End Station A at SLAC. The research was supported in part by the Department of Energy under contracts DE-AC03-76SF00515 (SLAC) and DE-AC02-76ER03075 (Yale), by the German Federal Ministry of Research and Technology, and by the Japan Society for the Promotion of Science.

REFERENCES

1. A. Abragam, in High Energy Physics with Polarized Beams and Polarized Targets, AIP Conf. Proc. 51, Ed. G. H. Thomas (AIP, New York, 1979), p. 1; R. C. Fernow, ibid., p. 15; S. Mango, Ö. Runólfsson, and M. Borghini, Nucl. Instrum. Methods 72 (1969) 45; M. Borghini, in Proceedings of IInd International Conference on Polarized Tagets, Ed. G. Shapiro (University of California, Berkeley, 1971), p. 1.
2. K. Scheffler, Nucl. Instrum. Methods 82 (1970) 205.
3. J. C. Solem and G. A. Rebka, Phys. Rev. Lett. 21 (1968) 19; J. C. Solem, Nucl. Instrum. Methods 117 (1974) 477.
4. B. Craven, thesis, University of Liverpool (1973), unpublished.
5. T. O. Niinikoski and J.-M. Rieubland, Phys. Lett. 72 (1979) 141; T. O. Niinikoski, in Proceedings of the Second Workshop on Polarized Target Materials, Ed. G. R. Court, S. F. J. Cox, D. A. Cragg, and T. O. Niinikoski (Rutherford, Oxford, 1980), p. 94.
6. M. L. Seely, M. R. Bergström, S. K. Dhawan, V. W. Hughes, R. F. Oppenheim, K. P. Schüler, P. A. Souder, K. Kondo, S. Miyashita, S. J. St. Lorant, and Y.-N. Guo in High-Energy Physics with Polarized Beams and Polarized Targets, Ed. C. Joseph and J. Soffer (Birkhäusen Verlag, Basel, 1981), p. 453; M. L. Seely et al., in Polarization Phenomena in Nuclear Physics - 1980, AIP Conf. Proc. 69, Ed. G. G. Ohlsen, R. E. Brown, N. Jarmie, W. W. McNaughton, and G. M. Hale (AIP, New York, 1981), p. 933; M. L. Seely et al., Bull. Amer. Phys. Soc. 25 (1980) 555; see also A. Krisch in Proceedings of the Second Workshop on Polarized Target Materials, Ed. G. R. Court, S. F. J. Cox, D. A. Cragg, and T. O. Niinikoski (Rutherford, Oxford, 1980), p. 39.

7. U. Hartel, O. Kaul, W. Meyer, K. Rennings, and E. Schilling in High-Energy Physics with Polarized Beams and Polarized Targets, Ed. C. Joseph and J. Soffer (Birkhäusen Verlag, Basel, 1981), pp. 447 and 451.
8. M. J. Alguard, W. W. Ash, G. Baum, M. R. Bergström, J. E. Clendenin, P. S. Cooper, D. H. Coward, R. D. Ehrlich, V. W. Hughes, K. Kondo, M. S. Lubell, R. H. Miller, S. Miyashita, D. A. Palmer, W. Raith, N. Sasao, K. P. Schüler, D. J. Sherden, P. A. Souder, and M. E. Zeller, Phys. Rev. Lett. 41 (1978) 70; W. W. Ash, in High Energy Physics with Polarized Beams and Targets, AIP Conf. Proc. 35, Ed. M. L. Marshak (AIP, New York, 1976), p. 485.
9. O. Hamada, S. Hiramatsu, S. Isagawa, S. Ishimoto, A. Masaike and K. Morimoto, Nucl. Instrum. Methods 189 (1981) 561.
10. V. W. Hughes et al., in High-Energy Physics with Polarized Beams and Polarized Targets, Ed. C. Joseph and J. Soffer (Birkhäuser Verlag, Basel, 1981), p. 331; SLAC-PUB-2674 (February 1981).
11. M. J. Alguard, J. E. Clendenin, R. D. Ehrlich, V. W. Hughes, J. S. Ladish, M. S. Lubell, K. P. Schüler, G. Baum, W. Raith, R. H. Miller, and W. Lysenko, Nucl. Instrum. Methods 163 (1979) 29.
12. C. Y. Prescott, W. B. Atwood, R. L. A. Cottrell, H. DeStaebler, E. L. Garwin, A. Gonidec, R. H. Miller, L. S. Rochester, T. Sato, D. J. Sherden, C. K. Sinclair, S. Stein, R. E. Taylor, C. Young, J. E. Clendenin, V. W. Hughes, N. Sasao, K. P. Schüler, M. G. Borghini, K. Lübelsmeyer, W. Jentschke, Phys. Lett. 84B (1979) 524.

TABLE I

Material	Formula	H or D Fraction	Studied at Dose to	Maximum Proton Polarization
Ammonia	NH_3	0.175	4×10^{15} e$^-$/cm^2	75%
Deuterated Ammonia	ND_3	0.175	5×10^{15} e$^-$/cm^2	25% (deuteron)
Borane Ammonia	BH_3NH_3	0.194	1×10^{15} e$^-$/cm^2	30%*
Ammonium Hydroxide	NH_4OH	0.143	5×10^{13} e$^-$/cm^2	+
Butanol/5% Water	$C_4H_9OH + H_2O$	0.135	8×10^{14} e$^-$/cm^2	21%*
Ethane	C_2H_6	0.200	6×10^{15} e$^-$/cm^2	10%
Lithium Borohydride	$LiBH_4$	0.183	1×10^{15} e$^-$/cm^2	10%
Amino Methane	CH_3NH_2	0.161	3×10^{14} e$^-$/cm^2	4%

* Polarization after irradiation and anneal. Polarization measured after irradiation only is lower.

+ No polarization measurement attempted. Beads of NH_4OH prepared by rapidly freezing in a mixture of $NH_3 + H_2O$ disintegrated rapidly when irradiated.

FIGURE CAPTIONS

fig. 1. Polarization vs time for an NH_3 target, showing the effects of irradiation and annealing. During the breaks in time the target was being irradiated but no polarization measurements were made.

fig. 2. Time constants for polarization growth (T_p) and proton spin-lattice relaxation (T_1) as functions of dose for NH_3. These are combined measurements from three different targets. The scatter of the points is believed to be due to systematic effects, e.g. those associated with cryostat temperature changes over long periods of time, to the use of different targets or to tuning conditions.

fig. 3. Growth of enhanced signal for ND_3 as the target is irradiated at 1 K. For ND_3, the dose rate is 1.65×10^{12} e$^-$/cm^2/min. The dose = 0 at time = 0.

fig. 4. Time constants for polarization growth (T_p) and deuteron spin relaxation (T_1) as functions of dose for the sum of the peak heights in ND_3. These are combined measurements from three different targets. See remark in fig. 2 caption on the scatter of the points.

fig. 5. Time constants for polarization growth (T_p) and deuteron spin relaxation (T_1) for the difference of the peak heights in ND_3. These are combined measurements from three different targets. See remark in fig. 2 caption on the scatter of the points.

fig. 6. Enhanced deuteron NMR signal for ND_3.

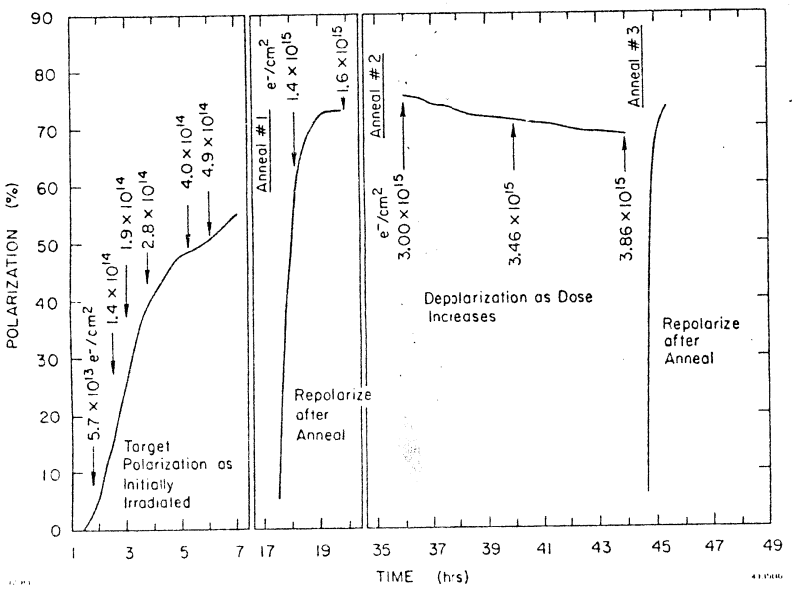
POLARIZATION (%)
TIME (hrs)
5.7 x 10^13 e⁻/cm²
1.4 x 10^14
1.9 x 10^14
2.8 x 10^14
4.0 x 10^14
4.9 x 10^14
Target Polarization as Initially Irradiated
Anneal #1
e⁻/cm²
1.4 x 10^15
1.6 x 10^15
Repolarize after Anneal
Anneal #2
e⁻/cm²
3.00 x 10^15
3.46 x 10^15
3.86 x 10^15
Depolarization as Dose Increases
Anneal #3
Repolarize after Anneal

Fig. 1

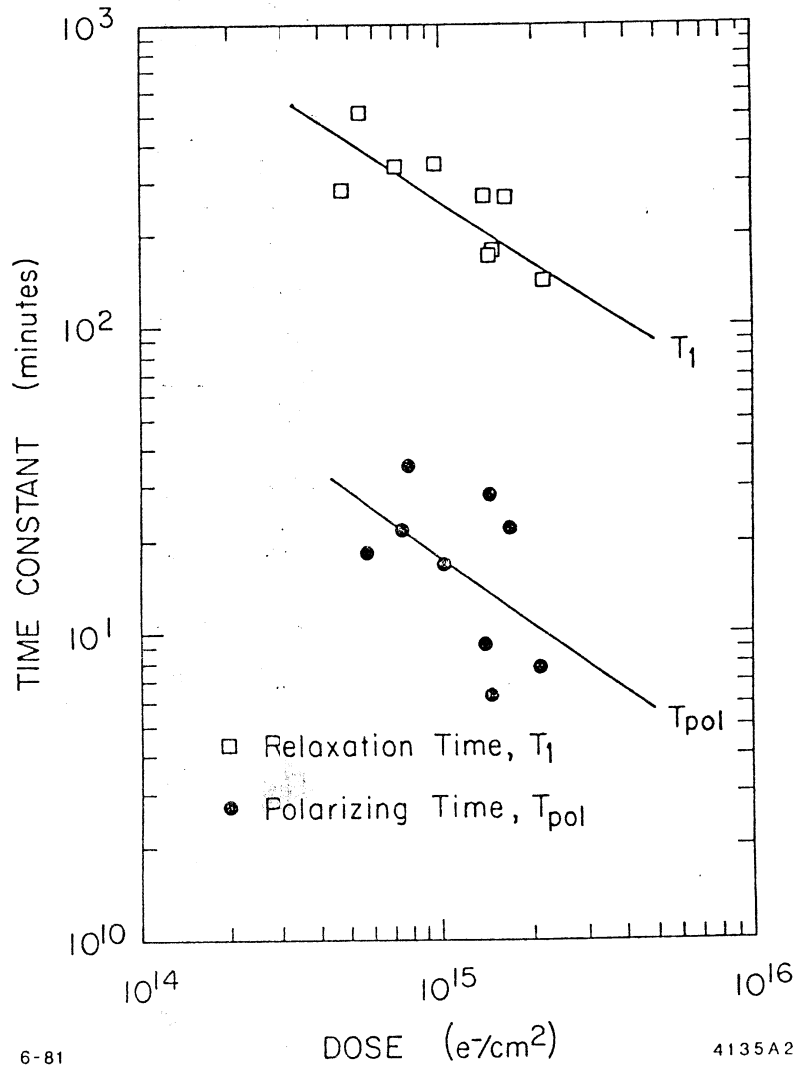
TIME CONSTANT (minutes)
DOSE (e⁻/cm²)
T1
Tpol
Relaxation Time, T1
Polarizing Time, Tpol
6-81
4135A2

Fig. 2

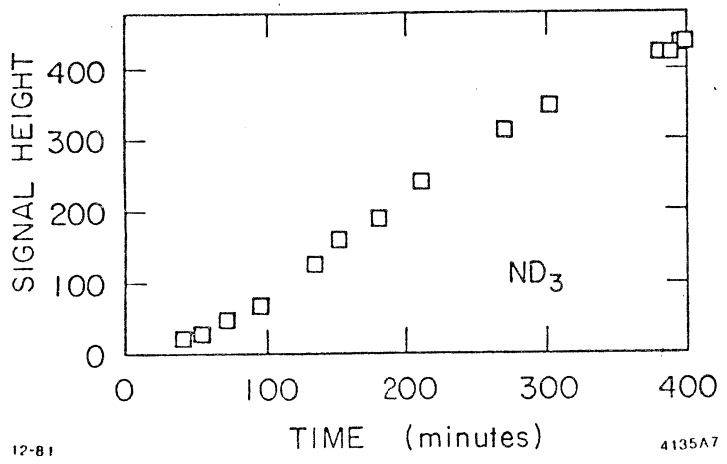
SIGNAL HEIGHT
400
300
200
100
0
0
100
200
300
400
TIME (minutes)
ND_3
12-81
4135A7

Fig. 3

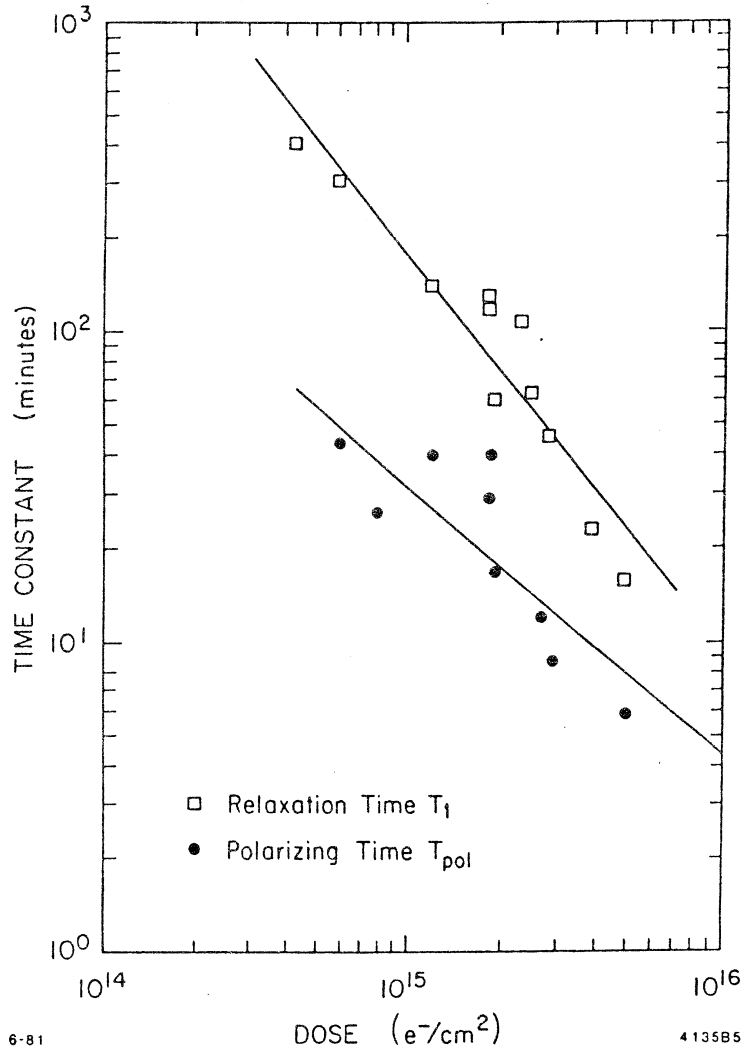
10^3
10^2
10^1
10^0
TIME CONSTANT (minutes)
10^{14}
10^{15}
10^{16}
DOSE (e^-/cm^2)
Relaxation Time T_1
Polarizing Time T_{pol}
6-81
4135B5

Fig. 4

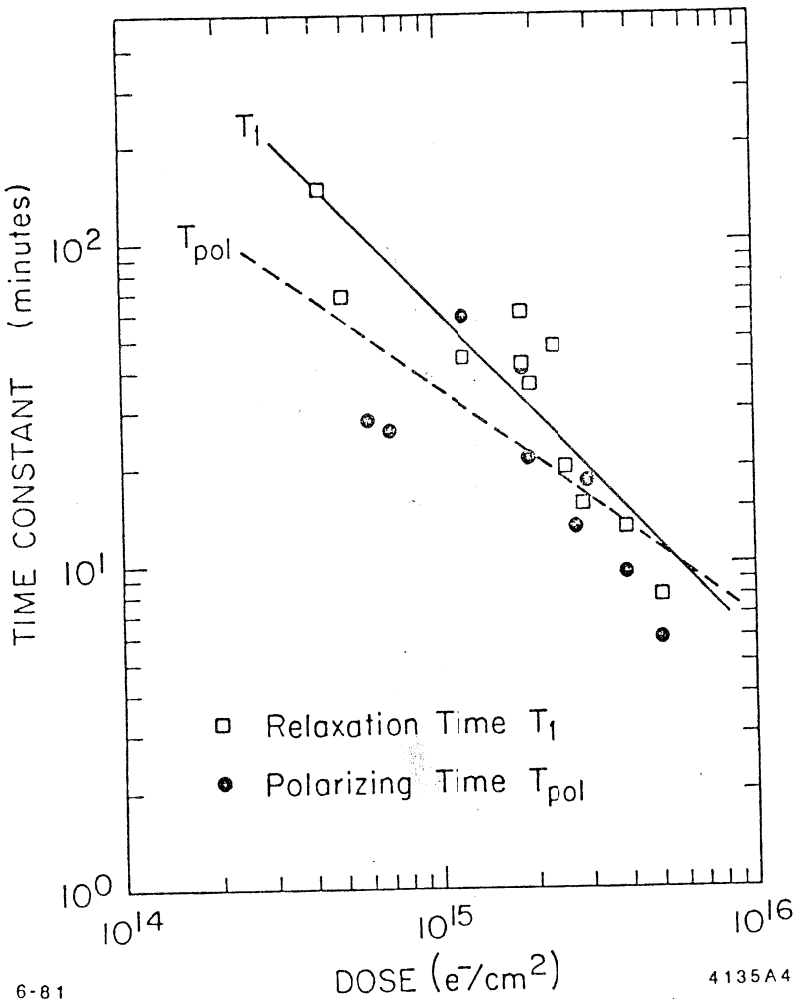
TIME CONSTANT (minutes)
10^2
10^1
10^0
T_1
T_{pol}
Relaxation Time T_1
Polarizing Time T_{pol}
10^{14}
10^{15}
10^{16}
DOSE (e^-/cm^2)
6-81
4135A4

Fig. 5

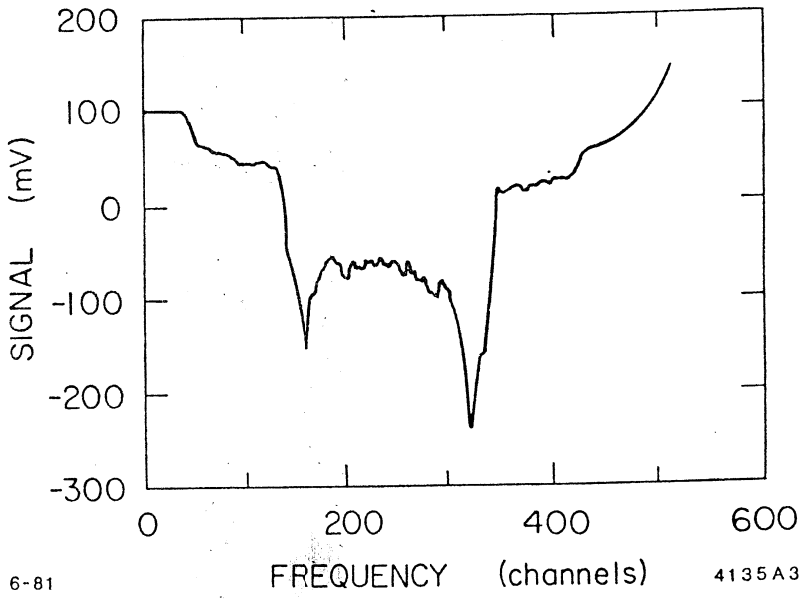
SIGNAL (mV)
200
100
0
-100
-200
-300
0
200
400
600
FREQUENCY (channels)
6-81
4135A3

Fig. 6